

INVESTIGATION OF DIAZABOROLE FORMATION AND DIAZABOROLE-LINKED  
MACROCYCLES WITH ETHYLHEXYL ESTER SUBSTITUENTS

---

A Thesis

Presented to

The Faculty of the Department of Chemistry

Sam Houston State University

---

In Partial Fulfillment

of the Requirements for the Degree of

Master of Science

---

by

Thao N. Nguyen

August, 2018

INVESTIGATION OF DIAZABOROLE FORMATION AND DIAZABOROLE-LINKED  
MACROCYCLES WITH ETHYLHEXYL ESTER SUBSTITUENTS

by

Thao N. Nguyen

---

APPROVED:

Dustin E. Gross, PhD  
Thesis Director

David E. Thompson, PhD  
Committee Member

Donovan C. Haines, PhD  
Committee Member

John B. Pascarella, PhD  
Dean, College of Science and Engineering  
Technology

## **DEDICATION**

To my friends, family and loved ones.

## ABSTRACT

Nguyen, Thao N., *Investigation of Diazaborole Formation and Diazaborole-Linked Macrocycles with EthylHexyl Ester Substituents*. Master of Science (Chemistry), August, 2018, Sam Houston State University, Huntsville, Texas.

Boron-containing polymers and macrocycles are currently an exciting field of study due to their wide variety of potential applications. The exploration of the dynamic covalent behavior of 2-phenyl-1,3,2-benzodiazaborole (**DAB**) under different solvent and temperature conditions may provide insight into the synthesis of larger diazaborole-based frameworks. The effects of solvent and temperature on the condensation of **DAB** were explored. The results showed that the **DAB** product formed faster in DMSO than in toluene. However, **DAB** formation showed higher percent conversion in toluene. In addition, Raman spectroscopy was used for *in situ* reaction monitoring of **DAB** formation. By using a calibration curve, we found that the formation of **DAB** in chloroform at 50 °C can achieve up to 68% conversion. However, the use of Raman spectroscopy for reaction monitoring of **DAB** formation was limited by solubility and by the baseline noise.

Furthermore, our research group is investigating the use of diazaboroles as the active linking unit in shape-persistent macrocycles. The present study describes the continuing efforts towards improving the solubility of monomers, oligomeric intermediates, and macrocyclic products. Ethylhexyl ester functional groups were installed on the monomer to improve solubility. The results illustrated that although the presence of branched 2-ethylhexyl ester had a positive effect on solubility of the monomer, the side chain interactions were not strong enough to overcome the pi-stacking forces of the macrocycles. The poor solubility of the co-reactant benzene-1,4-diboronic acid (**BDBA**) is a limiting factor for the formation of the macrocycle product. To overcome this issue,

we investigated the use of **BDBA**-based esters instead of **BDBA**. The results revealed that the reactions between **BDBA**-based esters with various di- and tetraamines in chloroform at room temperature were slow and intramolecular reactions to form the macrocycle could not compete with the stability of the **BDBA**-based esters.

**KEY WORDS:** Diazaborole, Dimethyl sulfoxide, Toluene, Temperature, Raman spectroscopy, Macrocycle, DC<sub>v</sub>C.

## ACKNOWLEDGEMENTS

First and foremost, I send my deepest appreciation to my advisor, Dr. Dustin Gross. Completing my masters degree would feel so unreachable without his continuing support and guidance throughout this project. He has done so much to affirm my love for the field of organic chemistry.

I would like to extend my gratitude to committee members, Dr. Donovan Haines and Dr. David Thompson, for their invaluable input during the revision of my thesis. I would additionally like to thank Dr. David Thompson and Waruni Senanayake for their limitless support on the Raman spectrometer.

Many thanks to the faculty and staff of the Chemistry Department for allowing me not to feel lost and ignored in the noise of an already challenging endeavor.

I would like to thank former group members Sanjaya Lokugama, Chamila Manankandayalage, and Angela Caffey, whose solid work provided the foundation for my research.

I would also like to acknowledge all of my colleagues in the Gross research group for their daily laboratory assistance.

Finally, I want to thank my friends, family and loved ones, especially Thomas Nguyen, for their limitless encouragement, love, and support while I pursue this degree.

## TABLE OF CONTENTS

	<b>Page</b>
DEDICATION .....	iii
ABSTRACT .....	iv
ACKNOWLEDGEMENTS .....	vi
TABLE OF CONTENTS.....	vii
LIST OF TABLES .....	ix
LIST OF FIGURES .....	x
CHAPTER	
I INTRODUCTION .....	1
1.1 Shape persistent arylene ethynylene macrocycles .....	1
1.2 Dynamic covalent chemistry .....	2
1.3 Boronic acid in DC <sub>v</sub> C.....	6
1.4 Diazaboroles .....	10
1.5 Previous work .....	12
1.6 Aims of this research.....	14
II EXAMINATION OF THE SYNTHESIS OF 2-PHENYL-1,3,2- BENZODIAZABOROLE .....	15
2.1 Introduction.....	15
2.2 Objectives .....	15
2.3 Results and discussion.....	16
2.4 Conclusions.....	35
2.5 Experimental.....	36

III SYNTHESIS AND REACTIONS OF AN ETHYLHEXYL-ESTER	
SUBSTITUTED TETRAAMINE MONOMER.....	42
3.1 Introduction.....	42
3.2 Objectives .....	42
3.3 Results and discussion.....	43
3.4 Conclusions.....	70
3.5 Experimental.....	72
REFERENCES.....	82
APPENDIX – NMR spectra for the synthesized compounds.....	87
VITA.....	110

## LIST OF TABLES

<b>Table</b>		<b>Page</b>
1	Raman data for the reaction of <b>OPD</b> and <b>PBA</b> in chloroform (308 mM) .....	28
2	Raman data for the reaction of <b>OPD</b> and <b>PBA</b> in chloroform with the inclusion of molecular sieves at the onset (308 mM) .....	29
3	Raman data for the reaction of <b>OPD</b> and <b>PBA</b> in chloroform (100 mM) .....	31
4	Raman data for the reaction of <b>OPD</b> and <b>PBA</b> in chloroform with the inclusion of molecular sieves at the onset (100 mM) .....	33
5	Solubilities of tetraamine monomers in chloroform .....	47

## LIST OF FIGURES

Figure	Page
1 Stabb's synthesis of SPAEMs .....	2
2 DC <sub>v</sub> C and ring-chain equilibrium lead to the most thermodynamically stable macrocyclic product.....	3
3 Synthesis of a SPAEM using alkyne metathesis .....	4
4 Synthesis of an imine-linked macrocycle.....	5
5 Dynamic B-O bond .....	6
6 Boronic acid in the anionic tetrahedral form.....	6
7 Synthesis of <b>COF-1</b> through boroxine formation.....	7
8 Synthesis of <b>COF-5</b> through boronate esterification.....	8
9 Synthesis of macrocycles via boronate ester formation.....	9
10 Synthesis of molecular cubes via boronate ester formation .....	9
11 Formation of <b>DAB</b> .....	10
12 Synthesis of diazaborole-based polymers .....	11
13 Oligodiazaborole-based materials.....	11
14 Synthesis of a highly porous <b>DBLP</b> .....	12
15 Synthesis of a diazaborole-based rectangular shaped macrocycle, <b>DBM-TM</b> .....	13
16 Diazaborole-based Tg functionalized macrocycle ( <b>DBM-TTg</b> ).....	13
17 Benzodiazaborole formation in CDCl <sub>3</sub> at 50 °C and in DMSO-d <sub>6</sub> at 100 °C .....	15
18 The reaction of <b>PBA</b> and <b>OPD</b> under different solvents and temperature conditions .....	16
19 The reaction of <b>PBA</b> and <b>OPD</b> in toluene-d <sub>8</sub> at 80 °C .....	16

20	Partial $^1\text{H}$ NMR spectra (aromatic region) for <b>DAB</b> formation in toluene- $\text{d}_8$ at 80 °C .....	17
21	Formation of <b>DAB</b> at a) 80, b)100 and c) 120 °C .....	18
22	Formation of <b>DAB</b> in toluene- $\text{d}_8$ (left) and DMSO- $\text{d}_6$ (right).....	19
23	Partial $^1\text{H}$ NMR spectra for the reaction in DMSO- $\text{d}_6$ at 120 °C with increasing integral values of the water signal.....	20
24	Raman spectra for <b>OPD</b> , <b>PBA</b> , and <b>DAB</b> in chloroform and pristine chloroform. The spectra were offset for clarity .....	22
25	a) Raman spectrometer set-up for Raman sampling. b) During the reaction, the glass vial was insulated in the aluminum block heaters to maintain the temperature. c) The glass vial was centered to the laser probe tip for Raman sampling. d) A black velvet fabric was used to cover the glass vial and the probe tip to avoid light interference during the analysis .....	22
26	The reaction of <b>PBA</b> and <b>OPD</b> in chloroform at 50 °C.....	23
27	Raman spectra during the formation of <b>DAB</b> (308 mM); top left: raw data; top right: normalized; bottom left: zoom; bottom right: peak heights at 850 $\text{cm}^{-1}$ vs. time .....	24
28	Raman spectra during the formation of <b>DAB</b> (308 mM) in presence of molecular sieves at the onset; top left: raw data; top right: normalized; bottom left: zoom; bottom right: peak heights at 850 $\text{cm}^{-1}$ vs. time.....	26
29	Peak heights at 850 $\text{cm}^{-1}$ vs. time for the reactions with molecular sieves added at 48 h and at the onset.....	27

30	Peak heights at 850 cm <sup>-1</sup> for various <b>DAB</b> dilutions (left) and calibration curve (right) .....	27
31	Raman spectra during the formation of <b>DAB</b> (100 mM); top left: raw data; top right: normalized; bottom left: zoom; bottom right: peak heights at 850 cm <sup>-1</sup> vs. time .....	31
32	Raman spectra during the formation of <b>DAB</b> with molecular sieves (100 mM); top left: raw data; top right: normalized; bottom left: zoom; bottom right: peak heights at 850 cm <sup>-1</sup> vs. time .....	32
33	<b>DAB</b> was heated in CDCl <sub>3</sub> at 50 °C.....	34
34	Partial <sup>1</sup> H NMR spectra of <b>DAB</b> in CDCl <sub>3</sub> at 50 °C for 10 days .....	35
35	<sup>1</sup> H NMR spectra of the isolated products from the reaction of <b>OPD</b> and <b>PBA</b> (308 mM) in chloroform at 50 °C.....	39
36	Retrosynthetic analysis of <b>TA-DEH</b> .....	43
37	Synthesis of 2-ethylhexyl 4-amino-3-bromo-5-nitrobenzoate ( <b>7</b> ).....	44
38	Synthesis of 2-ethylhexyl 4-amino-3-((trimethylsilyl)ethynyl)-5-nitrobenzoate ( <b>8</b> ).....	44
39	Synthetic route to <b>TA-DEH</b> from <b>8</b> .....	45
40	<sup>1</sup> H NMR spectrum of <b>TA-DEH</b> .....	46
41	Monomers with various pendent groups ( <b>TA-DEH</b> , <b>TA-DM</b> and <b>TA-DTg</b> ) .....	46
42	Synthesis of <b>DBM-TEH</b> from <b>TA-DEH</b> .....	48
43	<sup>1</sup> H NMR spectrum of the product mixture from Figure 42.....	49
44	MALDI mass spectrum of the reaction mixture from Figure 42.....	50
45	Reaction of <b>TA-DEH</b> and <b>BDBA</b> in DMSO-d <sub>6</sub> .....	50

46	<sup>1</sup> H NMR spectra of the reaction progress of <b>TA-DEH</b> and <b>BDBA</b> in DMSO- d <sub>6</sub> .....	52
47	Reaction of benzodioxaborole <b>11</b> and <b>OPD</b> .....	53
48	The exchange reaction of monomer <b>TA-DEH</b> and <b>BDBA</b> -based ester <b>13</b> .....	53
49	Synthesis of 2,2'-(1,4-phenylene)bis(1,3,2-benzodioxaborole) ( <b>13</b> ).....	54
50	Synthesis of a t-butyl substituted ester of <b>BDBA</b> ( <b>15</b> ).....	55
51	Reaction of <b>BDBA</b> -based ester <b>15</b> and <b>OPD</b> .....	56
52	<sup>1</sup> H NMR spectra of the reaction progress of t-butyl <b>BDBA</b> -based ester <b>15</b> and <b>OPD</b> .....	57
53	Monosubstituted diazaborole <b>17</b> .....	58
54	Reaction of monomer <b>TA-DEH</b> and <b>BDBA</b> -based ester <b>15</b> .....	58
55	<sup>1</sup> H NMR spectra of reaction progress of t-butyl <b>BDBA</b> -based ester <b>15</b> and monomer <b>TA-DEH</b> .....	60
56	Early study of the formation of B-N bonds by Letsinger.....	61
57	Synthesis of <b>BDBA</b> -based ester <b>19</b> .....	62
58	Reaction of monomer <b>TA-DEH</b> and <b>BDBA</b> -based ester <b>19</b> .....	63
59	<sup>1</sup> H NMR spectra of the reaction progress of monomer <b>TA-DEH</b> and <b>BDBA</b> - based ester <b>19</b> with increasing signal of <b>20</b> over time .....	64
60	Reaction of <b>19</b> and <b>OPD</b> .....	65
61	<sup>1</sup> H NMR spectra of the reaction progress of <b>BDBA</b> -based ester <b>19</b> and <b>OPD</b> .....	66
62	Monosubstituted diazaborole <b>21</b> .....	67
63	Synthesis of boronate ester <b>18</b> .....	67
64	Synthesis of <b>DAB</b> from <b>18</b> and <b>OPD</b> .....	68

65	$^1\text{H}$ NMR spectrum for the product of the reaction in Figure 64 .....	68
66	Reaction of <b>18</b> and <b>OPD</b> in different solvents .....	69
67	Partial $^1\text{H}$ NMR spectra for the reaction in Figure 66 after 10 days in benzene- $\text{d}_6$ and $\text{CDCl}_3$ .....	70

## CHAPTER I

### Introduction

#### 1.1 Shape persistent arylene ethynylene macrocycles

Shape persistent arylene ethynylene macrocycles (SPAEMs) have attracted noticeable research attention in supramolecular chemistry and materials science because they possess several advantages compared to their polymeric counterparts.<sup>1</sup> SPAEMs are typically composed of aromatic building blocks, which are linked by alkene or alkyne bridges. Since the repeating units have limited conformational freedom, their rigid backbones allow large molecular surfaces to organize into higher order structures.<sup>1</sup> The rigidity and planarity of SPAEMs has led to assemblies such as 2D monolayers,<sup>2</sup> liquid crystals, and nanotubes with well-defined inner pores.<sup>3,4</sup>

Traditional methods, such as cross-coupling reactions, have been widely applied to the synthesis of SPAEMs. The first synthesis of SPAEMs was introduced by Staab and Neunhoeffer in 1974.<sup>5</sup> Through a six-fold Stephens-Castro coupling of copper *m*-iodophenyl acetylide, the formation of a hexameric phenylene ethynylene macrocycle was accomplished in one-step (Figure 1).

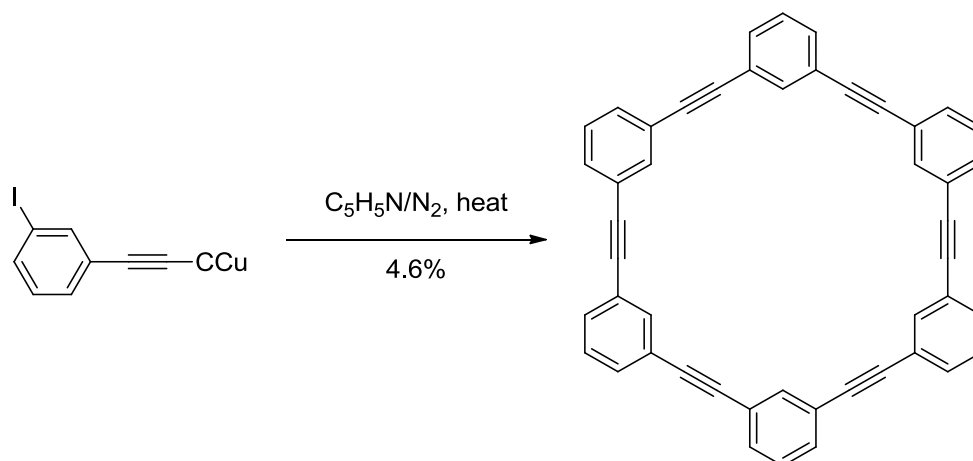
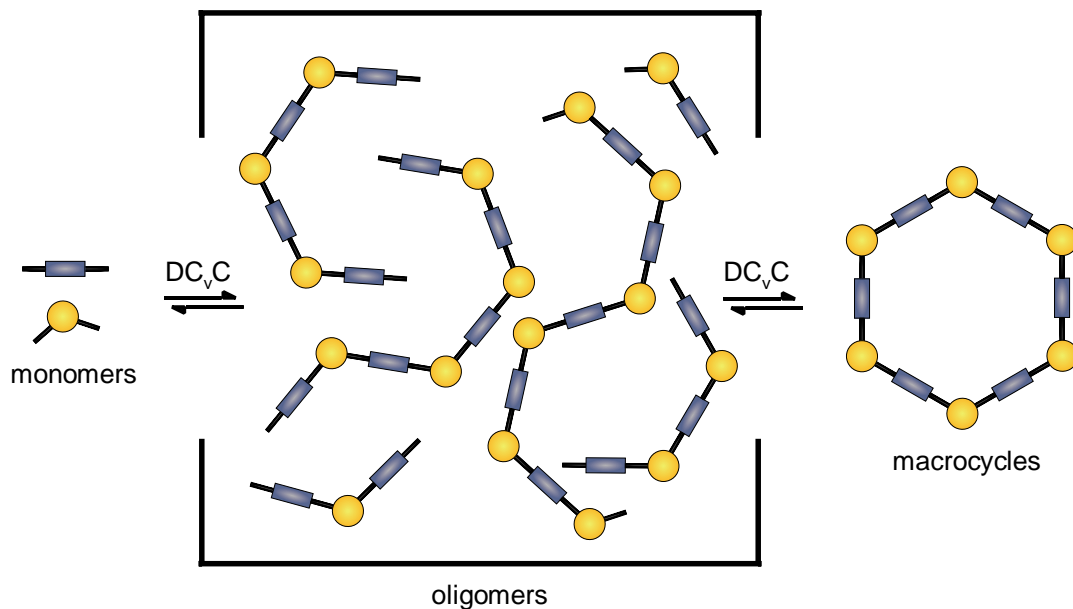


Figure 1. Stabb's synthesis of SPAEMs.<sup>5</sup>

However, the irreversible nature of these reactions leads to the formation of oligomeric, polymeric, and macrocyclic products of various sizes. The chain elongation competes with macrocyclization, which results in the low yield of the target macrocycles.<sup>6</sup> Hence, the overshooting to side products poses a problem during the synthesis of macrocycles using this method.

## 1.2 Dynamic covalent chemistry

Recently, dynamic covalent chemistry (DC<sub>v</sub>C) has emerged as a strategy to assemble thermodynamically stable macrocyclic architectures.<sup>7</sup> It involves reversible covalent bond formation, which is necessary to facilitate equilibrium between monomers, oligomers, and macrocycles. During the reaction, these components experience dynamic exchange with each other. Overshoot products are reintegrated into the process, allowing the system to “self-correct” to yield the most thermodynamically stable products, which are dependent on the bonding angles of the rigid monomer units (Figure 2).<sup>7</sup>



*Figure 2.* DCvC and ring-chain equilibrium lead to the most thermodynamically stable macrocyclic product.

Typical dynamic covalent reactions involve (1) the formation of new functional groups and (2) exchange reactions between reacting species to give products having identical bond types.<sup>8,9</sup> The types of dynamic covalent bonds may be divided into three categories: C-C, C-heteroatom, and heteroatom-heteroatom.<sup>9</sup>

Well-known covalent reactions that involve the formation of the dynamic C-C bonds include aldol, Diels-Alder, and Friedel-Crafts reactions. More recently, olefin and alkyne metathesis have been widely applied to the synthesis of complex macrocycles and cages. The assembly of SPAEMs using dynamic alkyne metathesis was first reported by Zhang and Moore in 2004 (Figure 3).<sup>10</sup> The precipitation of the diarylacetylene byproduct facilitates a shift in the reaction towards the macrocycle products.

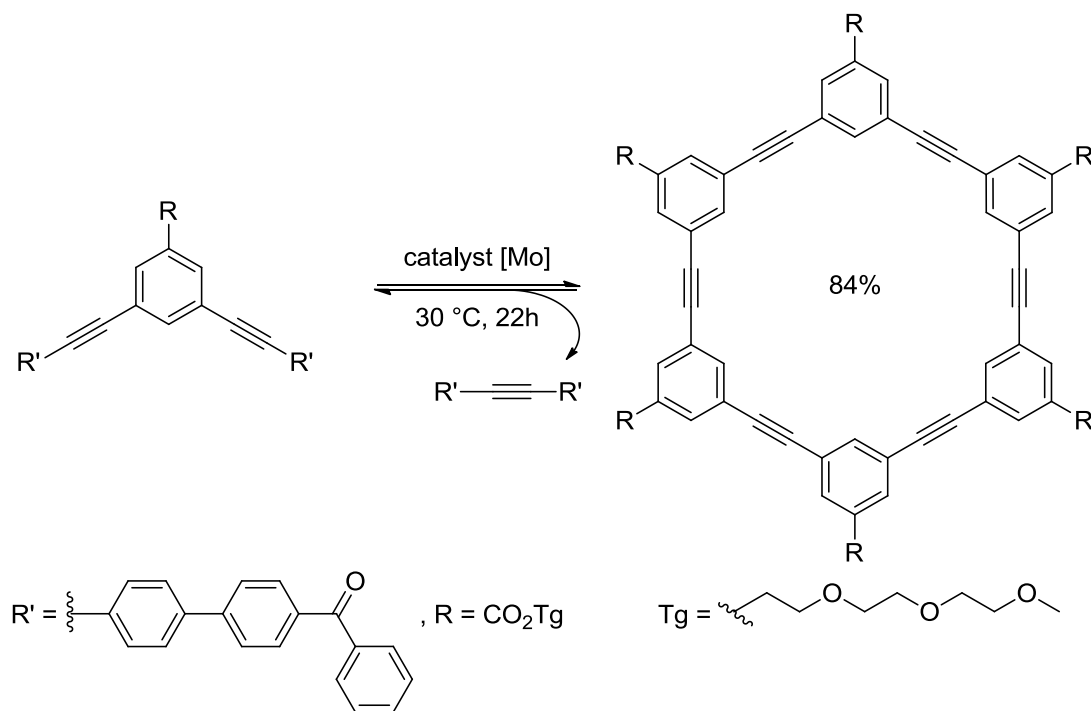


Figure 3. Synthesis of a SPAEM using alkyne metathesis.<sup>10</sup>

Imine formation between aldehydes and amines is a classic example of a C-heteroatom dynamic covalent reaction. Chavez and Dichtel have recently reported the formation of imine-linked macrocycles (Figure 4).<sup>11</sup> The starting materials are converted to the macrocycles, which aggregate into layered structures, driving macrocycle formation in high yield.

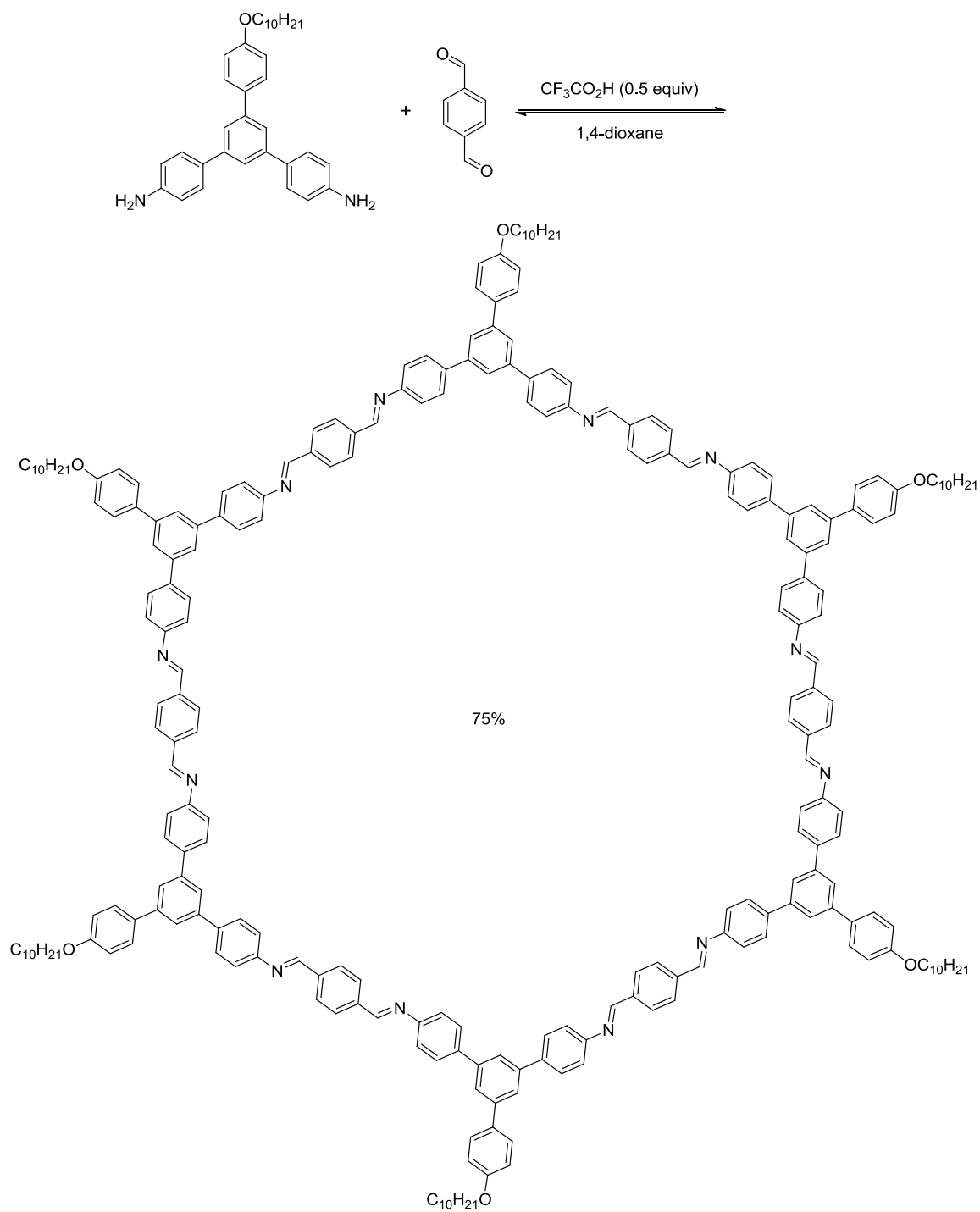


Figure 4. Synthesis of an imine-linked macrocycle.<sup>11</sup>

Dynamic heteroatom-heteroatom bonds have received great research attention, specifically the B-O bond. Commonly used reactions for the formation of the B-O bond

include boroxine anhydride formation from the self-condensation of boronic acids, and boronate ester formation from the condensation of boronic acids with diols (Figure 5). The use of boronic acids in the construction of macrocycles and polymeric systems will be discussed in the subsequent section.

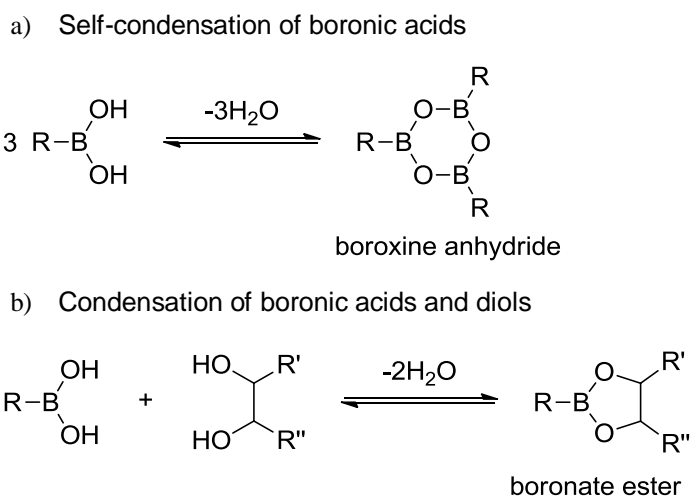


Figure 5. Dynamic B-O bond.

### 1.3 Boronic acid in DC<sub>v</sub>C

In general, the unique and advantageous chemistry of boronic acids arise from their properties as Lewis acids. Due to the low valency and the empty p orbital of the boron center, boronic acids can accept electron density from most Lewis bases, such as fluorides or hydroxides, or electron-donating centers, such as nitrogen or oxygen.<sup>12</sup> The binding of a Lewis base at the boron center results in a change in hybridization from sp<sup>2</sup> to sp<sup>3</sup>, with the boronic acid becoming a tetrahedral anionic hydroxyl coordinate species (Figure 6).<sup>12</sup>

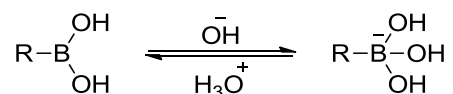


Figure 6. Boronic acid in the anionic tetrahedral form.

As discussed in section 1.2, boronic acids can form esters when reacted with diols. The boronate esterification has played an important role in the development of COFs. COFs are a class of porous materials that contain lightweight elements (H, B, C, N, and O) and strong covalent bonds. Porous COFs have high thermal stability and high surface area.<sup>13</sup> They have shown potential applications in gas storage,<sup>13</sup> catalysis,<sup>14</sup> and separation.<sup>15</sup> Yaghi and his research group were the first to report the successful synthesis of **COF-1** (Figure 7) through boroxine formation and **COF-5** through boronate esterification (Figure 8).<sup>16</sup>

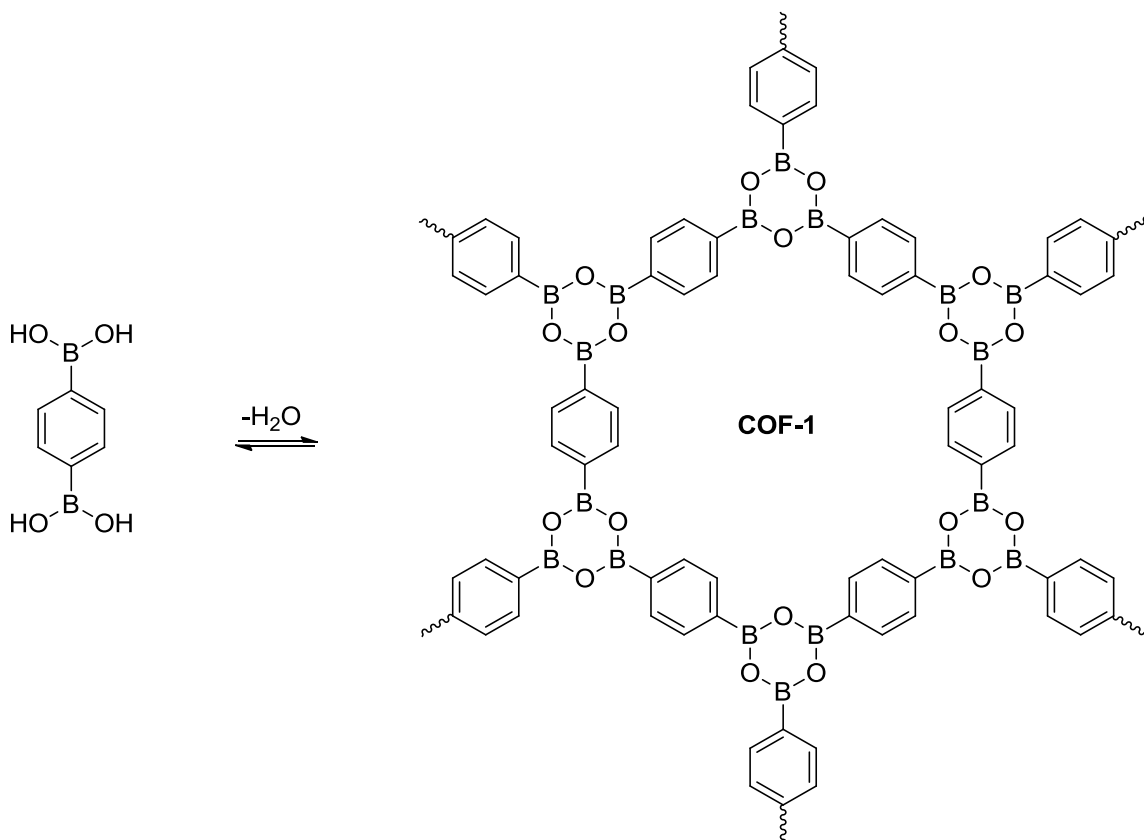


Figure 7. Synthesis of **COF-1** through boroxine formation.

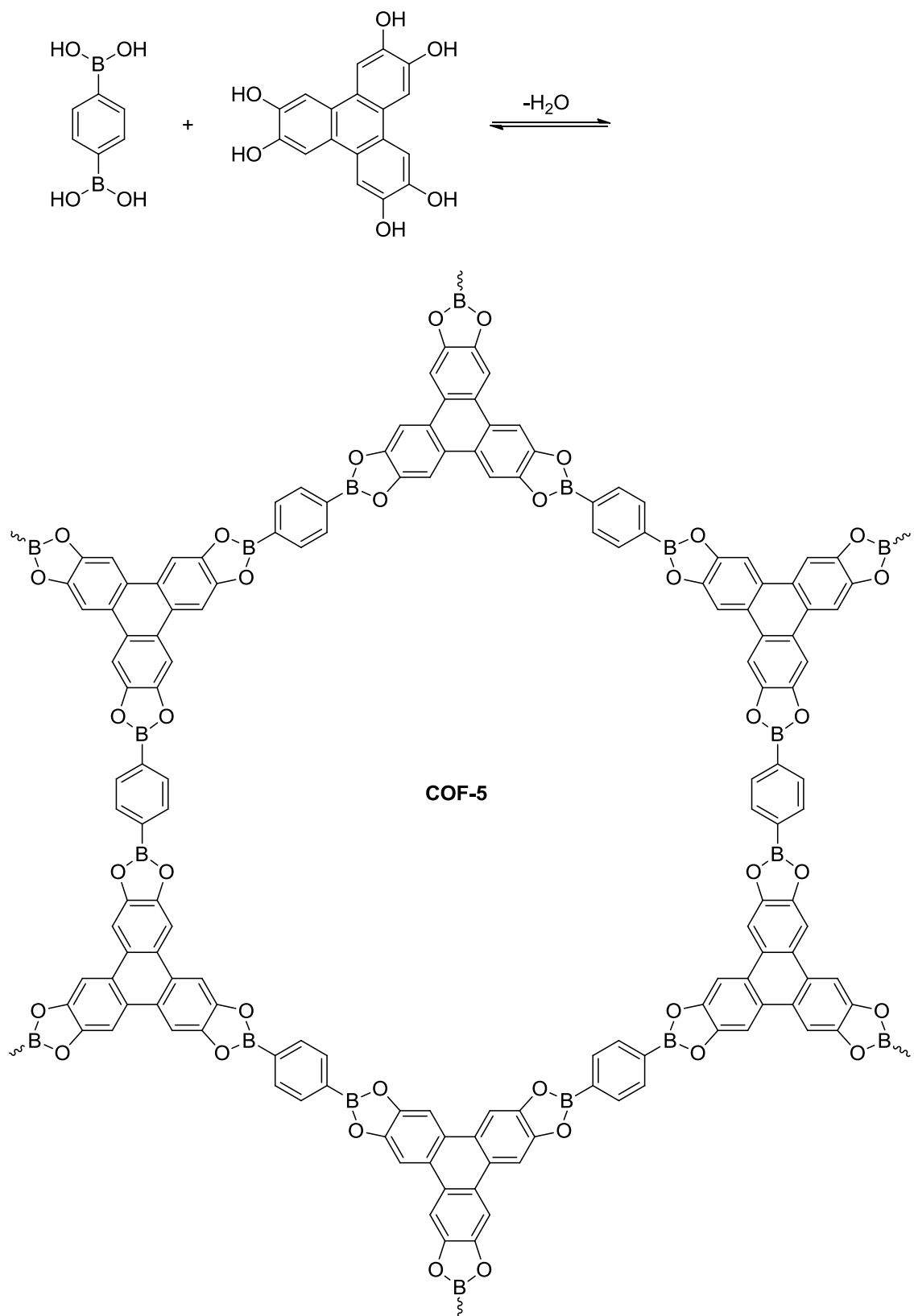


Figure 8. Synthesis of **COF-5** through boronate esterification.

These reactions have also been well studied for the preparation of macrocycles, cages, and polymeric frameworks. Northrop and his group reported the synthesis of soluble dioxaborole-based macrocycles from linear bis-catechols and benzene-1,4-diboronic acid (Figure 9).<sup>17</sup> The increased  $\pi$ -conjugation in these rectangles showed absorption and fluorescence properties.

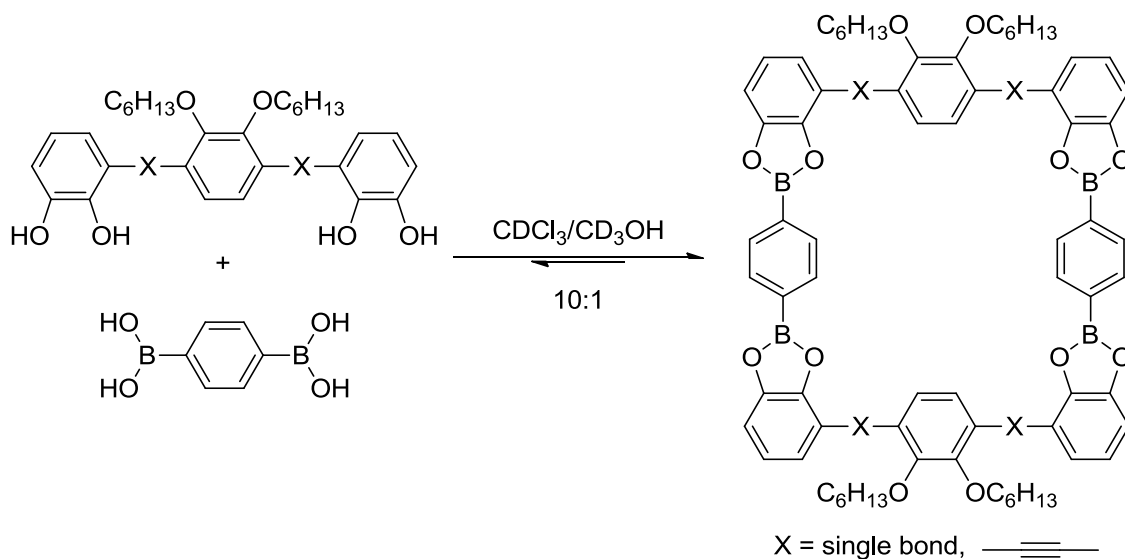


Figure 9. Synthesis of macrocycles via boronate ester formation.

Also through boronate esterification, Beuerler and coworkers synthesized molecular cubes by crosslinking of catechol-functionalized tribenzotriquinacenes and diboronic acids in a one-pot procedure (Figure 10).<sup>18</sup>

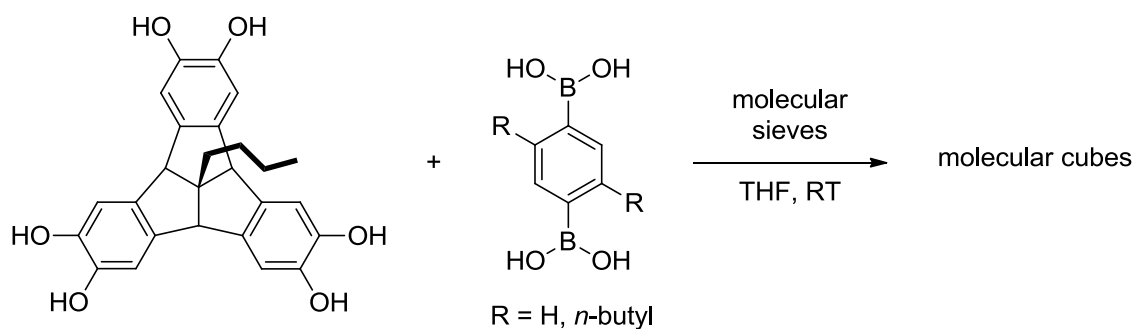


Figure 10. Synthesis of molecular cubes via boronate ester formation.

Boronic acids can also self-assemble with diamines to form diazaboroles. Diazaboroles represent a sub-category of B-N containing heterocyclic compounds. The formation of the B-N bonds has been explored for the synthesis of small molecule-based systems due to their potential application in linear and nonlinear optics,<sup>19</sup> signal amplification in sensory materials,<sup>20</sup> and in organic light emitting devices.<sup>21</sup>

#### 1.4 Diazaboroles

2-Phenyl-1,3,2-benzodiazaborole, also known as diazaborole (**DAB**), is an aromatic organic molecule that consists of two phenyl rings and a 5-membered B-N containing ring. Due to their extended  $\pi$ -conjugation, diazaboroles have attractive optical<sup>22</sup> and electrochemical properties.<sup>23</sup>

Diazaboroles are formed through the condensation of *o*-phenylenediamine (**OPD**) and phenylboronic acid (**PBA**) (Figure 11).<sup>24</sup> In order to drive the equilibrium toward the **DAB** product, water can easily be removed by using a Dean-Stark trap.

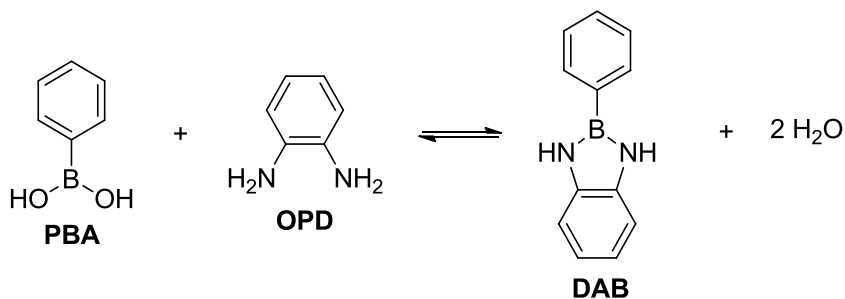


Figure 11. Formation of **DAB**.

The incorporation of **DAB** sub-unit has been used in the construction of polymers, and macrocycles. However, there are very few reported examples. In 1962, Marvel and his group reported syntheses of the first diazaborole polymers (Figure 12).<sup>25</sup> These polymers exhibit good thermal stability.

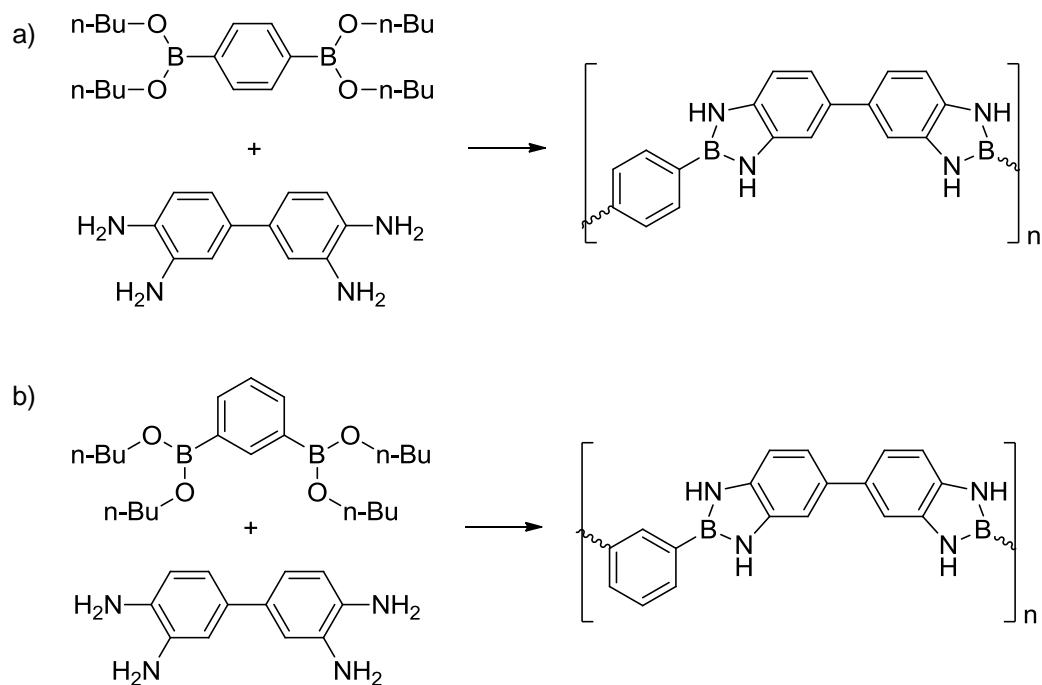


Figure 12. Synthesis of diazaborole-based polymers.

Since then, there have been reports of the formation of various oligodiazaboroles by condensing boronic acid derivatives with suitable amines (Figure 13a-b).<sup>26</sup>

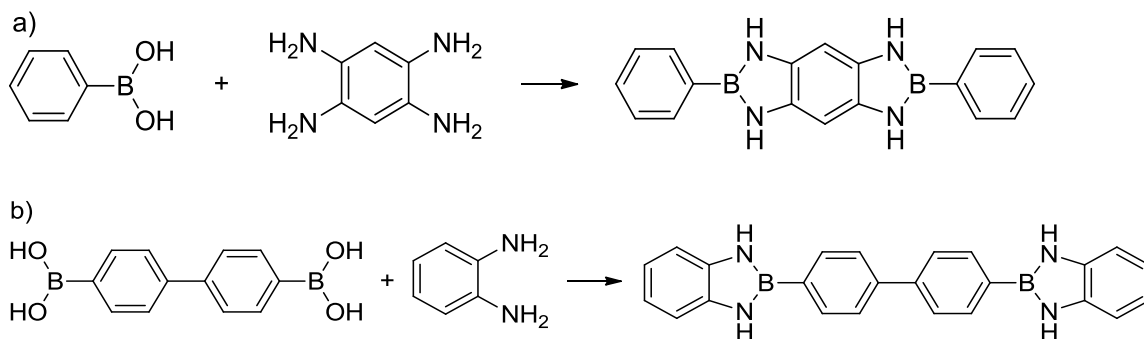


Figure 13. Oligodiazaborole-based materials.

Recently, El-Kaderi and his research group reported the syntheses of three highly porous diazaborole-linked polymers (DBLPs) by condensation reactions between a hexamine and aryl boronic acids (Figure 14).<sup>22</sup> These polymers demonstrated high gas

uptake ( $\text{CO}_2$  and  $\text{H}_2$ ), high surface area and high thermal stability. In addition, they are emissive upon UV irradiation, which could be useful for sensing anions.

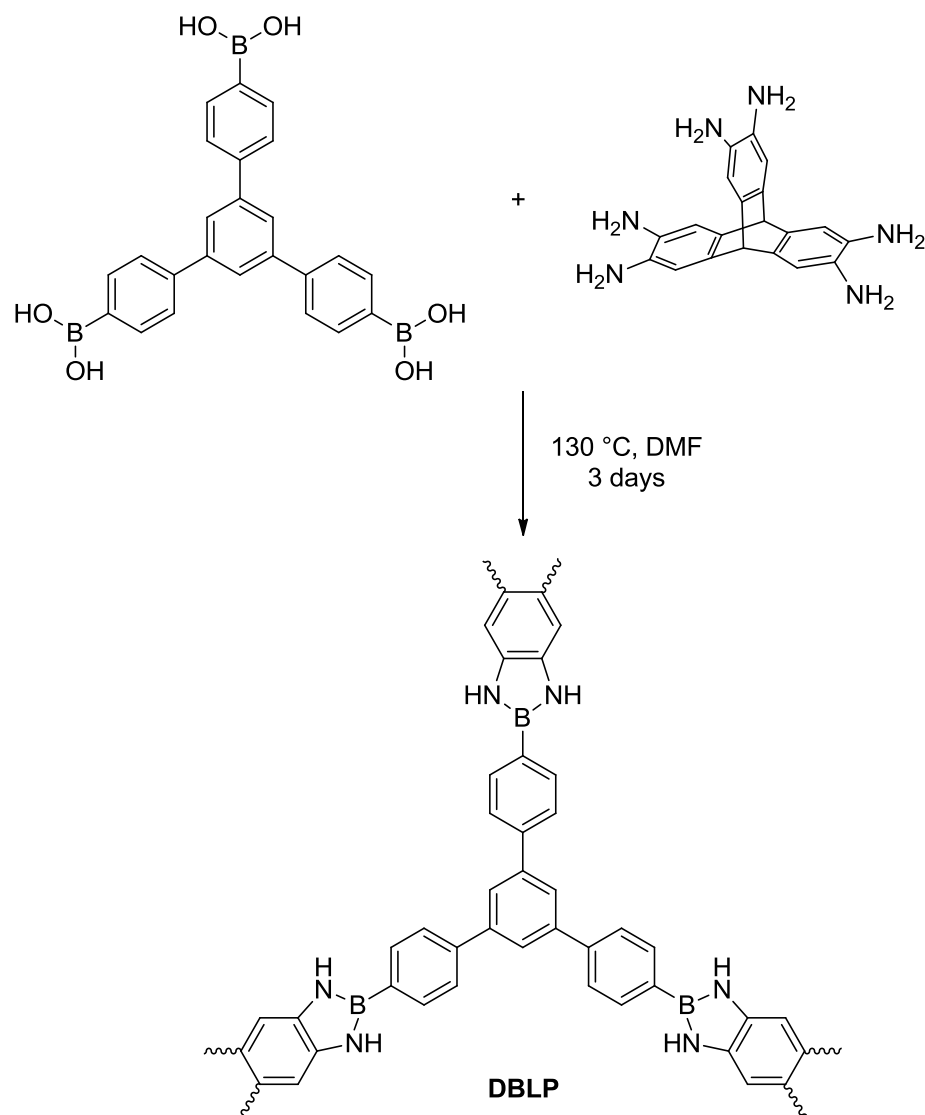


Figure 14. Synthesis of a highly porous **DBLP**.

### 1.5 Previous work

Previously a diazaborole-based rectangular-shaped macrocycle (**DBM-TM**) was synthesized by Sanjaya Lokugama using a dimethyl tetraamine monomer (**TA-DM**) and benzene-1,4-diboronic acid (**BDBA**) (Figure 15).<sup>27</sup>

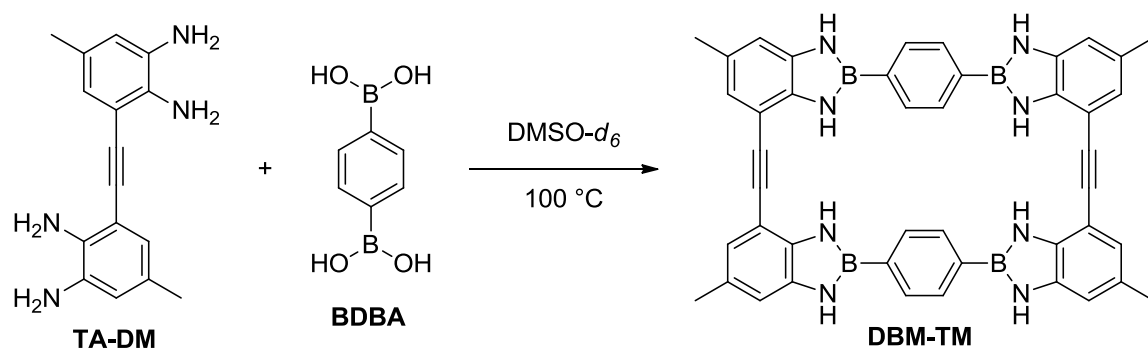


Figure 15. Synthesis of a diazaborole-based rectangular shaped macrocycle, **DBM-TM**.

The reaction was run in dimethyl sulfoxide (DMSO) because neither the **BDBA** nor the products were soluble in other common aprotic solvents. These limitations have inhibited characterization of intermediates during the reaction. Improving the solubility may not only help the self-assembly of the reactants, but also provide insight into the dynamics and kinetics of macrocycle formation.

To address the solubility limitation of intermediates during monomer and macrocycle synthesis, we propose to introduce solubilizing groups. Previously, a triethylene glycol (Tg) based ester was examined by Chamila Manankandayalage (Figure 16).<sup>28</sup>

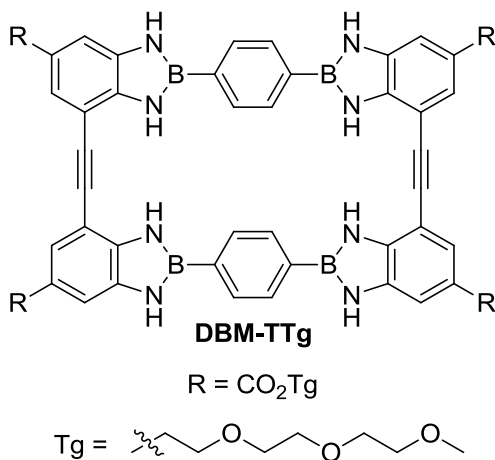


Figure 16. Diazaborole-based Tg functionalized macrocycle (**DBM-TTg**).

Chamila observed the successful formation of the Tg functionalized macrocycle (**DBM-TTg**) in DMSO as well as toluene. However, neither the macrocycle nor the oligomeric intermediates were found to be soluble in chloroform. The solubilizing power of the Tg ester sidechains was not enough to overcome the pi-pi stacking interactions among the aromatic cores of the macrocycles.<sup>28</sup>

### **1.6 Aims of this research**

In general, reflux under harsh conditions has been applied to the synthesis of various diazaboroles. However, the effect of elevated temperature and different organic solvents on product formation has yet to be fully realized. Understanding the impact of these conditions on diazaborole formation allows for their effective synthesis. Therefore, the influence of solvent and temperature on diazaborole formation was investigated. Moreover, real-time reaction monitoring of diazaborole formation using Raman spectroscopy as a convenient, cost-effective, and portable method was explored.

We introduced 2-ethylhexyl ester side chains as substituents to the tetraamine monomer in hopes of improving the overall solubility of the macrocycle unit. In addition, we investigated methods to enhance solubility of the co-reactant **BDBA** by using soluble **BDBA**-based esters.

## CHAPTER II

### Examination of the Synthesis of 2-Phenyl-1,3,2-Benzodiazaborole

#### 2.1 Introduction

In the late 1950s, Letsinger demonstrated that 2-phenyl-1,3,2-benzodiazaborole (**DAB**, **1**) formed readily by refluxing *o*-phenylenediamine (**OPD**, **2**) and phenylboronic acid (**PBA**, **3**) in toluene.<sup>24</sup> Since then, many studies have been reported using this method (toluene, reflux) as a simple and efficient way to synthesize various diazaboroles.<sup>7,29–33</sup> During the reflux, the azeotropic removal of water from the reaction medium facilitates product formation by shifting the equilibrium.

Solvents may affect reactions by stabilizing reactants, intermediates, or products, which can limit reversibility of the reaction.<sup>34</sup> Previously, our research group has examined the reaction of benzodiazaborole formation in  $\text{CDCl}_3$  and  $\text{DMSO-}d_6$  (Figure 17).<sup>27</sup> The reaction carried out in  $\text{CDCl}_3$  at 50 °C resulted in 72% benzodiazaborole formation after 200 h. On the other hand, the reaction carried out in  $\text{DMSO-}d_6$  at 100 °C established equilibrium after 60 h, ultimately reaching 80% conversion.

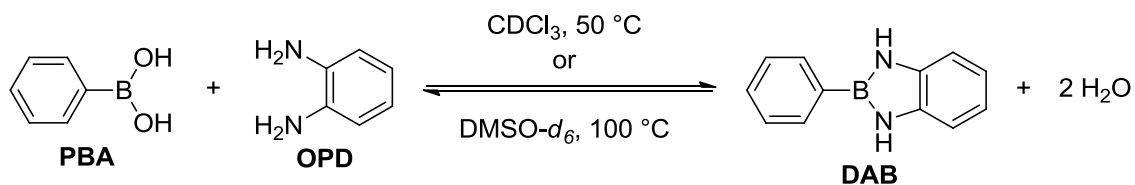


Figure 17. Benzodiazaborole formation in  $\text{CDCl}_3$  at 50 °C and in  $\text{DMSO-}d_6$  at 100 °C.

#### 2.2 Objectives

In order to optimize the yield of **DAB**, we need to know how different solvents and temperature affect the reaction. Although toluene and DMSO are commonly used solvents for diazaborole synthesis, their effect on diazaborole formation under milder conditions

were unknown at the time.  $^1\text{H}$  NMR was used to monitor the reaction in each solvent, toluene and dimethyl sulfoxide, at 80, 100, and 120 °C oil-bath temperatures (Figure 18).

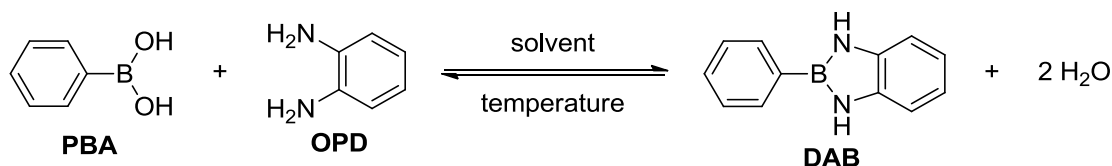


Figure 18. The reaction of **PBA** and **OPD** under different solvents and temperature conditions.

Additionally, even though a number of studies have been reported regarding diazaboroles, there are very few reports of the *in situ* reaction monitoring of its formation.<sup>35</sup> Considering its advantages, Raman spectroscopy was utilized for real-time reaction monitoring. These efforts will be described in this chapter.

## 2.3 Results and discussion

### 2.3.1 The influence of solvents and temperature on DAB formation

Initial attempts to examine the formation of **DAB** between **PBA** and **OPD** were performed in toluene-*d*<sub>8</sub>. To begin, **PBA** was mixed with a stoichiometric amount of **OPD** in toluene-*d*<sub>8</sub> and heated to 80 °C (Figure 19).

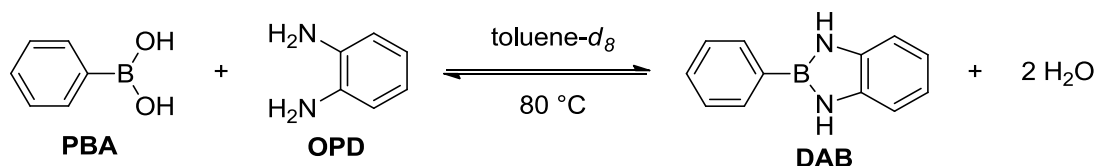


Figure 19. The reaction of **PBA** and **OPD** in toluene-*d*<sub>8</sub> at 80 °C.

$^1\text{H}$  NMR analysis provided both qualitative and quantitative evidence of the conversion of **PBA** and **OPD** to **DAB**. The reaction progress was monitored by integrating the change of the aromatic signals corresponding to **OPD** (H<sub>a</sub>) and **DAB** (H<sub>b</sub>) (Figure 20). These signals were chosen because they are distinct and well separated from the others,

which allows for the quantification of conversion. The consumption of the starting material **OPD** ( $H_a$ ) and formation of the product **DAB** ( $H_b$ ) was observed.

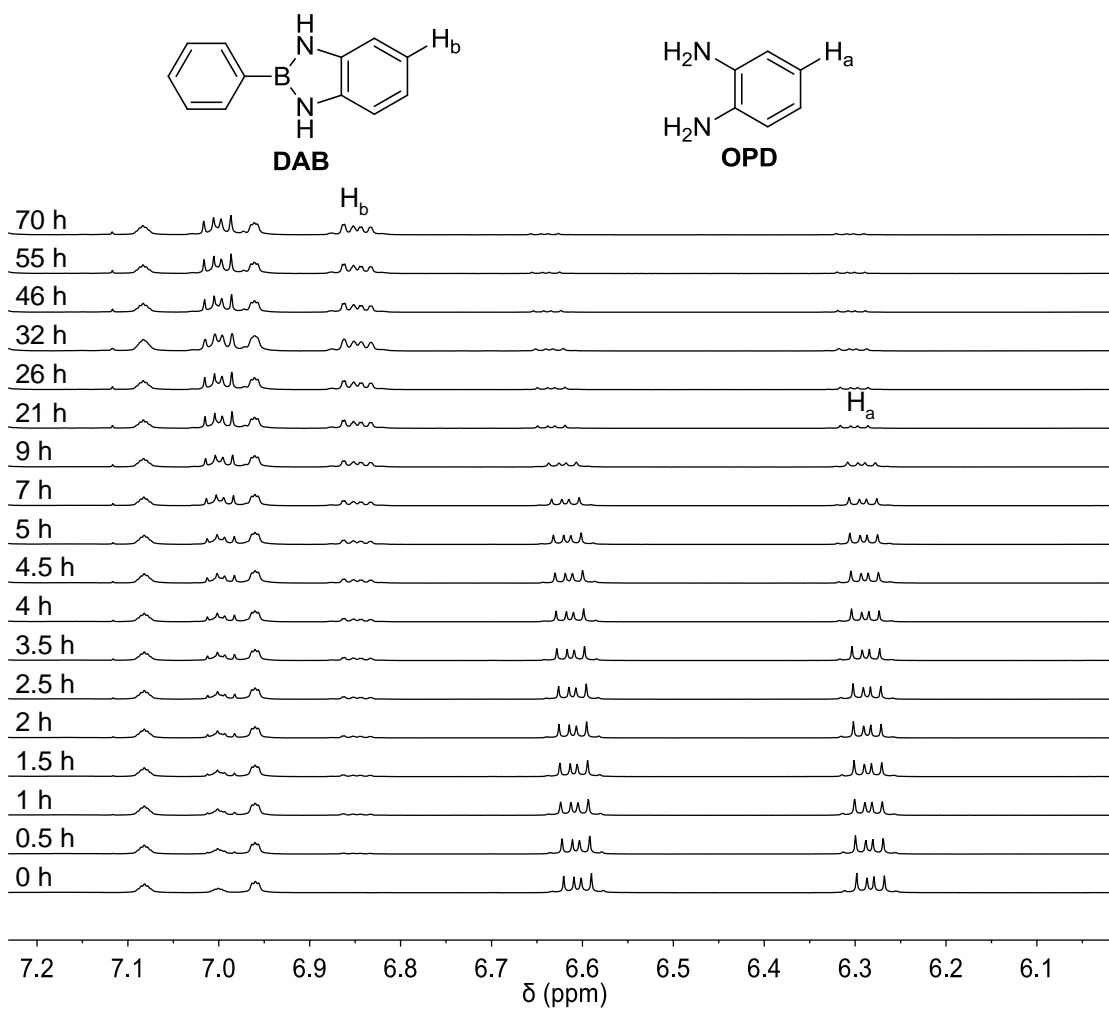


Figure 20. Partial  $^1\text{H}$  NMR spectra (aromatic region) for **DAB** formation in toluene- $d_8$  at 80 °C.

A similar procedure was carried out in toluene- $d_8$  at 100 and 120 °C and in DMSO- $d_6$  at 80, 100, and 120 °C. The percent conversions are summarized in Figure 21.

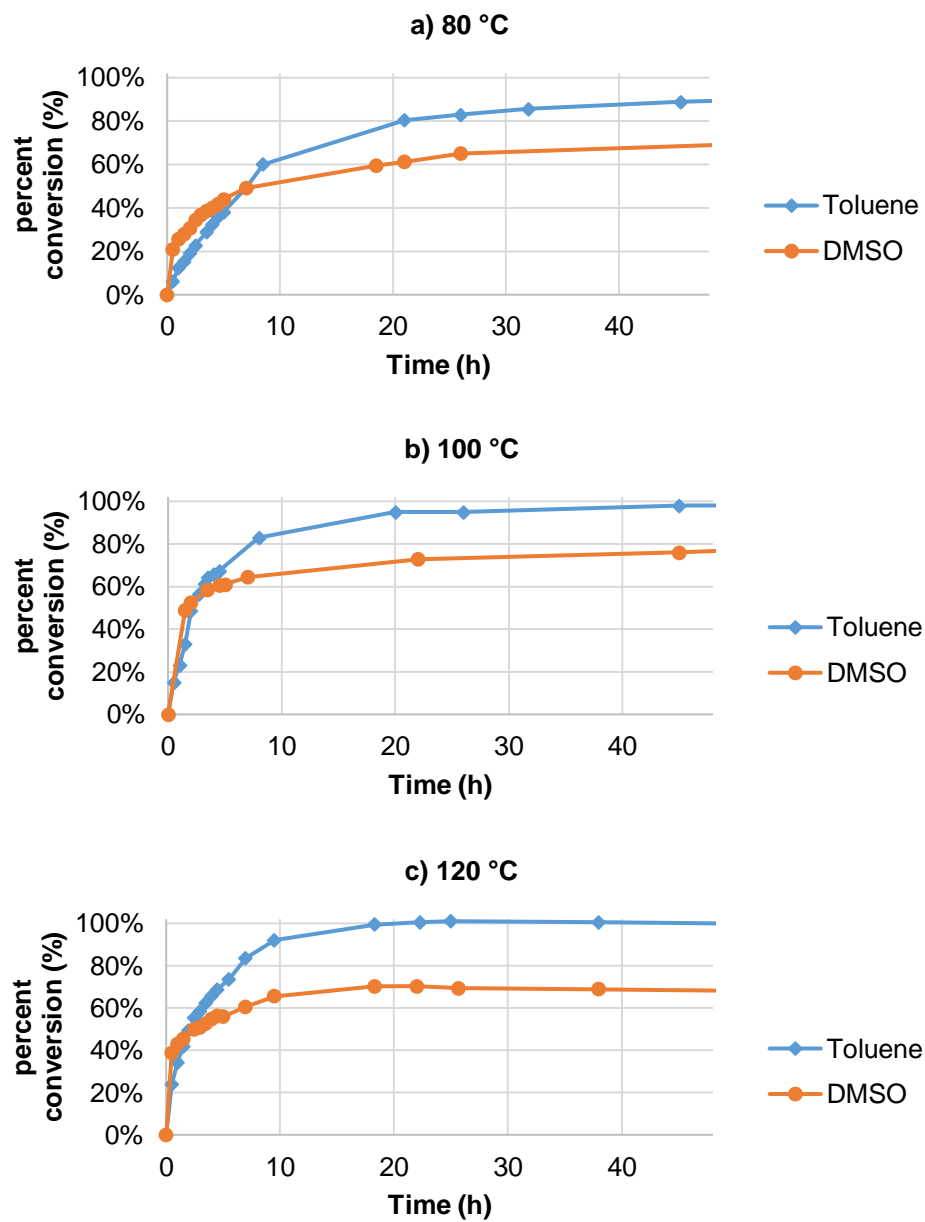


Figure 21. Formation of **DAB** at a) 80, b) 100 and c) 120 °C.

Figure 21 shows that the starting materials were consumed faster in DMSO compared to toluene. DMSO is a very polar, aprotic solvent and is capable of accepting hydrogen bonds. This can help stabilize the charged intermediates (and transition states) and facilitate proton transfers during the reaction, which results in an increase in rate.

As time progressed, however, the formation of **DAB** was greater in toluene (Figure 22). The reaction reached 100% conversion after heating for 23 h at 120 °C oil-bath. Since toluene is a less hygroscopic solvent, increasing the reaction temperature may have allowed water to evaporate from the system more easily than from DMSO, helping shift the equilibrium toward the product side. For the reaction in DMSO, the increasing presence of water in the medium is evident due to the increasing integral values at  $\delta$  3.32 ppm (Figure 23). We hypothesized that this caused the reactions to establish equilibrium at ~70% conversion.

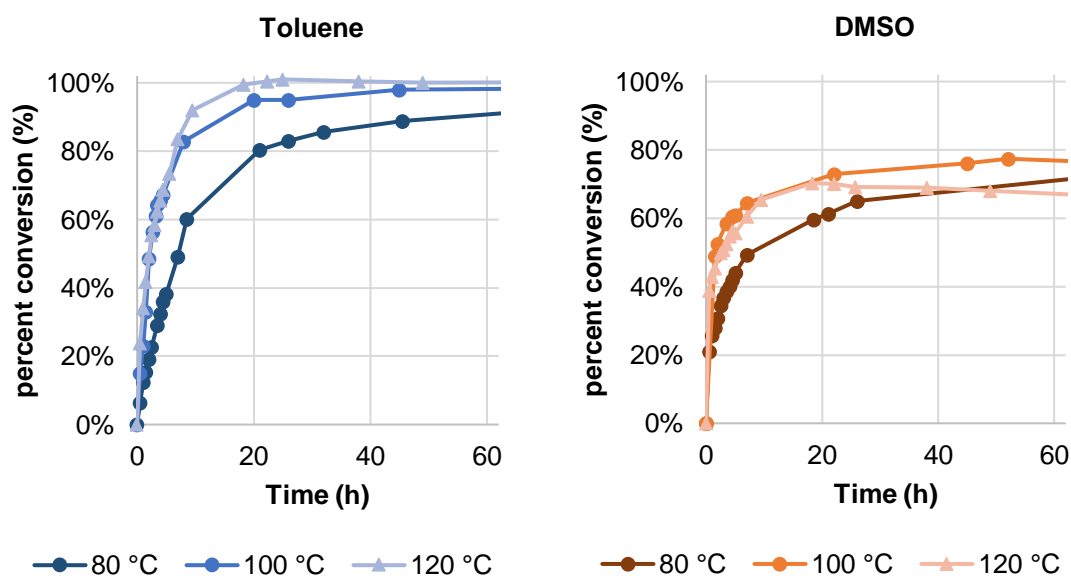
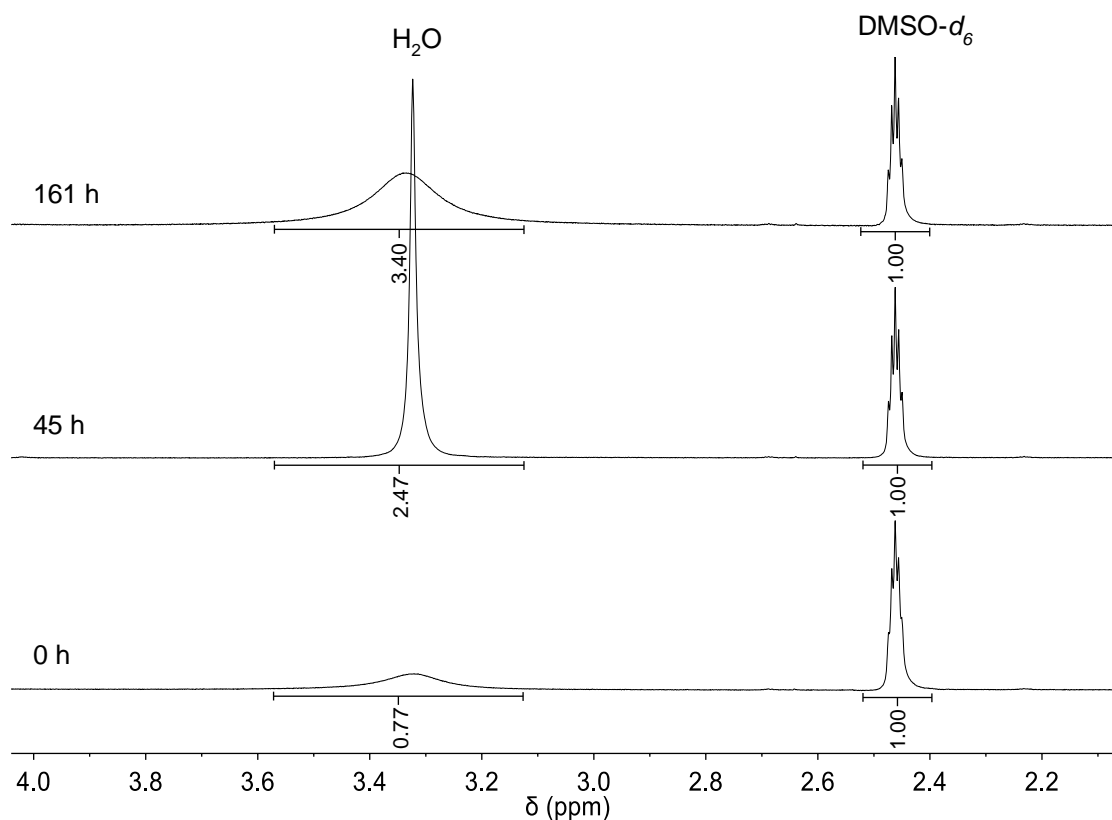


Figure 22. Formation of **DAB** in toluene- $d_8$  (left) and DMSO- $d_6$  (right).



*Figure 23.* Partial  $^1\text{H}$  NMR spectra for the reaction in  $\text{DMSO-}d_6$  at  $120\text{ }^\circ\text{C}$  with increasing integral values of the water signal.

The results in this experiment are similar with earlier studies done in DMSO by Sanjaya Lokugama,<sup>27</sup> where **DAB** formation in DMSO at  $100\text{ }^\circ\text{C}$  only reached  $\sim 80\%$  after 60 h of reaction. These results further support that the presence of water in hygroscopic solvents hinders the complete formation of diazaborole.

The use of NMR spectroscopy for reaction monitoring of organic syntheses is widely applied because it is powerful and sensitive. However, it often requires complex sample preparation and serial analysis steps that are time consuming. In addition, conventional NMR instruments are not portable and expensive. Raman spectroscopy is a

technique that provides the potential for portable, sensitive, and real-time analysis of organic reactions.

### 2.3.2 Monitor DAB formation using Raman spectroscopy

Raman spectroscopy probes vibrational transitions by exciting the sample with an intense beam of light, and monitoring the inelastic scattering of that light.<sup>36</sup> It has become a technique for *in situ* reaction monitoring in chemical syntheses. The chemical reaction investigated in this study mainly involves three compounds that may be Raman active, the starting materials **OPD** and **PBA** and the target product **DAB**. During the reaction, the main structural molecular change is the conversion of C-B-O into C-B-N. As a result, the appearance and disappearance of peaks or change in intensities of the peaks associated with the structural changes will be utilized for reaction monitoring.

In order to mitigate the influence of polar aprotic solvents on **DAB** formation and also to ensure the greater solubility of all participating analytes, chloroform was chosen over DMSO and toluene. Chloroform is relatively nonreactive and will not affect the working solutes. Since room temperature condensation of diazaboroles in chloroform is relatively slow,<sup>7,25</sup> the temperature is elevated for this reaction to increase the rate.

The first set of experiments was carried out to obtain Raman spectra of pure reactants and products (**OPD**, **PBA**, and **DAB**) and pristine chloroform (Figure 24). Raman spectra were collected using the assembled Raman system with the Bayspec probe shown in Figure 25. The Raman spectrum of **DAB** in Figure 24 shows Raman-active stretching mode at 850 cm<sup>-1</sup> while the **OPD** and **PBA** starting materials show minimal Raman activity in this area. In addition, the peak at 1016 cm<sup>-1</sup> is overlapping with neighboring peaks and the one at 1426 cm<sup>-1</sup> had baseline correction complications.

Therefore, the peak at  $850\text{ cm}^{-1}$  was identified as a potential signal to monitor reaction progress.

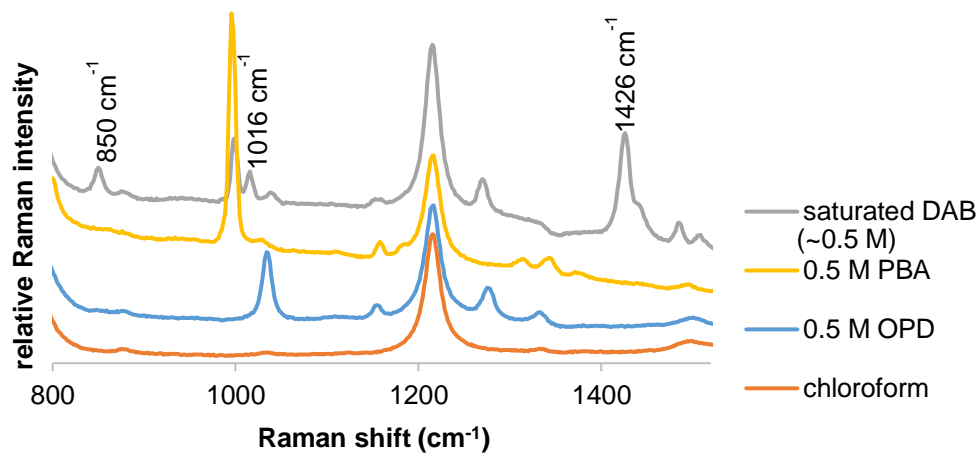


Figure 24. Raman spectra for **OPD**, **PBA**, and **DAB** in chloroform and pristine chloroform. The spectra were offset for clarity.

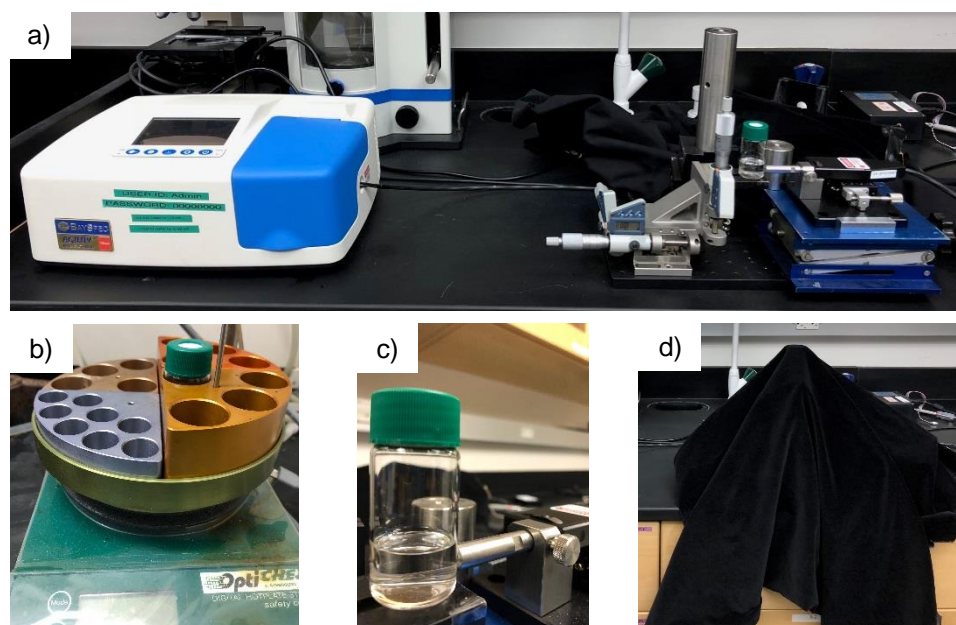


Figure 25. a) Raman spectrometer set-up for Raman sampling. b) During the reaction, the glass vial was insulated in the aluminum block heaters to maintain the temperature. c) The glass vial was centered to the laser probe tip for Raman sampling. d) A black velvet fabric was used to cover the glass vial and the probe tip to avoid light interference during the analysis.

With this signal in mind, the reaction was ran at 308 mM in chloroform in a glass vial. The reaction was heated to 50 °C with stirring and Raman spectra were obtained over time (Figure 26).

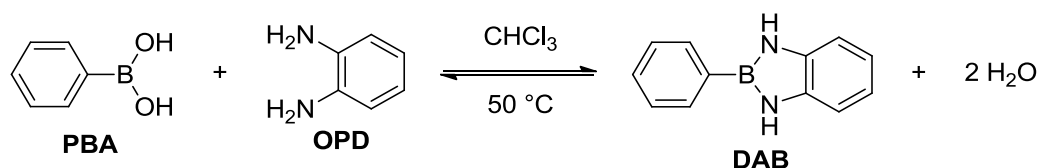


Figure 26. The reaction of **PBA** and **OPD** in chloroform at 50 °C.

The Raman spectra obtained during the reaction of **PBA** and **OPD** are shown in Figure 27 (top left). Normalization was performed using Microsoft Excel, where the baseline (831 cm<sup>-1</sup>) was set to zero near the peak of interest (850 cm<sup>-1</sup>) and the solvent peak (1215 cm<sup>-1</sup>) was set to 1 (Figure 27, top right). The changes in Raman intensities at 850 cm<sup>-1</sup> ( $H_{850}$ ) were then plotted *versus* time (Figure 27, bottom right). The sharp change in Raman intensity during the first 12 h of the reaction suggests the relatively fast product formation. Since little change was observed in the Raman signal after 12-38 h of reaction, the reaction may have established equilibrium. Molecular sieves (3 Å) were added at the 48 hour mark in an attempt to remove the water byproduct and shift the reaction to the products. This led to the formation of a white precipitate at 56 h of reaction. After 68 h, the reaction mixture became more turbid, indicating the formation of more precipitate. The solution turbidity increases Rayleigh scattering, which interferes with the Raman signal detection by varying the baseline. Therefore the reaction vial was removed from heating at the 68 h mark. The precipitate was isolated (see Experimental Methods) and identified as **DAB** (61% yield) using <sup>1</sup>H NMR.

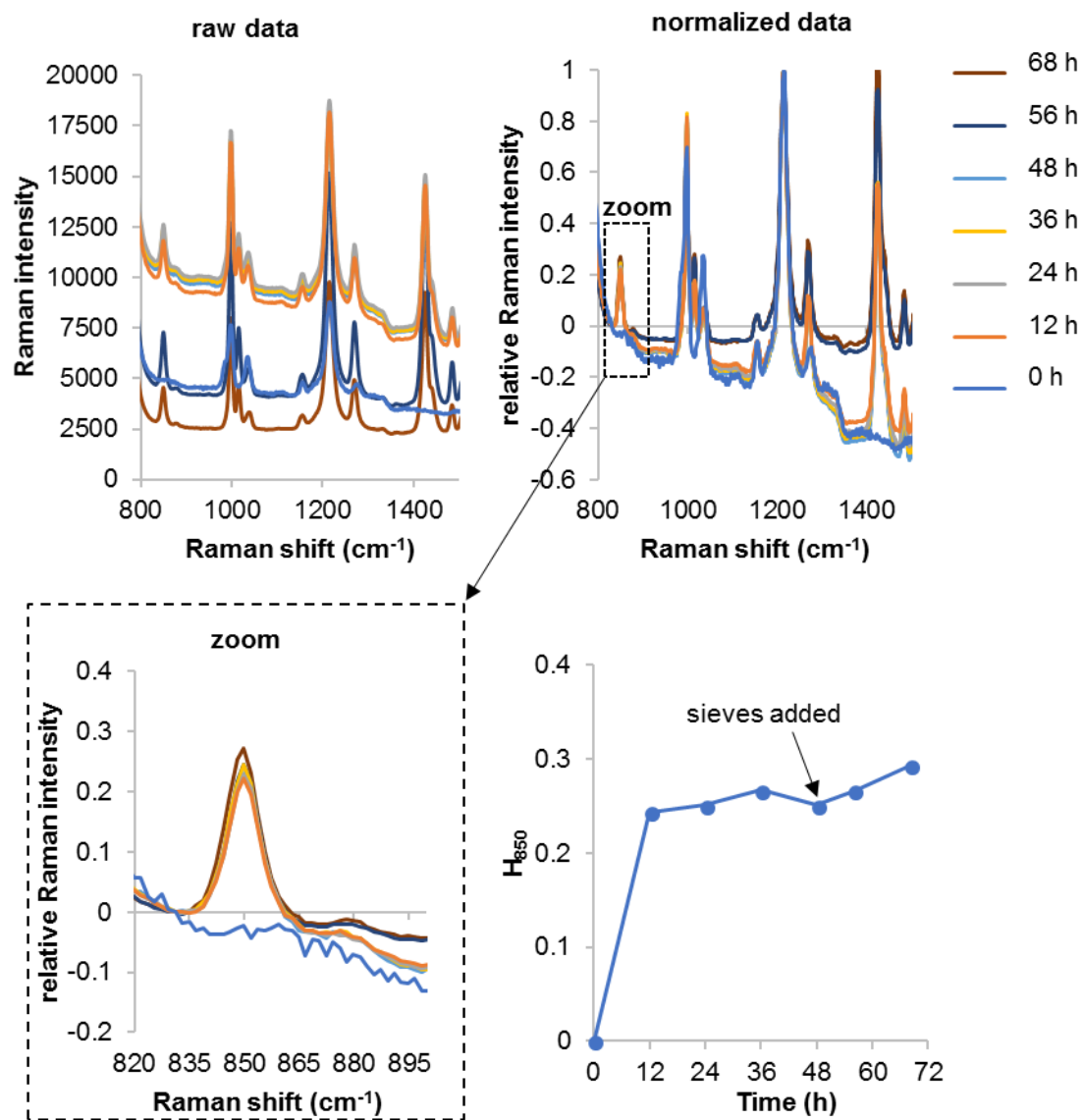
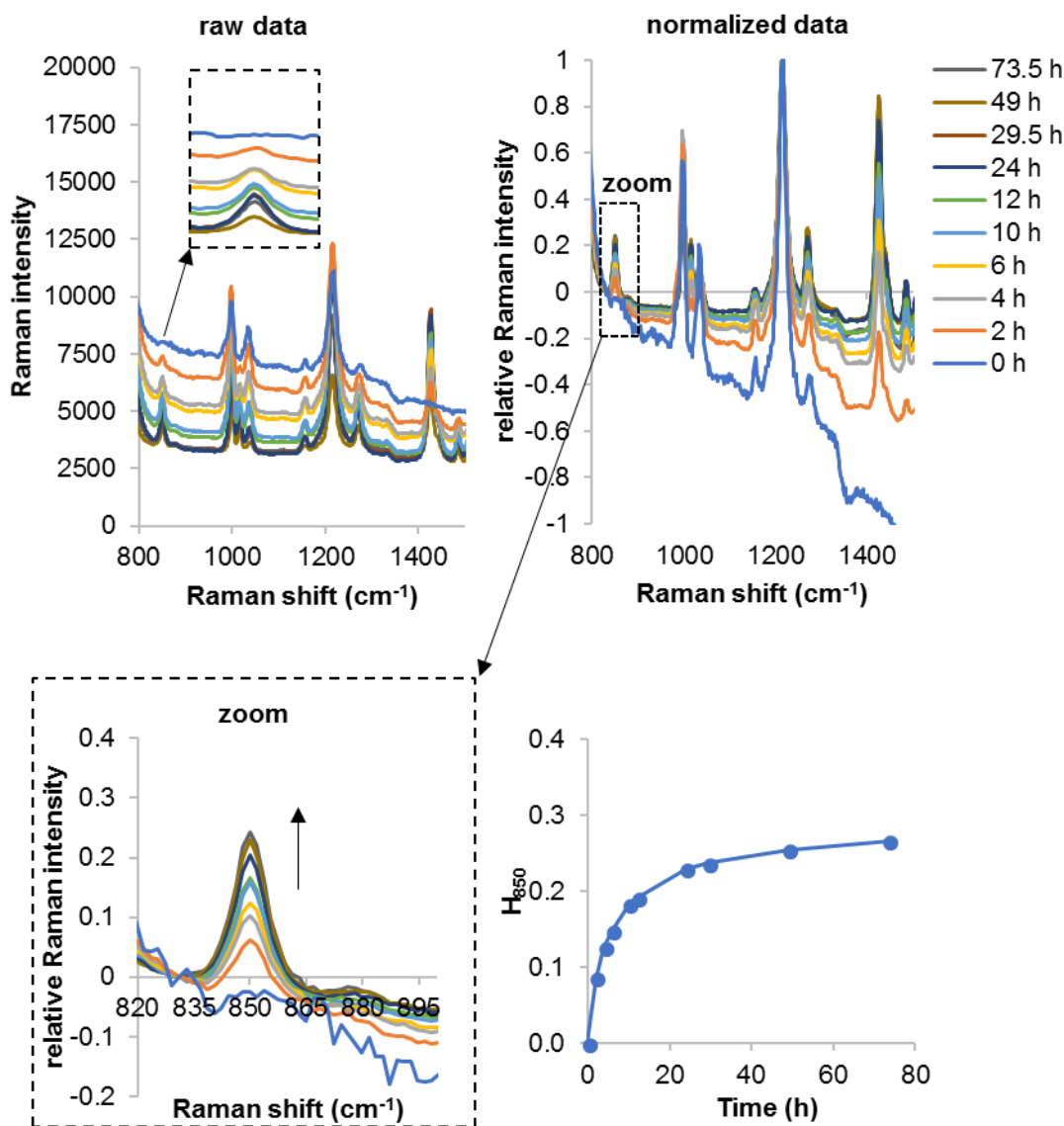


Figure 27. Raman spectra during the formation of **DAB** (308 mM); top left: raw data; top right: normalized; bottom left: zoom; bottom right: peak heights at  $850\text{ cm}^{-1}$  vs. time.

Since the addition of molecular sieves seemed to help with product formation, the experiment was repeated with the inclusion of molecular sieves ( $3\text{ \AA}$ , 2 equiv by mass relative to **PBA**) at the onset. Spectra were obtained every 2-4 h to better observe the change in product formation during the first 12 h of reaction (Figure 28, top left). Similar normalization was performed (Figure 28, top right) and the changes in Raman intensities at  $850\text{ cm}^{-1}$  ( $H_{850}$ ) were plotted *versus* time (Figure 28, bottom right).

Figure 28 (bottom right) shows a gradual change in Raman intensities during the first 30 h of reaction. After 49 h, the reaction mixture became turbid due to precipitation and the Raman spectrum obtained had a less intense solvent signals as well as the signal at  $850\text{ cm}^{-1}$  than the same bands recorded at 24 h of reaction. The turbidity of the solution leads to the decrease in the amount of product exposed to the light coming from the laser. This causes the intensity of Raman scattering to reduce. After 73.5 h, the reaction mixture became very turbid and therefore, was removed from heating. The precipitate was isolated (see Experimental Methods) and identified as **DAB** (57% yield) using  $^1\text{H}$  NMR.



*Figure 28.* Raman spectra during the formation of **DAB** (308 mM) in presence of molecular sieves at the onset; top left: raw data; top right: normalized; bottom left: zoom; bottom right: peak heights at 850 cm<sup>-1</sup> vs. time.

For the reaction with molecular sieves added at the onset, **DAB** formation was fast within the first 6 h of reaction (Figure 29, right). After 24 h, small changes in Raman intensities were observed. The inclusion of molecular sieves at the onset allowed for the gradual removal of water from the reaction medium, leading to the continuing shift in

equilibrium to the right of the reaction shown in Figure 26. However, this resulted in little change in reaction outcome (Figure 29).

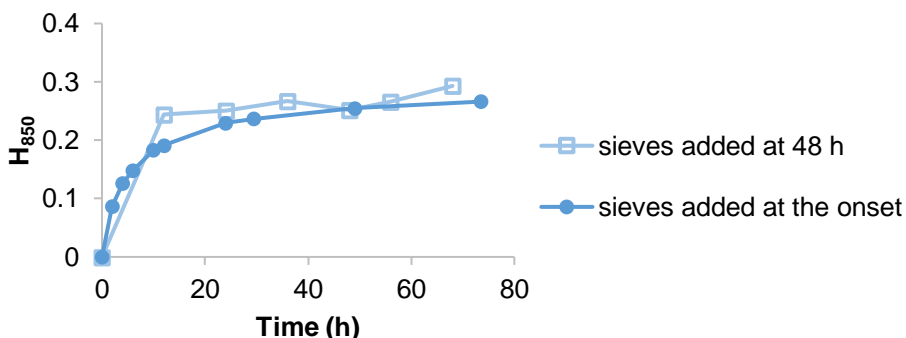


Figure 29. Peak heights at  $850\text{ cm}^{-1}$  vs. time for the reactions with molecular sieves added at 48 h and at the onset.

In an attempt to quantify **DAB** formation in solution, a calibration curve was obtained to relate the Raman intensity to units of concentration. To achieve this, solutions of **DAB** having various concentrations were prepared and measured. The spectra were normalized in the same manner, where the baseline ( $831\text{ cm}^{-1}$ ) was set to zero near the peak of interest ( $850\text{ cm}^{-1}$ ) and the solvent peak ( $1215\text{ cm}^{-1}$ ) was set to one. When the signal intensity at  $850\text{ cm}^{-1}$  ( $H_{850}$ ) was plotted against concentration  $[\text{DAB}]$ , it showed a linear relationship (Figure 30).

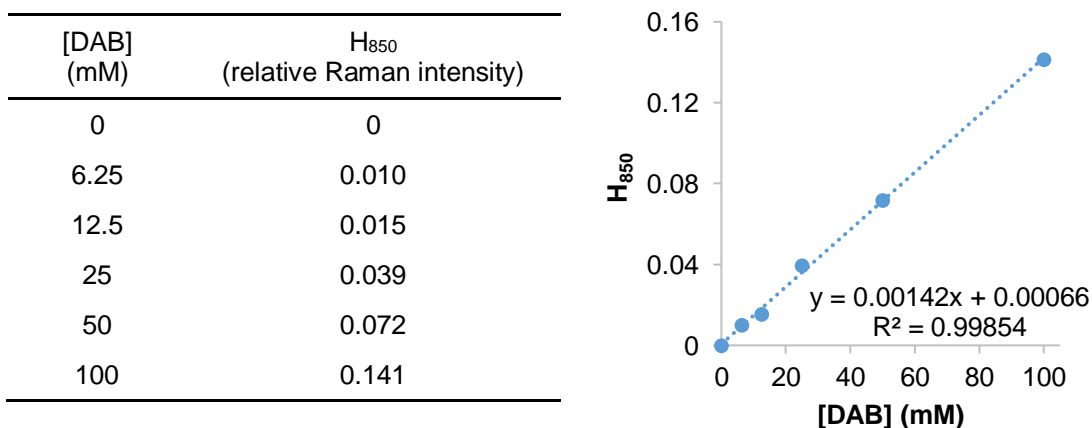


Figure 30. Peak heights at  $850\text{ cm}^{-1}$  for various **DAB** dilutions (left) and calibration curve (right).

A least linear squares fit for the data in Figure 30 yielded the concentration calibration equation shown on the graph, which can be written in terms of the peak height  $H_{850}$  and concentration  $[DAB]$  for each solution, as shown in the equation below.

$$H_{850} = 0.0014 [DAB] + 0.00066 \quad (\text{Equation 1})$$

The equation can be rearranged in terms of **DAB** concentration.

$$[DAB] = \frac{H_{850} - 0.00066}{0.0014} \quad (\text{Equation 2})$$

Using Equation 2, the concentration of **DAB** was estimated for the first reaction between **OPD** and **PBA**, where molecular sieves were added at 48 h of reaction in Table 1. From this data, its ratio with the expected concentration of the product (308 mM) gives percent conversion values. Since the reaction mixture showed turbidity at 56 h, the saturation concentration of **DAB** is estimated to be less than or equal to 190 mM.

Table 1

*Raman data for the reaction of OPD and PBA in chloroform (308 mM)*

Time (h)	$H_{850}$ (rel. Raman intensity)	$[DAB]$ (mM)	Conversion (%)
0 h	0	0	0 %
12 h	0.24	173	56 %
24 h	0.25	179	58 %
36 h	0.27	190	62 %
48 h	0.25	179	58 %
56 h	0.27	190	62 %
68 h	0.29	209	68 %

Similarly, the concentration of **DAB** was estimated for the second reaction, where molecular sieves were included at the onset (Table 2). Since the reaction mixture showed

turbidity at 49 h, the saturation concentration of **DAB** is estimated to be in between 169 to 181 mM. Due to the surface of the molecular sieves, their presence at the onset induced crystallization, causing **DAB** to precipitate sooner than the previous experiment.

Table 2

*Raman data for the reaction of OPD and PBA in chloroform with the inclusion of molecular sieves at the onset (308 mM)*

Time (h)	H <sub>850</sub>	[DAB] (mM)	Conversion (%)
0 h	0.00	0	0%
2 h	0.09	61	20%
4 h	0.13	90	29%
6 h	0.15	106	34%
10 h	0.18	130	42%
24 h	0.23	163	53%
29.5 h	0.24	169	55%
49 h	0.25	181	59%
73.5 h	0.27	190	62%

Despite the change in turbidity of the reaction mixture, **DAB** formation in these conditions is estimated to reach up to 68% conversion. These results are similar with earlier studies of **DAB** in chloroform at 50 °C, where **DAB** reached 70% after 150 h.<sup>27</sup> This means that using the solvent peak at 1215 cm<sup>-1</sup> as internal standard, variation in the laser intensity can be corrected for and change in turbidity of the reaction mixture can be overcome. Also, the isolated yield of pure **DAB** for these reactions, which are 61% and 57%, respectively, are in agreement with the estimates.

It should be noted that the above concentrations ( $>100$  mM) are not in the range of the calibration standards (1-100 mM), and this is only an estimate for the amount of **DAB** formed in the reaction mixture. Therefore, a new set of experiments was performed at a lower concentration within the range of the calibration standards. Equimolar amounts of **OPD** and **PBA** (100 mM) in chloroform were allowed to react at 50 °C and Raman spectra were obtained over time (Figure 31, top left). At the 68 h mark, unlike the previous reactions, a red precipitate was observed, indicating side reactions may have taken place. The reaction vial was then removed from heating. Normalization at the baseline ( $831\text{ cm}^{-1}$ ) near the peak of interest ( $850\text{ cm}^{-1}$ ) and the solvent peak ( $1215\text{ cm}^{-1}$ ) was performed using Microsoft Excel (Figure 31, top right). The changes in Raman intensities at  $850\text{ cm}^{-1}$  were plotted *versus* time (Figure 31, bottom right).

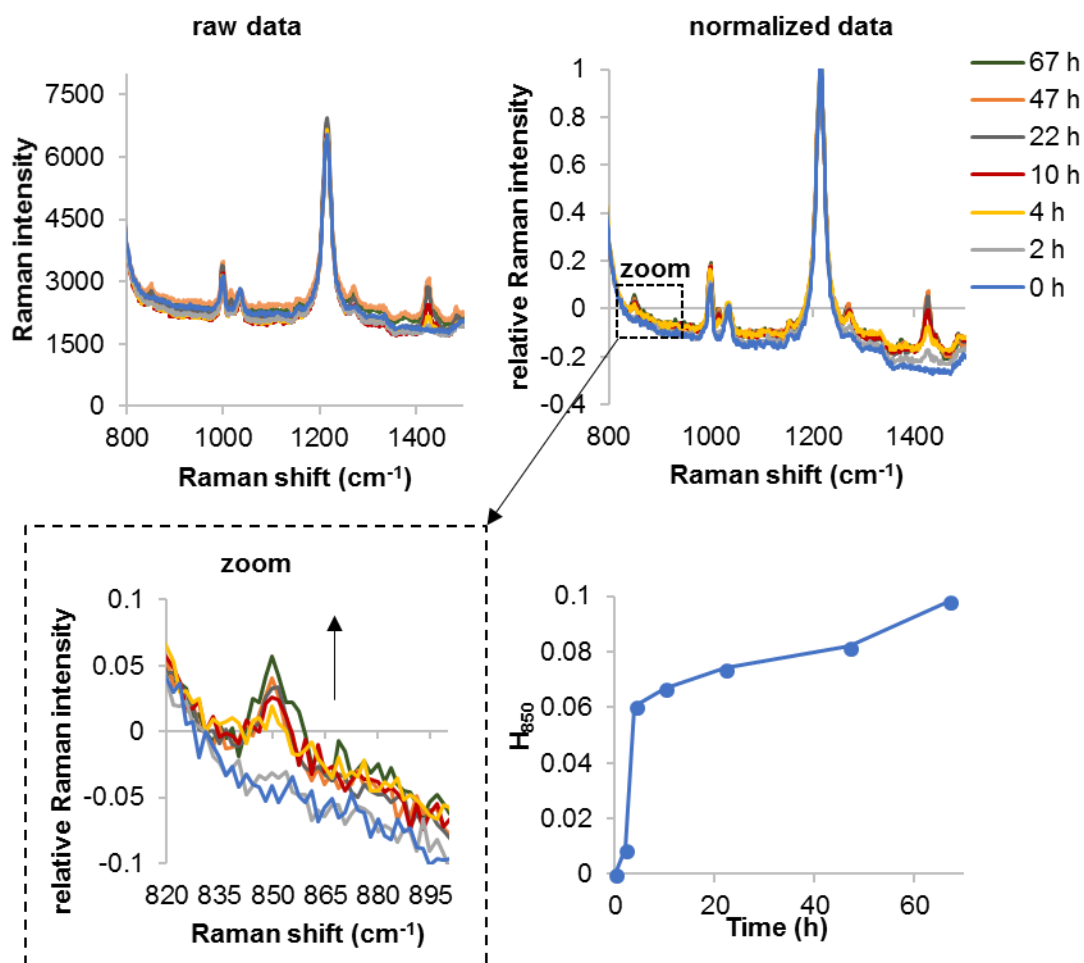


Figure 31. Raman spectra during the formation of **DAB** (100 mM); top left: raw data; top right: normalized; bottom left: zoom; bottom right: peak heights at  $850\text{ cm}^{-1}$  vs. time.

Using Equation 2, the concentration of **DAB** was estimated (Table 3).

Table 3

*Raman data for the reaction of OPD and PBA in chloroform (100 mM)*

Time (h)	$H_{850}$	[DAB] (mM)	Conversion (%)
0 h	0.000	0	0 %
2 h	0.017	11	11 %
4 h	0.054	38	38 %

(continued)

Time (h)	$H_{850}$	[DAB] (mM)	Conversion (%)
10 h	0.074	52	52 %
22 h	0.079	56	56 %
47 h	0.080	57 %	
67 h	0.094	67	67 %

The reaction was repeated with the inclusion of molecular sieves at the onset.

Similar data processing was performed to obtain the data shown in Figure 32.

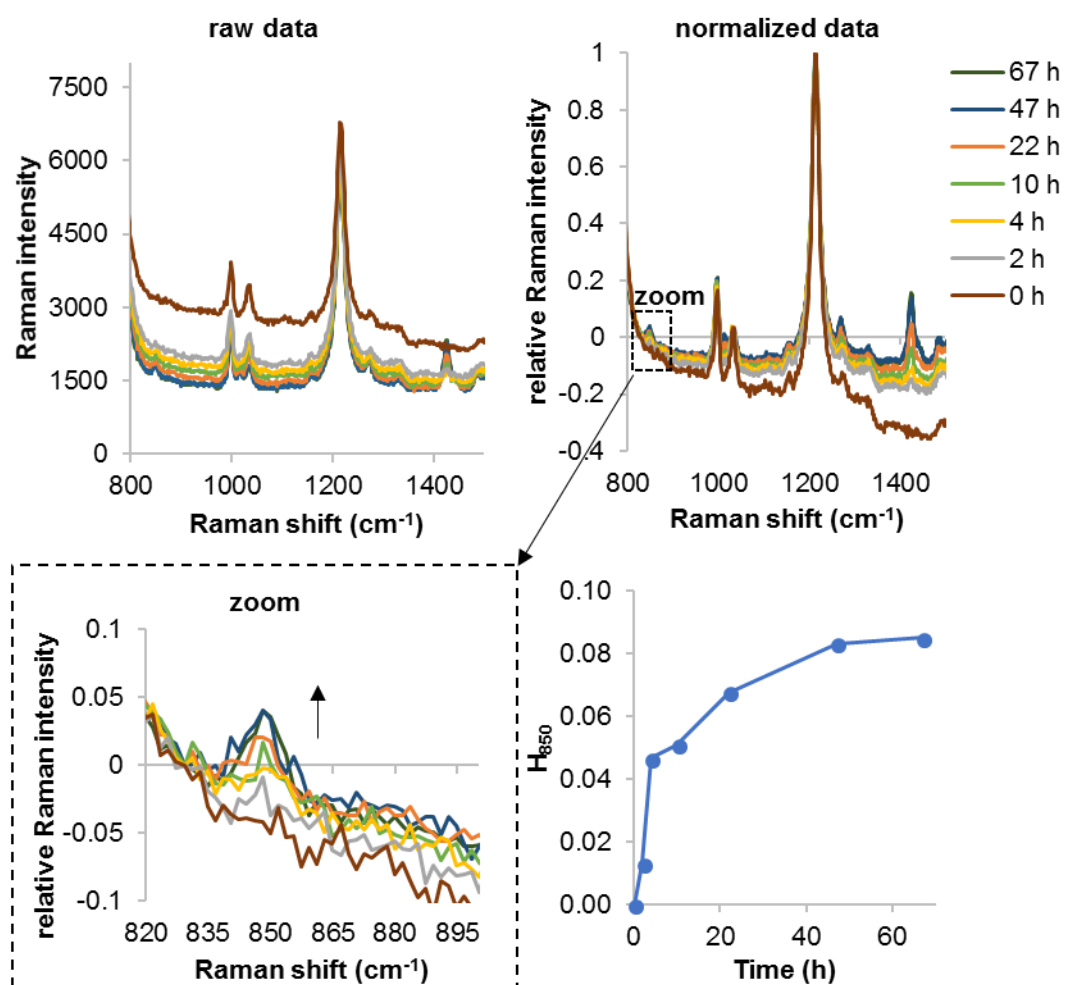


Figure 32. Raman spectra during the formation of **DAB** with molecular sieves (100 mM); top left: raw data; top right: normalized; bottom left: zoom; bottom right: peak heights at 850 cm<sup>-1</sup> vs. time.

Using Equation 2 established from the calibration curve, the concentration of **DAB** was estimated (Table 4).

Table 4

*Raman data for the reaction of **OPD** and **PBA** in chloroform with the inclusion of molecular sieves at the onset (100 mM)*

Time (h)	H <sub>850</sub>	[DAB] (mM)	Conversion (%)
0 h	0.000	0	0%
2 h	0.013	9	9%
4 h	0.047	33	33%
10 h	0.051	36	36%
22 h	0.068	48	48%
47 h	0.083	59	59%
67 h	0.085	60	60%

Similarly, **DAB** formation under these conditions is estimated to reach up to 67% conversion. Overall, these results are in agreement with the results of the reaction monitoring using <sup>1</sup>H NMR. However, the baseline noise in the Raman experiments is almost as large as some of the signals. This will limit not only the accuracy for the estimates of percent conversions, but also the range of concentrations that may be used for reaction monitoring.

The incomplete conversion of **OPD** and **PBA** to **DAB** may be due to limitation on the stability of the product under these conditions. This prediction was examined by heating **DAB** in CDCl<sub>3</sub> at 50 °C and <sup>1</sup>H NMR spectra were obtained for 10 days (Figures 33 and 34). The <sup>1</sup>H NMR spectra reveal that peaks corresponding to **OPD** (H<sub>j,k</sub>) and boroxine (**4**, H<sub>a</sub> and H<sub>c,d</sub>), which is an anhydride form of **PBA**, appear over time. This

indicates that hydrolysis of the **DAB** occurred. Although no water was added to the **DAB** sample, ambient moisture or water present in the deuterated solvent caused the molecule to hydrolyze overtime. By integrating the signals related to **DAB** (7.74 ppm, H<sub>b</sub>) and those of boroxine (8.25 ppm, H<sub>a</sub>), hydrolysis of **DAB** was estimated to be 12%. The result suggests that the potential reversibility of the **DAB** in solution under these conditions precluded the forward reaction from going to completion. Future investigations may involve the addition of water to the **DAB** sample to examine the equilibration point of the reaction.

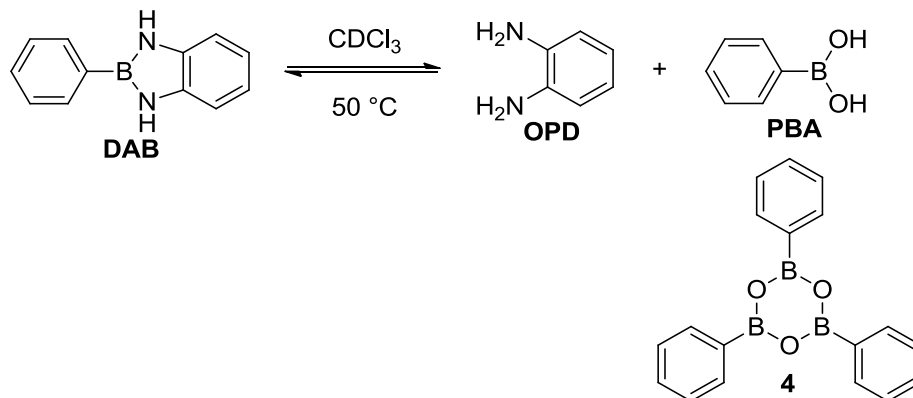


Figure 33. **DAB** was heated in  $\text{CDCl}_3$  at  $50\text{ }^\circ\text{C}$ .

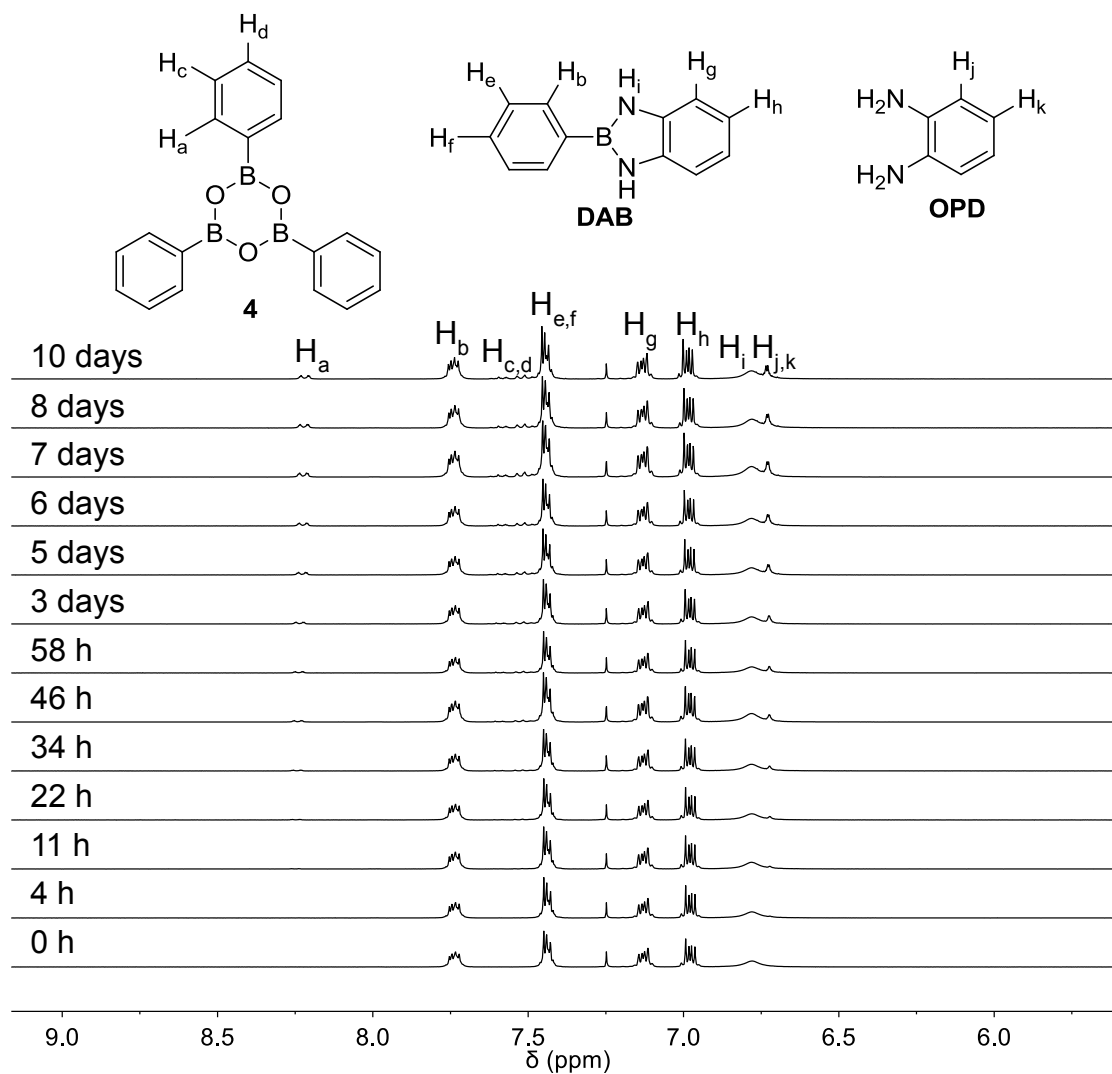


Figure 34. Partial  $^1\text{H}$  NMR spectra of **DAB** in  $\text{CDCl}_3$  at  $50\text{ }^\circ\text{C}$  for 10 days.

## 2.4 Conclusions

In summary, **DAB** formation is influenced by the nature of the solvent and temperature. The starting materials were consumed and products formed faster in DMSO than in toluene because DMSO is more polar, which results in stabilization of charged intermediates. This can help stabilize the charged intermediates and facilitate the proton transfers during the reaction, which results in an increase in rate. However, the percent conversion was lower in DMSO since the water byproduct was less able to leave the

reaction medium under these conditions. As a result, the reactions in DMSO established equilibrium at ~70% conversion. On the other hand, **DAB** formation favored reaction conditions in less polar toluene and at higher temperatures, where complete formation of **DAB** can be achieved within 23 h reaction time at an oil-bath temperature of 120 °C.

By using a calibration curve, product formation was determined from Raman spectral data. The saturation concentration of **DAB** is estimated to be less than or equal to 190 mM in chloroform at 50 °C. The use of molecular sieves had little effect in the overall yield of **DAB**. However, their presence in the reaction medium induces crystallization, thus decreasing the homogeneity of the reaction mixture. Using solvent as an internal standard, variations due to the change in turbidity of the reaction mixture can be overcome. The reactions between **OPD** and **PBA** in chloroform at 50 °C can achieve up to 68% conversion. The potential reversibility of **DAB** due to presence of water in the reaction medium may hinder the complete formation of **DAB**.

## 2.5 Experimental

All starting materials and reagents were purchased from commercial sources (Frontier Scientific, Alfa Aesar, Macron, J.T.Baker, and Cambridge Isotope Laboratories) and used without further purification, unless otherwise mentioned. The NMR solvents, CDCl<sub>3</sub>, toluene-*d*<sub>8</sub> and DMSO-*d*<sub>6</sub>, were stored over activated 3 Å molecular sieves. These sieves were activated by heating at 130 °C under vacuum for 3 hours.

<sup>1</sup>H NMR spectra were collected using JEOL Eclipse 300+ spectrometer. The Raman spectra were collected using a BaySpec Agility 785 nm Raman spectrometer.

**Reactions in different solvents and temperatures.** An equimolar amount of *o*-phenylenediamine (**OPD**, 4.0 mg, 0.037 mmol, 1 equiv) and phenylboronic acid (**PBA**, 4.5

mg, 0.037 mmol, 1 equiv) were mixed in an NMR tube in toluene- $d_8$  (0.8 mL). The reaction tube was submerged in an oil bath at 80 °C.  $^1\text{H}$  NMR spectra were obtained over time. This reaction was repeated (using the same amounts) in the same solvent at oil-bath temperatures of 100 and 120 °C, and in DMSO- $d_6$  at oil-bath temperatures of 80, 100, and 120 °C.

**Synthesis of 2-phenyl-1,3,2-benzodiazaborole (DAB, 3).** A mixture of **OPD** (0.68 g, 6.2 mmol, 1 equiv) and **PBA** (0.75 g, 6.2 mmol, 1 equiv) were dissolved in toluene (50 mL) and refluxed using a Dean-Stark trap for 20 h. Then, the solution was concentrated and cooled to room temperature. The resulting crystals were isolated by vacuum filtration and washed with cold toluene (10 mL) and cold hexane (5 mL) to give a white solid (0.94 g, 78%).  $^1\text{H}$  NMR (301 MHz,  $\text{CDCl}_3$ )  $\delta$  7.75-7.72 (m, 2H), 7.46-7.41 (m, 3H), 7.16-1.10 (m, 2H), 7.00-6.95 (m, 2H), 6.78 (br. s, 2H).

**Pure solutions in chloroform.** Each of the pure solutions of **OPD**, **PBA**, and **DAB** was freshly prepared in a glass vial. **OPD** (0.5 M) was prepared by dissolving **OPD** (540.5 mg, 0.005 mol) in chloroform (10 mL) in a glass vial (20 mL). **PBA** (0.5 M) was prepared by dissolving **PBA** (121.9 mg, 0.001 mol) in chloroform (2 mL) in a glass vial (20 mL). A saturated solution of **DAB** (~0.5 M) was prepared by mixing **DAB** (194.0 mg, 0.001 mol) in chloroform (2 mL) in a glass vial (20 mL). Raman spectra were obtained and exported to Microsoft Excel for processing.

**Reaction in chloroform at 50 °C (308 mM).** **PBA** (333.4 mg, 3.083 mmol, 1 equiv) and **OPD** (375.9 mg, 3.083 mmol, 1 equiv) were dissolved in chloroform (10 mL) in a 20 mL glass vial. The reaction mixture was stirred at 50 °C. The reaction progress was monitored using the Raman spectrometer. After 48 h of reaction, molecular sieves (3

Å, ~800 mg) were added. At 68 h of reaction, the glass vial was removed from heating. The white precipitate that formed was filtered and washed with a small amount of chloroform. This product was collected as crop 1 and identified as **DAB** (362.6 mg, 61% yield) using  $^1\text{H}$  NMR in  $\text{CDCl}_3$  (Figure 35). Any crystals formed on the edge of the filter paper that were visibly different in color were collected as crop 2 (46.7 mg). All washings and filtrate were combined and solvent was removed to obtain crop 3 (202.3 mg).  $^1\text{H}$  NMR analyses of crops 2 and 3 were obtained in  $\text{CDCl}_3$ . The results revealed that these two crops contained mostly **DAB**, with a small amount of boroxine (**4**) and starting material **OPD**.

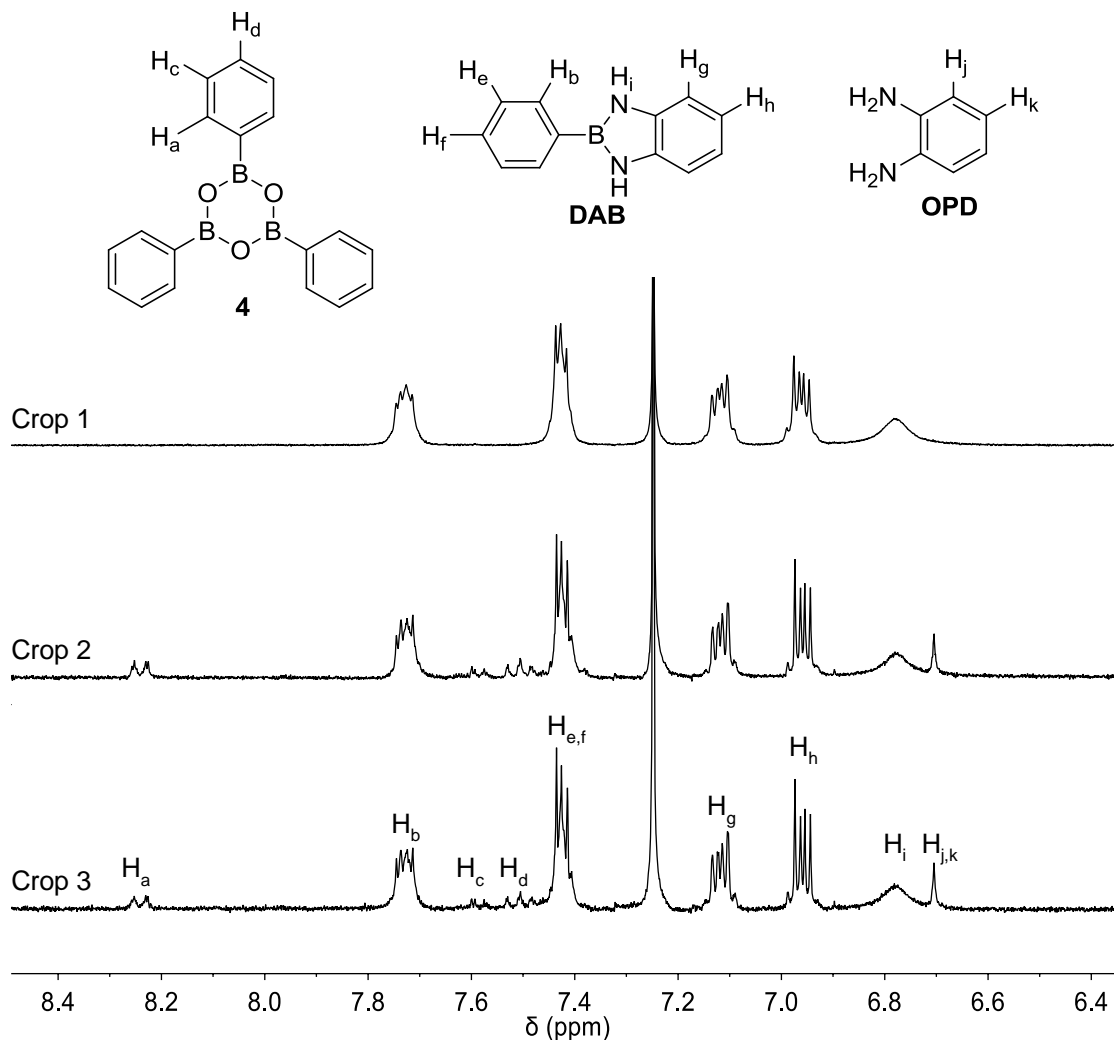


Figure 35. Partial  $^1\text{H}$  NMR spectra of the isolated products from the reaction of **OPD** and **PBA** (308 mM) in chloroform at 50 °C.

**Reaction in chloroform at 50 °C with molecular sieves at the onset (308 mM).**

**PBA** (333.4 mg, 3.083 mmol, 1 equiv) and **OPD** (375.9 mg, 3.083 mmol, 1 equiv) were dissolved in chloroform (10 mL) in a 20 mL glass vial. Molecular sieves (3 Å: 754.7 mg) were added to the reaction mixture, which was stirred at 50 °C. The reaction progress was monitored over time using the Raman spectrometer. At 73.5 h of reaction, the glass vial was removed from heating. After the removal of the molecular sieves, the white precipitate that formed was filtered and washed with a small amount of chloroform. This product was

collected as crop 1 and identified as **DAB** (340.3 mg, 57 % yield) by  $^1\text{H}$  NMR analysis in  $\text{CDCl}_3$ . All washings and filtrate were combined and solvent was removed to obtain crop 2 (109.5 mg).  $^1\text{H}$  NMR analysis of crop 2 in  $\text{CDCl}_3$  revealed the presence of **DAB** and a small amount of boroxine (**4**) and **OPD**.

**Serial dilutions for DAB concentration calibration curve.** Chloroform was heated to 50 °C for 1 h before use. A 100 mM **DAB** stock solution was prepared by completely dissolving **DAB** (194.0 mg, 1.0 mmol) to the mark with 50 °C chloroform in a volumetric flask (10 mL). From this stock solution, **DAB** calibration standards ranging from 6.25 to 50 mM were prepared by serial dilution. Each standard solution (5 mL) was transferred into glass vials (20 mL). The collection of Raman spectra began immediately after completing the preparation of the calibration solutions. Linear least squares regression was used to fit a line to the data in Microsoft Excel.

**Reaction in chloroform at 50 °C (100mM).** **PBA** (122.0 mg, 1.000 mmol, 1 equiv) and **OPD** (108.3 mg, 1.000 mmol, 1 equiv) were dissolved in chloroform (10 mL) in a 20 mL glass vial. The reaction mixture was stirred at 50 °C. The reaction progress was monitored periodically using the Raman spectrometer. At 67 h of reaction, a red precipitate was observed. The glass vial was removed from heating. The red precipitate was filtered and isolated as crop 1. Chloroform was evaporated from the filtrate under vacuum until the volume was reduced by half. The crystals which formed were filtered and washed with chloroform (2 mL). This product was collected as crop 2 and identified as **DAB** (125.0 mg, 64% yield) using  $^1\text{H}$  NMR analysis in  $\text{CDCl}_3$ .

All washings and filtrate were combined with crop 1. Chloroform was removed under vacuum to give a dark brown solid mixture (23.0 mg), which was identified as a combination of **DAB**, boroxine (**4**), and unreacted **OPD** using  $^1\text{H}$  NMR analysis in  $\text{CDCl}_3$ .

**Reaction in chloroform at 50 °C with molecular sieves (100mM).** **PBA** (122.0 mg, 1.000 mmol, 1 equiv) and **OPD** (108.3 mg, 1.000 mmol, 1 equiv) were dissolved in chloroform (10 mL) in a glass vial (20 mL). Molecular sieves (3 Å: 195.6 mg) were added to the reaction mixture, which was stirred at 50 °C. The reaction progress was monitored using Raman spectrometer. At 67 h of reaction, a red precipitate was observed. The glass vial was removed from heating. After the removal of the molecular sieves, the red precipitate was isolated as crop 1. Chloroform was evaporated from the filtrate under vacuum until the volume was reduced by half. The crystals which formed were filtered and washed with chloroform (2 mL). This product was collected as crop 2 and identified as **DAB** (107.4 mg, 55% yield) using  $^1\text{H}$  NMR ( $\text{CDCl}_3$ ).

All washings and filtrate were combined with crop 1. Chloroform was removed under vacuum to give a dark brown solid mixture (42.5 mg), which was identified as a combination of **DAB**, boroxine (**4**), and unreacted **OPD** using  $^1\text{H}$  NMR analysis in  $\text{CDCl}_3$ .

## CHAPTER III

### Synthesis and Reactions of an Ethylhexyl-Ester Substituted Tetraamine Monomer

#### 3.1 Introduction

The use of diazaboroles in oligomeric systems such as macrocycles and covalent organic frameworks is being investigated by our research group. Herein, we introduce a 2-ethylhexyl side chain to increase the solubility of the tetraamine (**TA**) monomer in common organic solvents such as chloroform, tetrahydrofuran, and ethyl acetate, as discussed in chapter 1. It was predicted that the 2-ethylhexyl groups may increase the stacking distance between the target macrocycles due to steric hindrance allowing for greater solubility.

The solubility of the co-monomer **BDBA** is also another limiting factor due to the formation of polymeric boroxine structure. Instead, using ester precursor may overcome this solubility problem.

#### 3.2 Objectives

The work described in this chapter is aimed at the development of a diazaborole-based macrocyclic system with improved solubility by incorporating 2-ethylhexyl groups. The following retrosynthetic analysis shows the undoing of an ethylhexyl ester substituted tetraamine monomer (**TA-DEH**) to a commercially available derivative of benzoic acid **5** (Figure 36). The synthetic details will be discussed in the results and discussion section.

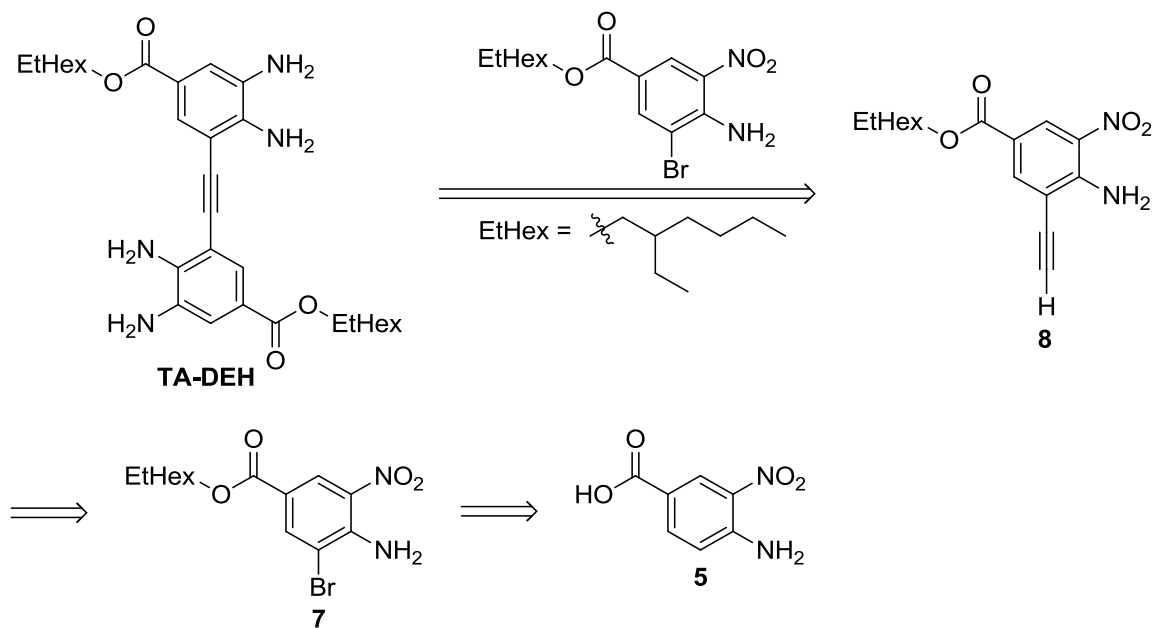


Figure 36. Retrosynthetic analysis of **TA-DEH**.

Additionally, the poor solubility of benzene-1,4-diboronic acid (**BDBA**) is a limiting factor in the formation of complex macrocyclic systems. To overcome this issue, the ability of monomer **TA-DEH** to participate in the dynamic exchange with functionalized **BDBA**-based esters to form macrocyclic diazaboroles was explored.

### 3.3 Results and discussion

The synthesis of an ethylhexyl ester substituted tetraamine monomer (**TA-DEH**) started with 4-amino-3-nitrobenzoic acid (**5**) (Figure 37). Fischer esterification gave 2-ethylhexyl 4-amino-3-nitrobenzoate (**6**) as a dark yellow solid in 83% yield. Subsequent bromination in dichloromethane (DCM) resulted in 2-ethylhexyl 4-amino-3-bromo-5-nitrobenzoate (**7**) as a yellow solid in 80% yield.

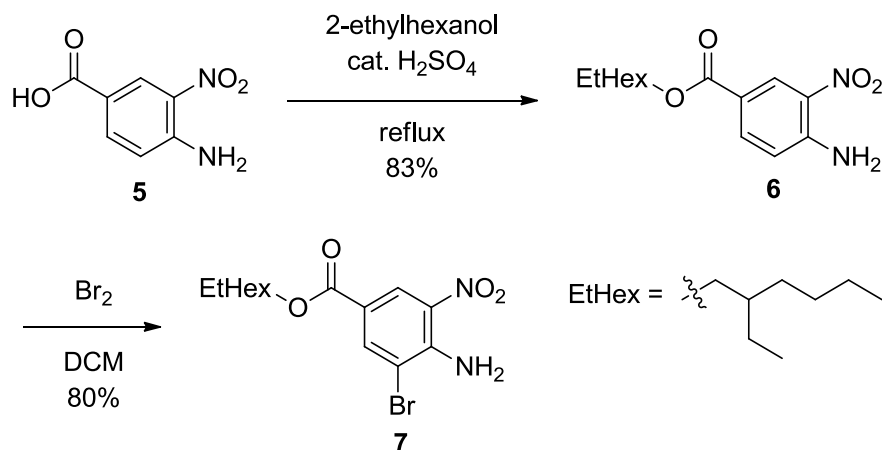


Figure 37. Synthesis of 2-ethylhexyl 4-amino-3-bromo-5-nitrobenzoate (**7**).

Next, bromide **7** was subjected to Sonogashira coupling conditions with trimethylsilylacetylene (TMSA, Figure 38). Initially, the reaction was carried out using bis(triphenylphosphine)palladium(II) dichloride (Pd(PPh<sub>3</sub>)<sub>2</sub>Cl<sub>2</sub>) and copper iodide (CuI) as the catalyst system. 2-Ethylhexyl 4-amino-3-((trimethylsilyl)ethynyl)-5-nitrobenzoate (**8**) was isolated in 37% yield. The low yield of the reaction was likely due to the premature decomposition of the palladium catalyst. Therefore, additional triphenylphosphine (PPh<sub>3</sub>) ligand was included in the reaction to help stabilize the palladium. This resulted in an increased yield of 82%. The formation of the product was verified using <sup>1</sup>H NMR analysis.

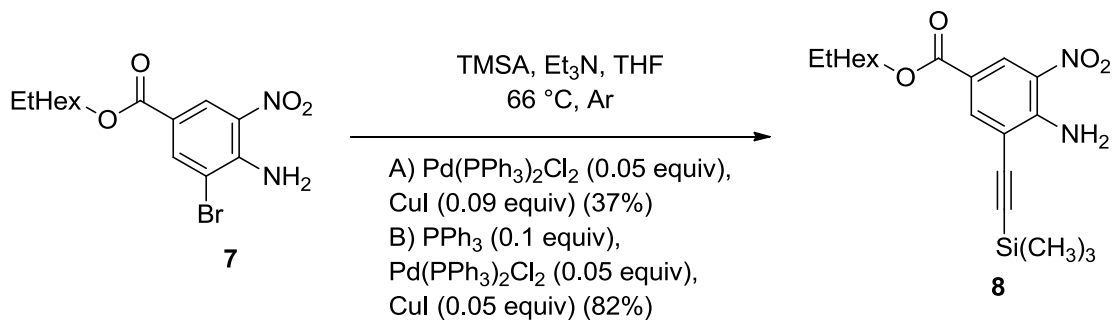


Figure 38. Synthesis of 2-ethylhexyl 4-amino-3-((trimethylsilyl)ethynyl)-5-nitrobenzoate (**8**).

Subsequent deprotection of the trimethylsilyl group gave 2-ethylhexyl 4-amino-3-ethynyl-5-nitrobenzoate (**9**) as a brown oil in 68% yield (Figure 39). Alkyne **9** was then coupled with the previously synthesized bromoarene **7** under Sonogashira coupling reaction conditions. 3,3'-(Ethyne-1,2-diyl)bis(2-ethylhexyl 5-nitro-4-aminobenzoate) (**10**) was isolated as a yellow solid in 67% yield. Finally, tin based reduction of the nitro group resulted in the formation of the tetraamine monomer **TA-DEH** having ethylhexyl ester side chains in 71% yield.  $^1\text{H}$  NMR analysis supported the formation and purity of the expected product (Figure 40).

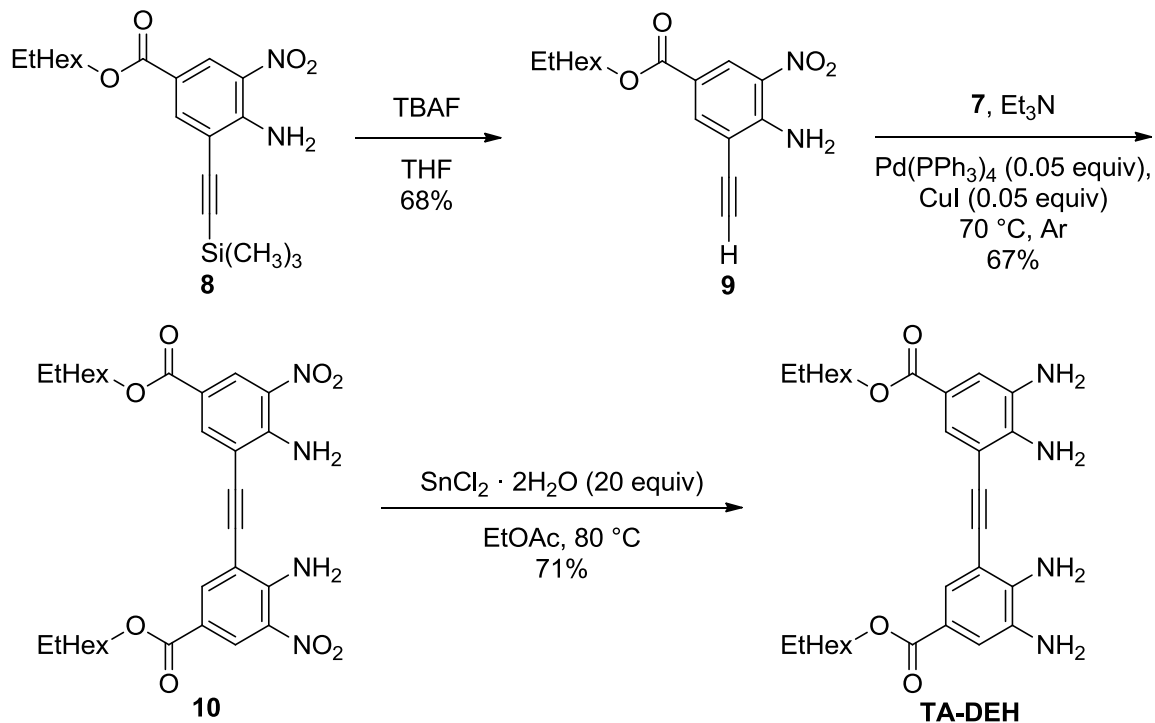


Figure 39. Synthetic route to **TA-DEH** from **8**.

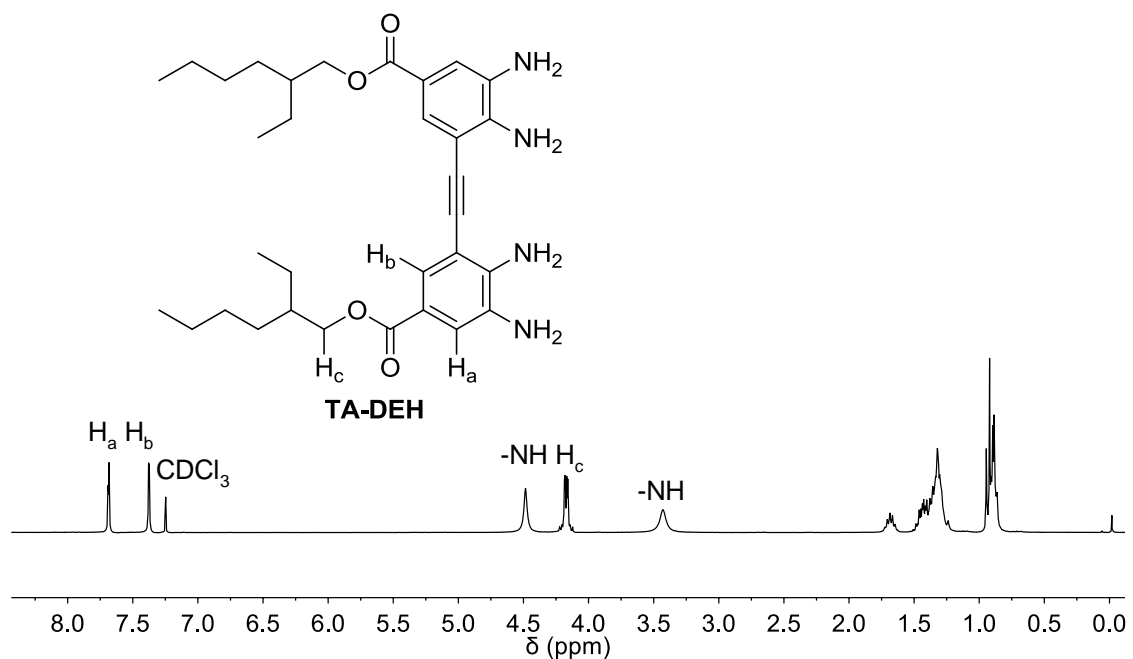


Figure 40.  $^1\text{H}$  NMR spectrum of **TA-DEH**.

Improved solubility of **TA-DEH**, as well as intermediates **8**, **9** and **10** in common organic solvents such as ethyl acetate, chloroform, and tetrahydrofuran, was observed throughout the multi-step synthesis toward **TA-DEH**. To probe to solubility further, a qualitative solubility study with chloroform was performed with the **TA-DEH**, **TA-DM**<sup>27</sup> and **TA-DTg**<sup>28</sup> (Figure 41).

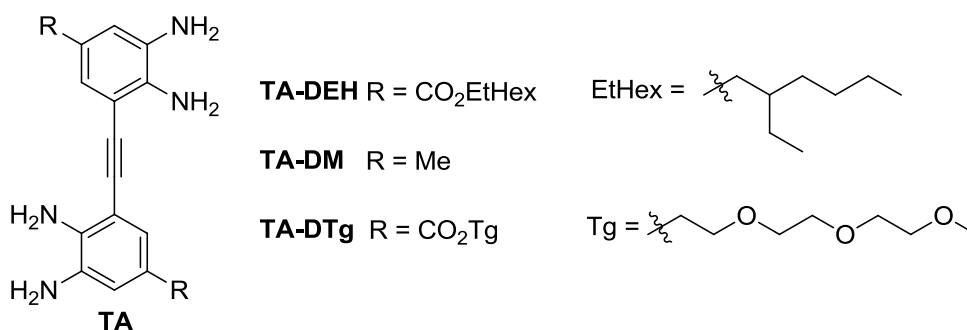


Figure 41. Monomers with various pendent groups (**TA-DEH**, **TA-DM** and **TA-DTg**).

Equal moles of each material were dissolved in chloroform (see Experimental Methods) and the results were recorded in Table 5. The estimated solubilities of the

monomers were calculated as their saturated concentration in chloroform in terms of molality.

Table 5.

*Solubilities of tetraamine monomers in chloroform*

Monomer	Mols of the monomer (mol)	Amount of CHCl <sub>3</sub> used (kg)	Estimated saturated concentration (molality, mol/kg)
<b>TA-DEH</b>	$4.2 \times 10^{-6}$	$4.8 \times 10^{-5}$	$8.8 \times 10^{-2}$
<b>TA-DM</b>	$4.1 \times 10^{-6}$	$5.0 \times 10^{-4}$	$8.2 \times 10^{-3}$
<b>TA-DTg</b>	$4.2 \times 10^{-6}$	$1.3 \times 10^{-3}$	$3.2 \times 10^{-3}$

We expected the **TA-DTg** monomer to be more soluble in chloroform compared to **TA-DM** monomer because of the solubilizing Tg ester sidechains. However, the estimated solubility of **TA-DTg** was lower than that of **TA-DM**. **TA-DEH** was more soluble than **TA-DM** and **TA-DTg** by greater than a factor of 10 in terms of molality. This can be attributed to the presence of branched 2-ethylhexyl ester side chains instead of methyl or Tg ester groups in the monomer.

With the more soluble tetraamine monomer (**TA-DEH**) in hand, the reaction with benzene-1,4-diboronic acid (**BDBA**) to form the ethylhexyl ester substituted diazaborole-based macrocycle (**DBM-TEH**) was performed under reflux conditions using a Dean-Stark apparatus (Figure 42). The starting materials were initially dissolved in ethanol to improve solubility of the **BDBA**.<sup>37</sup>

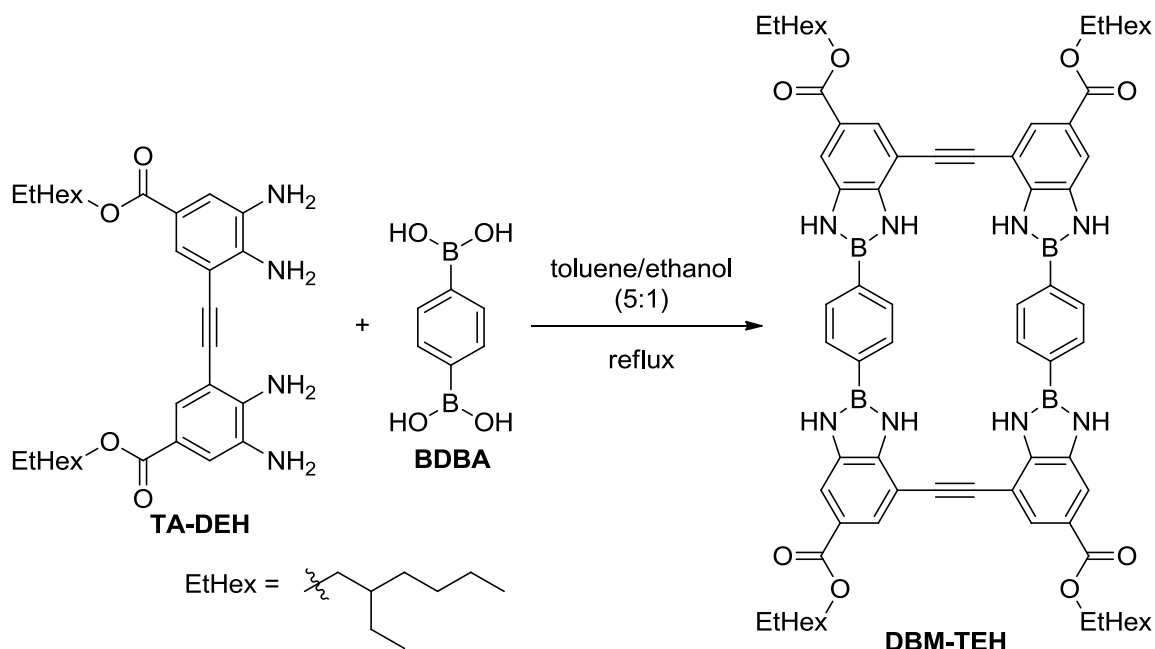


Figure 42. Synthesis of **DBM-TEH** from **TA-DEH**.

After 5 days of refluxing, the reaction mixture was concentrated and cooled to room temperature to induce precipitation. Upon filtering, a light color solid was obtained.  $^1\text{H}$  NMR analysis was initially attempted in chloroform. However, unlike the tetraamine monomer starting material, the solid was not soluble. We suspect this is due to the formation of oligomers. This also indicates that the addition of the ethylhexyl groups was not enough to overcome solubility issues.  $^1\text{H}$  NMR analysis was again attempted in  $\text{DMSO-}d_6$ . After 2 h of sonication and heating to  $100\text{ }^\circ\text{C}$ , evidence for formation of the macrocycle was observed by  $^1\text{H}$  NMR (Figure 43).

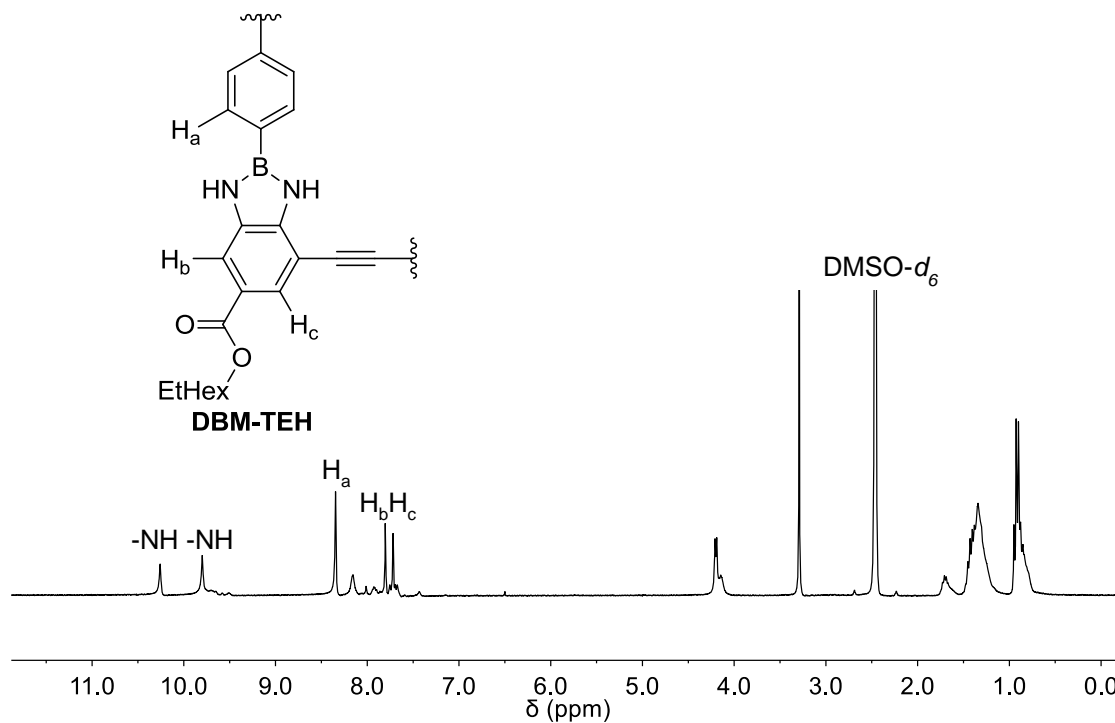


Figure 43.  $^1\text{H}$  NMR spectrum of the product mixture from Figure 42.

The  $^1\text{H}$  signals at 10.26 and 9.80 ppm are attributed to the NH protons. The aromatic protons of the phenylene groups appear at 8.35, 7.80, and 7.72 ppm ( $\text{H}_a$ ,  $\text{H}_b$ , and  $\text{H}_c$ , respectively). The  $\text{CH}_2$  directly linked to the oxygen of the ethylhexyl ester side chains are assigned to the signal at 4.21 ppm. All other CH,  $\text{CH}_2$  and  $\text{CH}_3$  protons of the ethylhexyl sidechains show signals in the range 1.71-0.88 ppm. The shoulder off of the signal for NH at 9.80 ppm as well as overlapping signals in the aromatic region 8.22-7.42 ppm suggest the presence of oligomeric intermediates. Despite the contamination of potential oligomers, it is clear that macrocycle formation occurred. Furthermore, MALDI mass spectra analysis of the reaction mixture reveals the presence of the macrocycle due to the signal at  $m/z = 1288.752$   $[\text{M}]^+$ , which is in agreement with the calculated value of 1288.84.

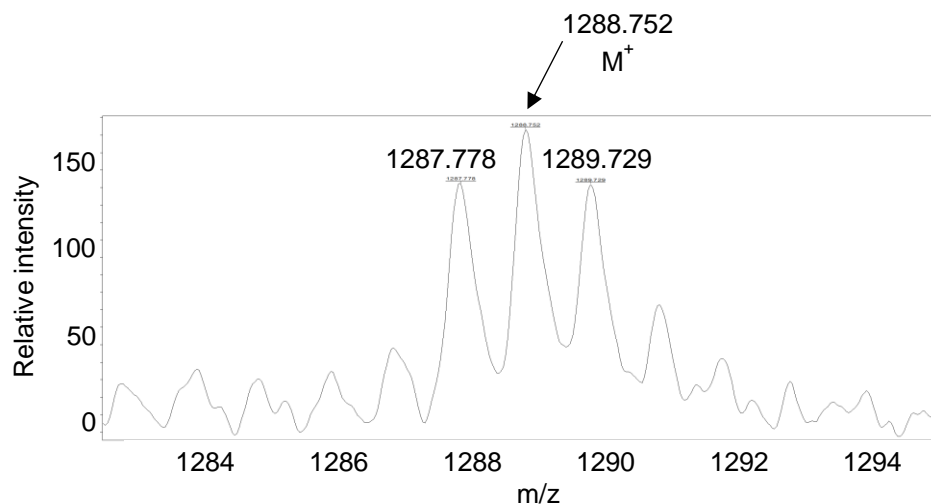


Figure 44. MALDI mass spectrum of the reaction mixture from Figure 42.

The same reaction was carried out in DMSO-*d*<sub>6</sub> at 100 °C in an NMR tube (Figure 45). This experiment allowed for the direct examination of the reaction progress using <sup>1</sup>H NMR (Figure 46) and to observe the potential oligomeric intermediates.

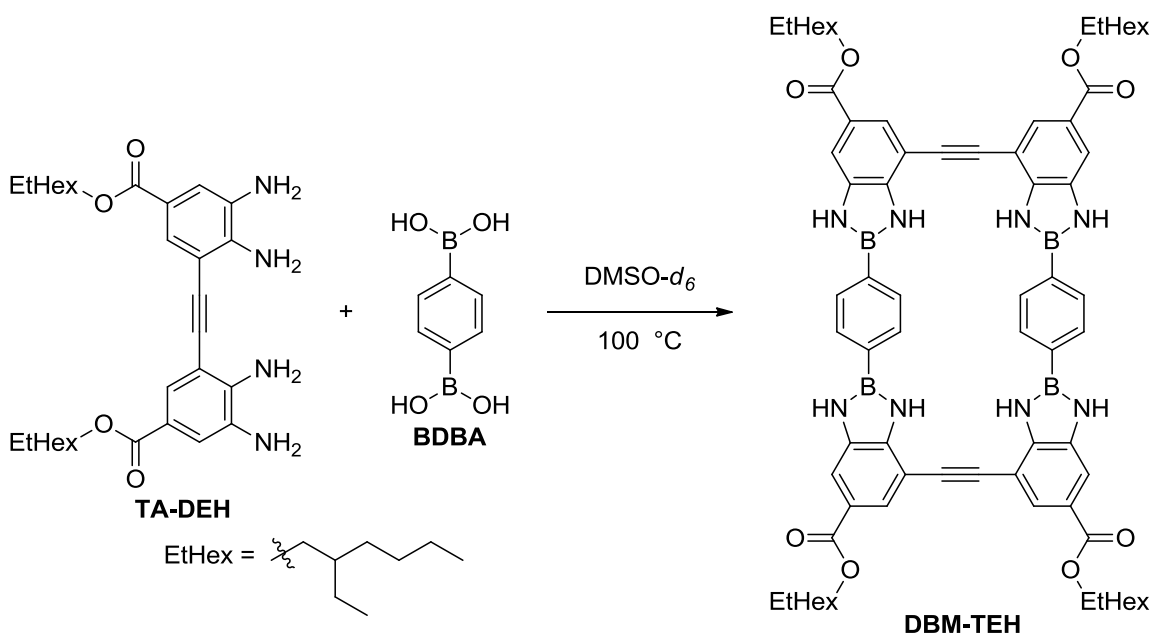


Figure 45. Reaction of **TA-DEH** and **BDBA** in DMSO-*d*<sub>6</sub>.

Figure 46 shows the consumption of the starting materials in the <sup>1</sup>H NMR spectra over time. After 11 h, evidence for formation of diazaborole was observed due to the broad

singlets at  $\delta$  10.26 and 9.80 ppm, which correspond to the protons of the NH groups. Oligomeric intermediates were also observed with many overlapping signals in the aromatic region. For this reason, it was difficult to identify oligomeric intermediates only by analyzing the  $^1\text{H}$  NMR. However, distinct peaks started to become more prevalent with time. This is evidence that oligomeric products experienced self-assembly to form the more symmetric and thermodynamically stable macrocycle. At 121 h, the reaction did not progress further. The signals related to the macrocycle actually decreased at 412 h of reaction, which was likely due to hydrolysis due to the increasing presence of water in the reaction medium. In addition, the proton signals from this experiment correlate to the proton signals in the earlier experiment performed in toluene under reflux conditions (Figure 43). This further confirms the formation of **DBM-TEH** in DMSO.

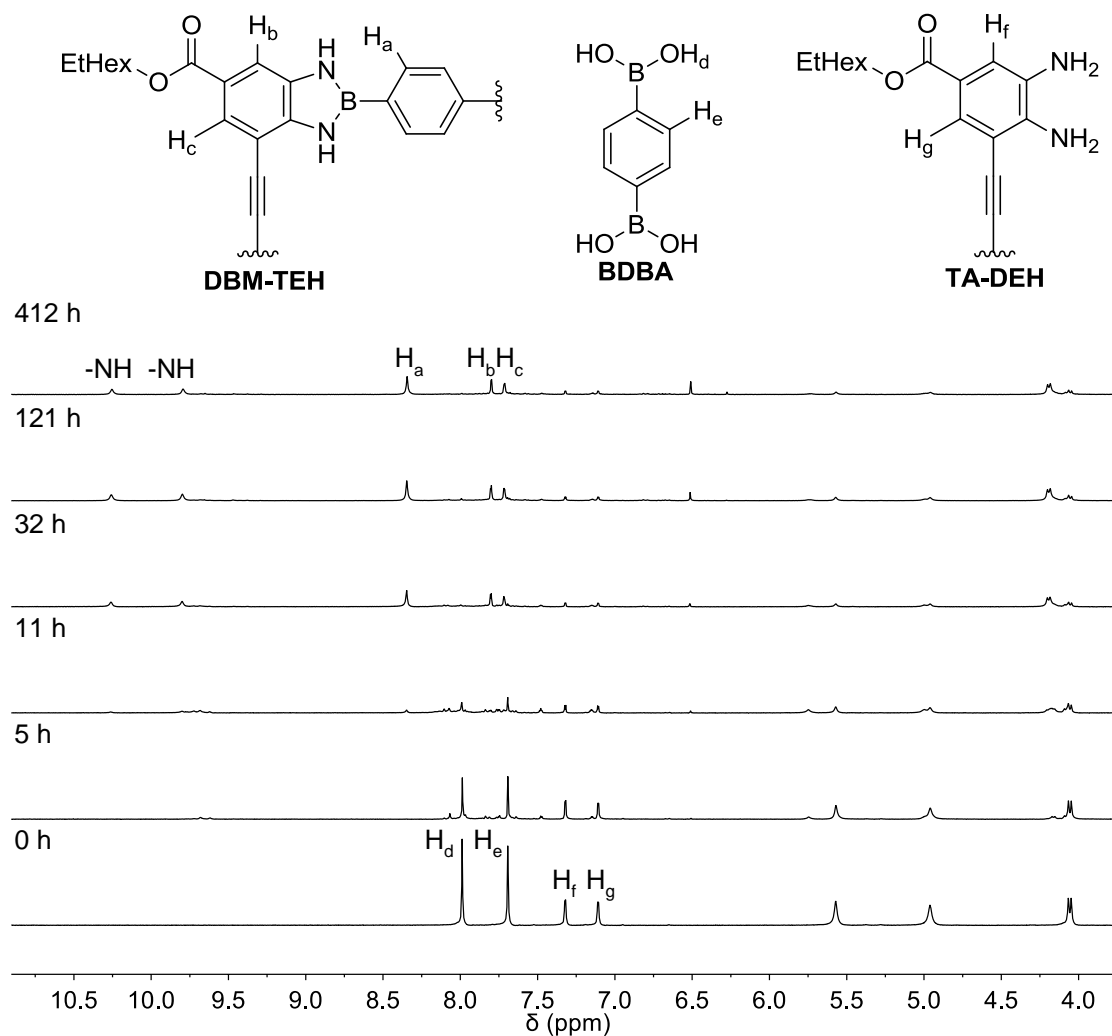


Figure 46.  $^1\text{H}$  NMR spectra of the reaction progress of **TA-DEH** and **BDBA** in  $\text{DMSO-d}_6$ .

The formation of the macrocycle product is limited in part by the poor solubility of benzene-1,4-diboronic acid (**BDBA**). To overcome this, we pursued more soluble **BDBA**-based esters, which can easily be obtained from the esterification of **BDBA** and commercial inexpensive diols, such as catechol, *tert*-butyl catechol, and diethyl tartrate.

The dynamic exchange of simple catechol ester (**7**) and *o*-phenylenediamine (**OPD**) was previously examined in our group.<sup>38</sup> In this study, the reagents were mixed at room

temperature in chloroform, and the reaction progress was monitored using  $^1\text{H}$  NMR spectroscopy.

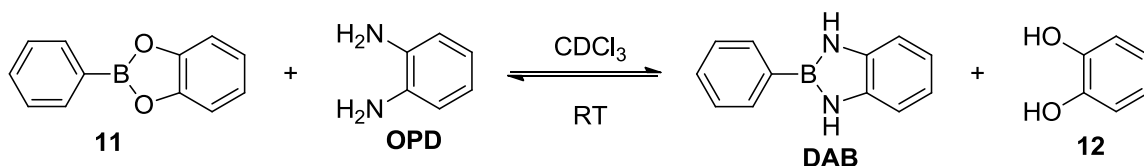


Figure 47. Reaction of benzodioxaborole **11** and OPD.

Under these conditions, the reaction was very slow and only 10% of the reactants had converted to **DAB** and catechol **12**. For our purpose, macrocyclization might overcome the 10% conversion due to intra vs. intermolecular reactions. At room temperature, the **TA-DEH** monomer may participate in dynamic covalent exchange with 2,2'-(1,4-phenylene)bis(1,3,2-benzodioxaborole) (**13**), instead of **BDBA** (Figure 48).

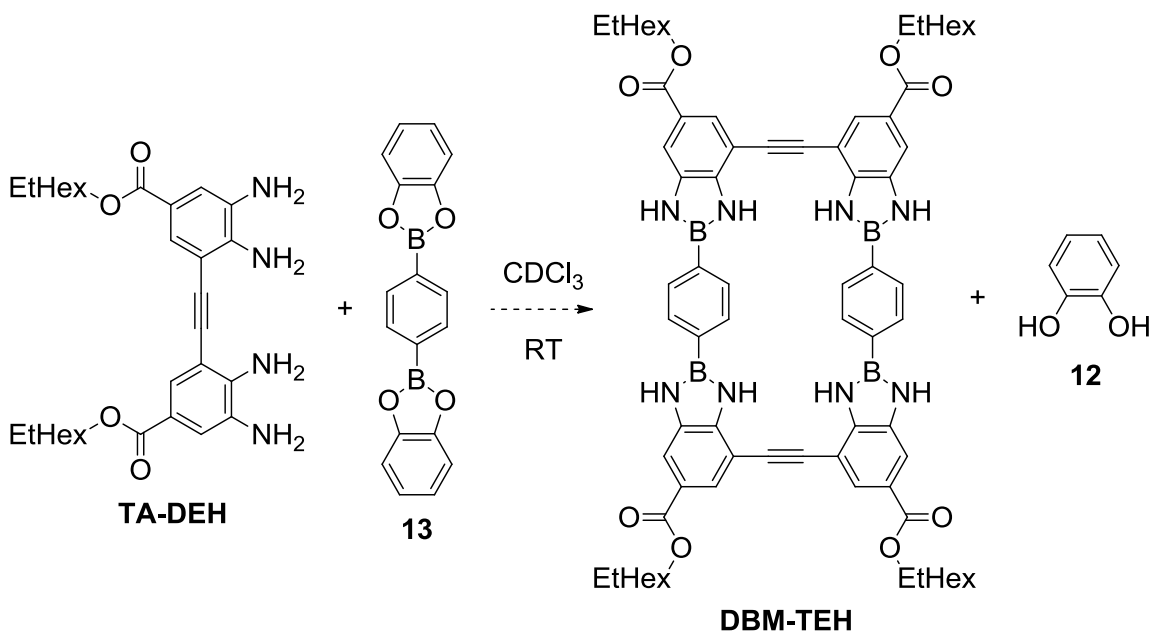


Figure 48. The exchange reaction of monomer **TA-DEH** and **BDBA**-based ester **13**.

First, the synthesis of 2,2'-(1,4-phenylene)bis(1,3,2-benzodioxaborole) (**13**) was accomplished by following a reported procedure.<sup>37</sup> **BDBA** and catechol **12** were mixed in

toluene under reflux conditions for 90 min using a Dean-Stark apparatus. Methanol was added to increase the solubility of **BDBA**, and 3 Å molecular sieves were added to help with the removal of water (Figure 49). After 90 min, a white precipitate formed in the reaction mixture. The resulting solid was isolated by vacuum filtration and did not require further purification. However, it was sparingly soluble in  $\text{CDCl}_3$ . Even though  $^1\text{H}$  NMR analysis revealed no trace of contaminants, the analysis was repeated at higher concentration in  $\text{DMSO-}d_6$  to verify the purity of the expected product.

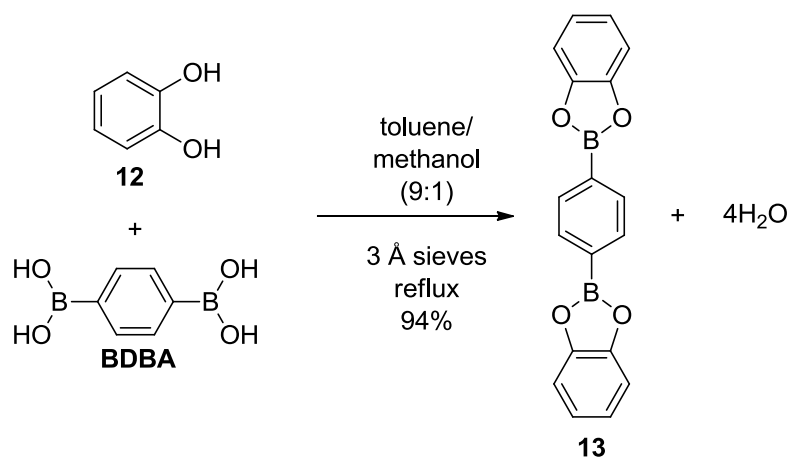


Figure 49. Synthesis of 2,2'-(1,4-phenylene)bis(1,3,2-benzodioxaborole) (**13**).

To increase solubility, *t*-butyl catechol **14** and **BDBA** were reacted and isolated under similar conditions to give a *t*-butyl substituted ester of **BDBA** (**15**).  $^1\text{H}$  NMR analysis of the resulting white solid in  $\text{CDCl}_3$  supported the formation of the product.

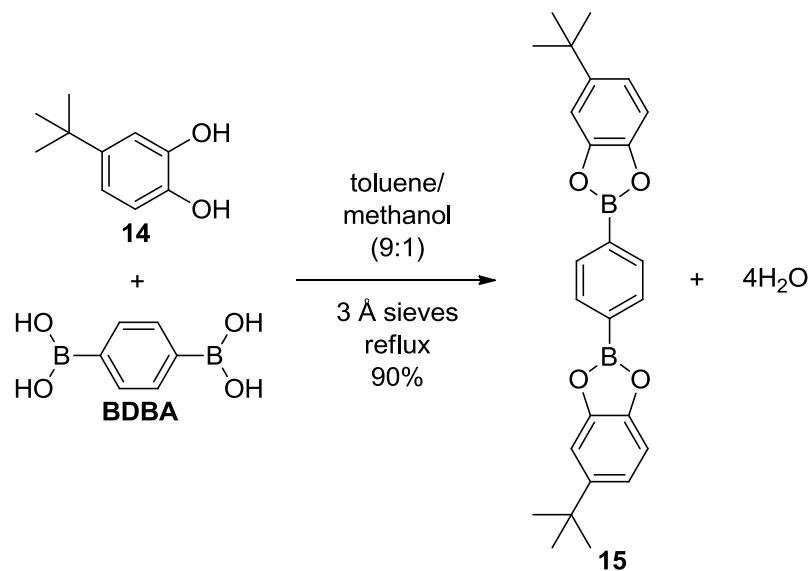


Figure 50. Synthesis of a *t*-butyl substituted ester of **BDBA** (**15**).

With the more soluble **BDBA**-based ester **15** in hand, the exchange reaction with simple *o*-phenylenediamine (**OPD**) was first investigated (Figure 51). The reaction was monitored for 9 days in CDCl<sub>3</sub> at room temperature using <sup>1</sup>H NMR. Since the potential product, bis(diazaborole) **16**, is not readily soluble in chloroform, it should precipitate from the solution and help shift the equilibrium towards the products.

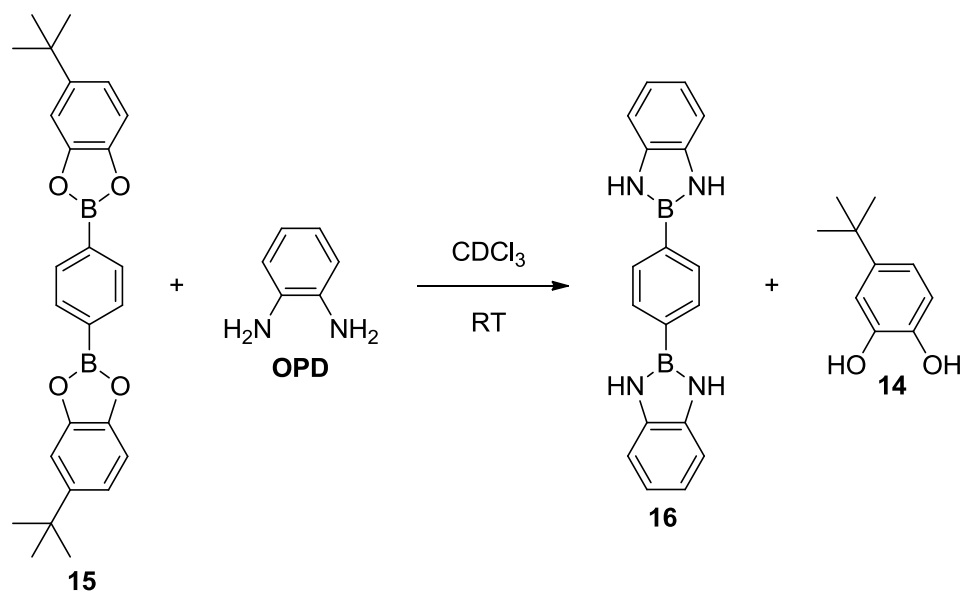


Figure 51. Reaction of **BDBA**-based ester **15** and **OPD**.

Analysis by <sup>1</sup>H NMR spectroscopy revealed a decrease of the aromatic signals of the starting materials (H<sub>a-f</sub>, Figure 52). There was no evidence of the target bis(diazaborole) **16** even after 9 days, neither by visible observation of any precipitation nor by analyzing the <sup>1</sup>H NMR spectra. The appearance of the signals at δ = 8.06 (H<sub>g</sub>) and 7.78 (H<sub>h</sub>) ppm may result from the monosubstituted diazaborole **17** (Figure 53). This intermediate is a less symmetrical molecule than the reactant **15** and therefore there are two doublets associated with the phenylene protons (H<sub>g</sub> and H<sub>h</sub>). By integrating these <sup>1</sup>H NMR signals and those of **15** (8.17 ppm, H<sub>a</sub>), we estimate 22% conversion of **15** to **17** or 11% overall conversion of dioxaborole to diazaborole.

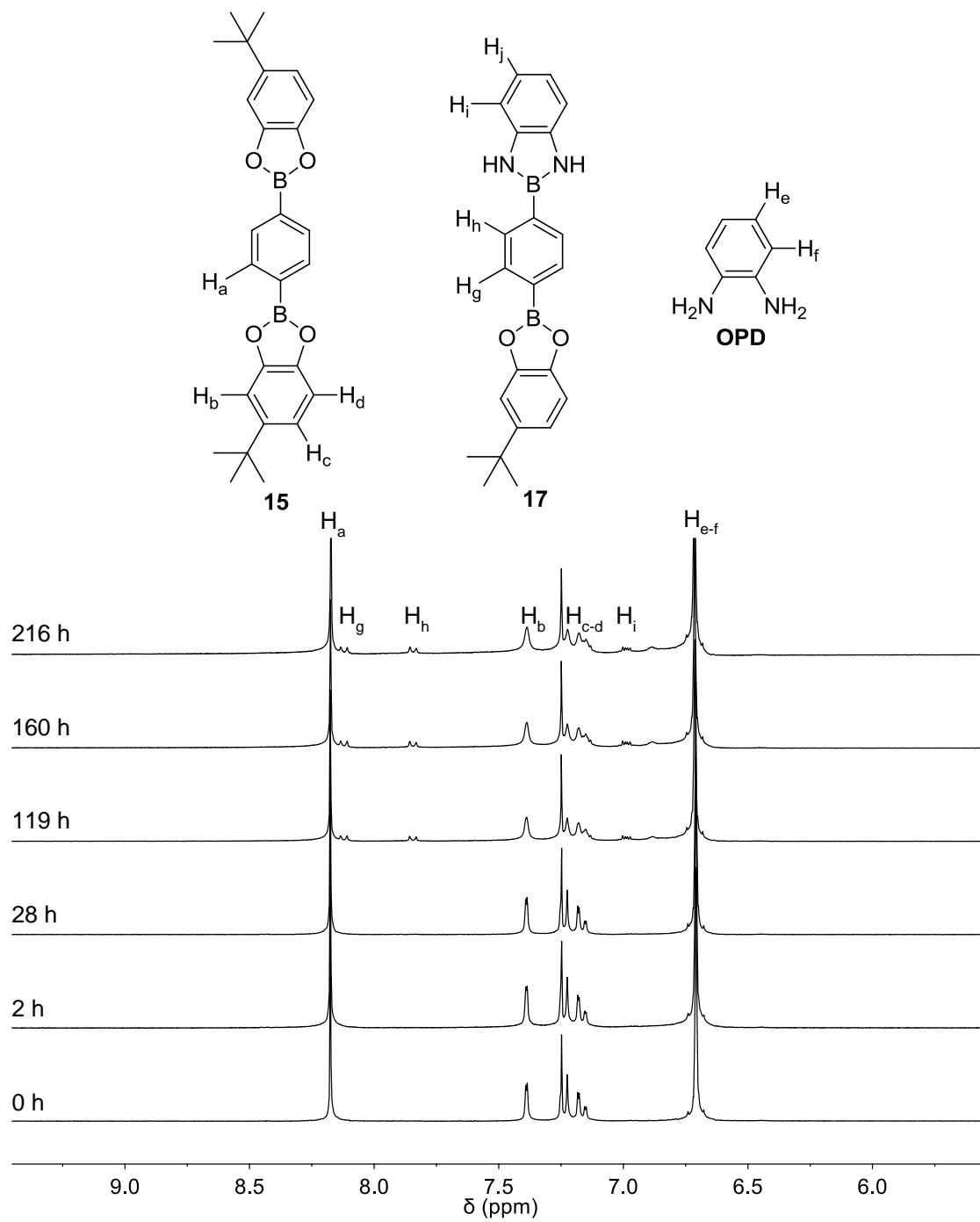


Figure 52.  $^1\text{H}$  NMR spectra of the reaction progress of *t*-butyl BDBA-based ester **15** and OPD.

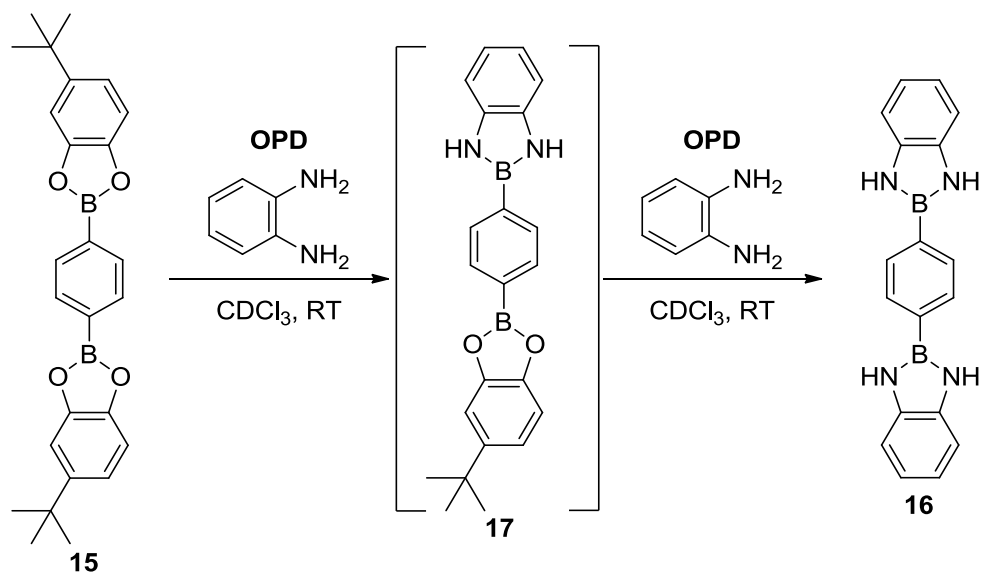


Figure 53. Monosubstituted diazaborole **17**.

Even though the target product bis(diazaborole) **16** did not form, we still pursued the reaction between bis(dioxaborole) **15** with monomer **TA-DEH** since the intramolecular macrocyclization vs. intermolecular reactions may act as a driving force. Therefore, the reactants were mixed under similar conditions (Figure 54).

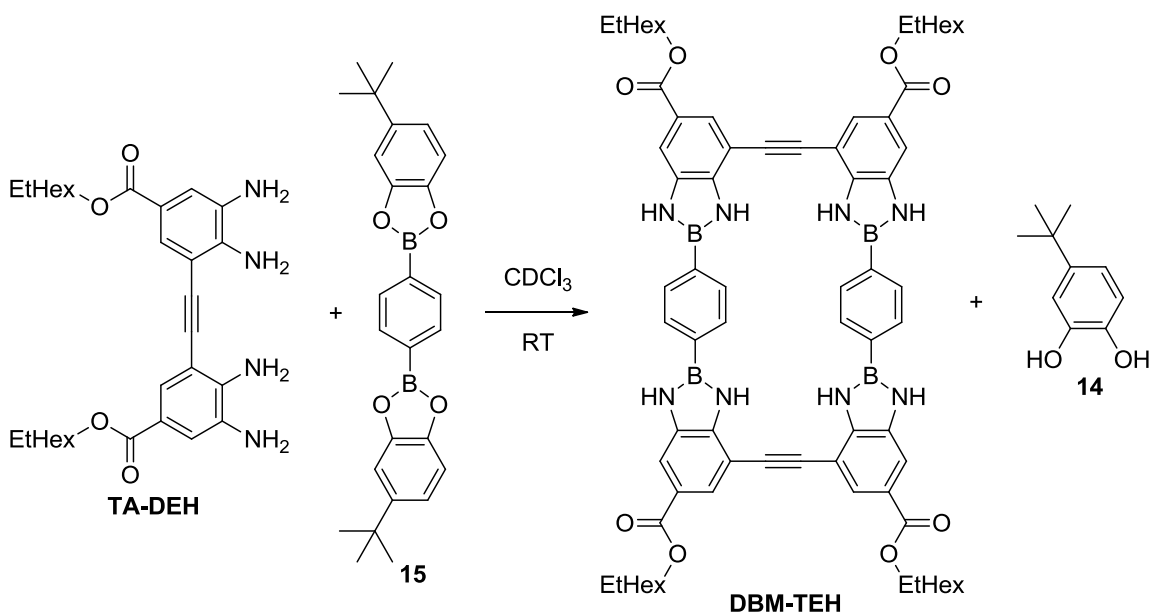


Figure 54. Reaction of monomer **TA-DEH** and **BDBA**-based ester **15**.

<sup>1</sup>H NMR analysis showed the appearance of signals at  $\delta$  6.77-6.89 ppm ( $H_{g-i}$ ) consistent with the formation of *t*-butyl catechol **14**. The appearance of **14** could be due to the hydrolysis of the **BDBA**-based ester **15** (Figure 55). Although the signals related to the starting materials have broadened, they showed no significant changes even after 357 h. No distinct peaks related to the macrocycle were observed in the aromatic region. Additionally, there was no precipitation to indicate the formation of the target **DBM-TEH**.

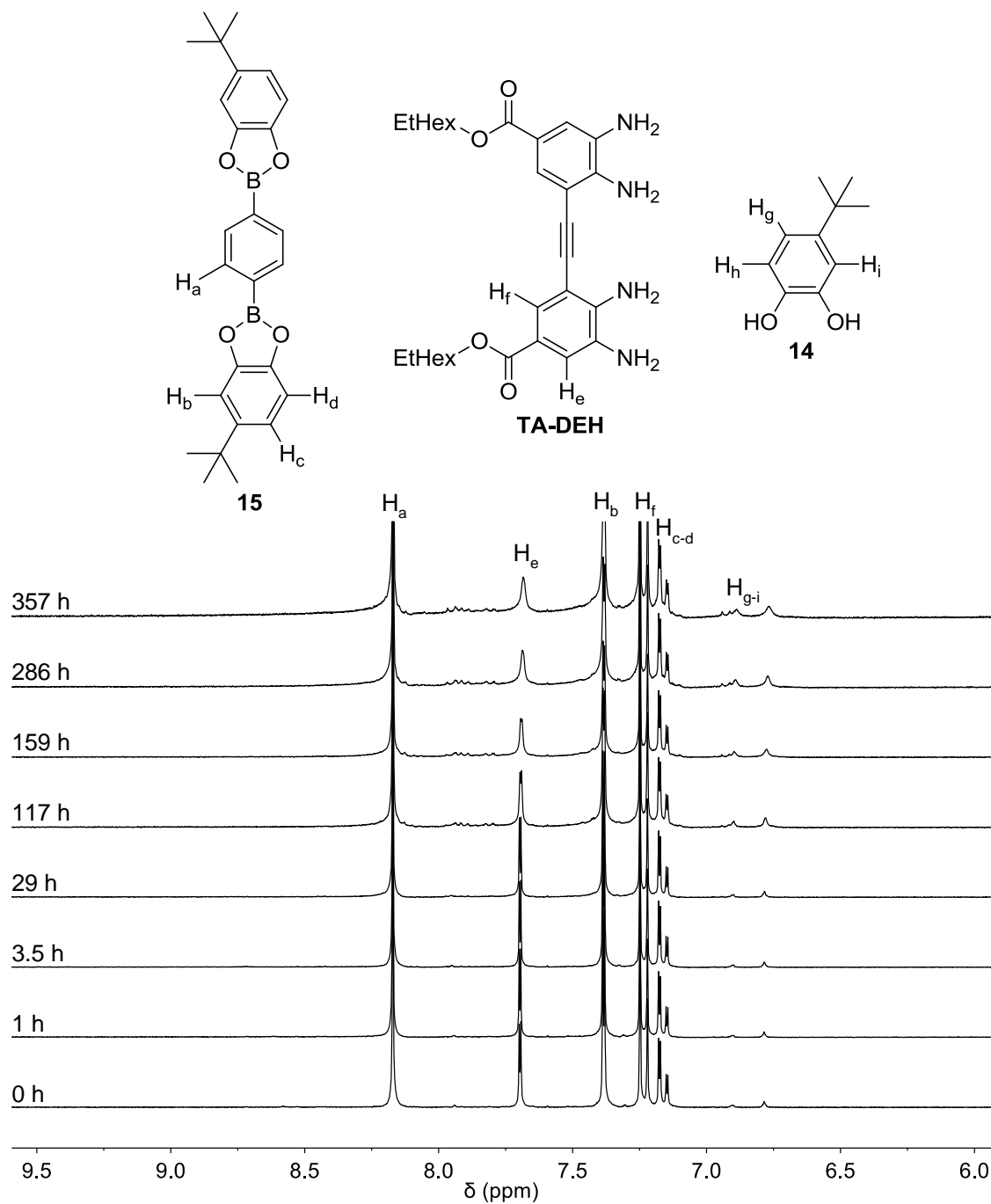


Figure 55. <sup>1</sup>H NMR spectra of reaction progress of *t*-butyl BDBA-based ester **15** and monomer **TA-DEH**.

Tartrate based boronate esters are known to have low stability due to the steric repulsions between the substituents.<sup>39</sup> This may lead to faster dynamic exchange with monomer **TA-DEH**. Furthermore, Letsinger and Hamilton serendipitously prepared 2-

phenyl-1,3,2-benzodiazaborole (**DAB**) in an attempt to accelerate amide formation between ethyl tartrate ester of phenylboronic acid (**18**) and *o*-phenylenediamine (**OPD**) (Figure 56).<sup>24</sup> It was observed that the B-N compound was formed readily even at room temperature by cleavage of a B-O bond. This was assumed to be caused by the unusual reactivity of the *o*-phenylenediamine due to its particular geometry and the stability of the ring system that was formed.<sup>24</sup>

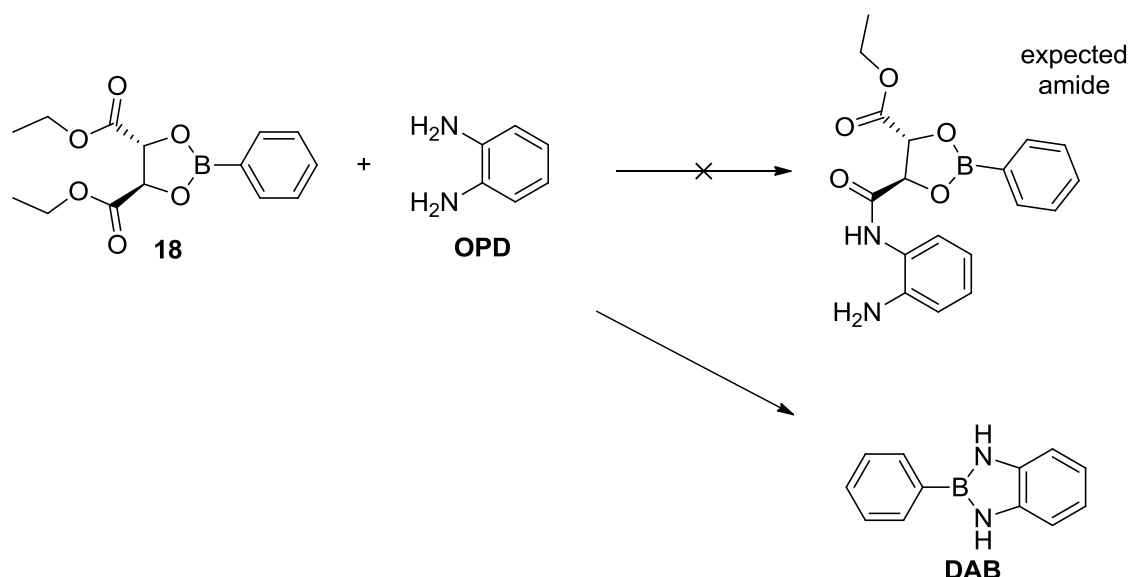


Figure 56. Early study of the formation of B-N bonds by Letsinger.<sup>24</sup>

Therefore, a strategy for formation of the B-N bond between a tartrate ester of **BDBA** and an aromatic amine was employed for larger macrocyclic systems. First, the synthesis of tartrate ester **19** was performed. **BDBA** and (2*R*,3*R*)-diethyl tartrate (**20**) were mixed in toluene under reflux conditions for 90 min using a Dean-Stark apparatus (Figure 57). The reaction was facilitated by the addition of ethanol to help dissolve the **BDBA**. The reaction mixture was concentrated and cooled to induce precipitation. Diboronate ester **19** was then isolated by vacuum filtration and washed with cold toluene to remove

unreacted diethyl tartrate.  $^1\text{H}$  NMR analysis of the resulting white solid in  $\text{CDCl}_3$  supported the formation of the expected product.

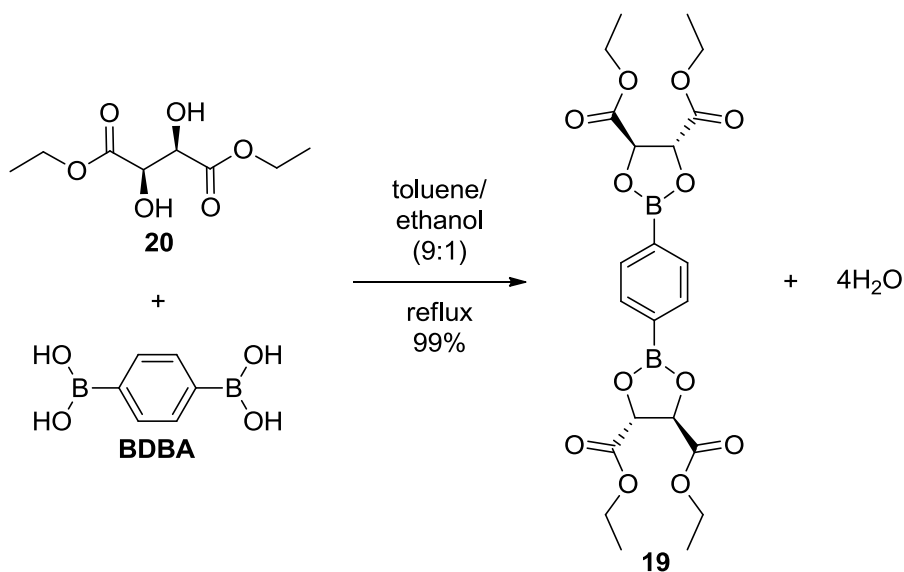


Figure 57. Synthesis of BDBA-based ester **19**.

The exchange reaction of BDBA-based ester **19** and monomer TA-DEH was then studied in a similar manner (Figure 58). Mixing an equimolar amount of each of the reagents resulted in very slow exchange. Analysis by  $^1\text{H}$  NMR spectroscopy revealed the decrease of aromatic signals at  $\delta = 7.67$  (H<sub>e</sub>) and 7.38 ppm (H<sub>f</sub>) related to the tetraamine along with the appearance of the signal at  $\delta = 4.62$  ppm (H<sub>d</sub>) consistent with the formation of the diethyl tartrate **20** byproduct (Figure 59). Similar to the exchange reaction of TA-DEH and ester **15**, however, no distinct peaks related to the target DBM-TEH were observed in the aromatic region even after 6 days. In addition, there was no precipitate to indicate the formation of the macrocycle.

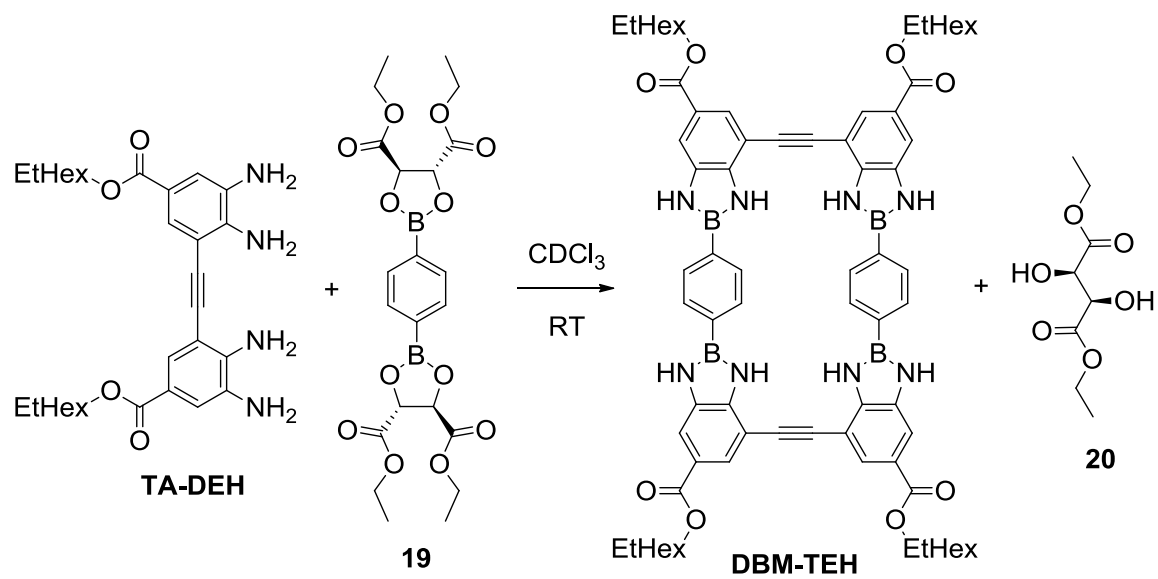


Figure 58. Reaction of monomer **TA-DEH** and **BDBA**-based ester **19**.

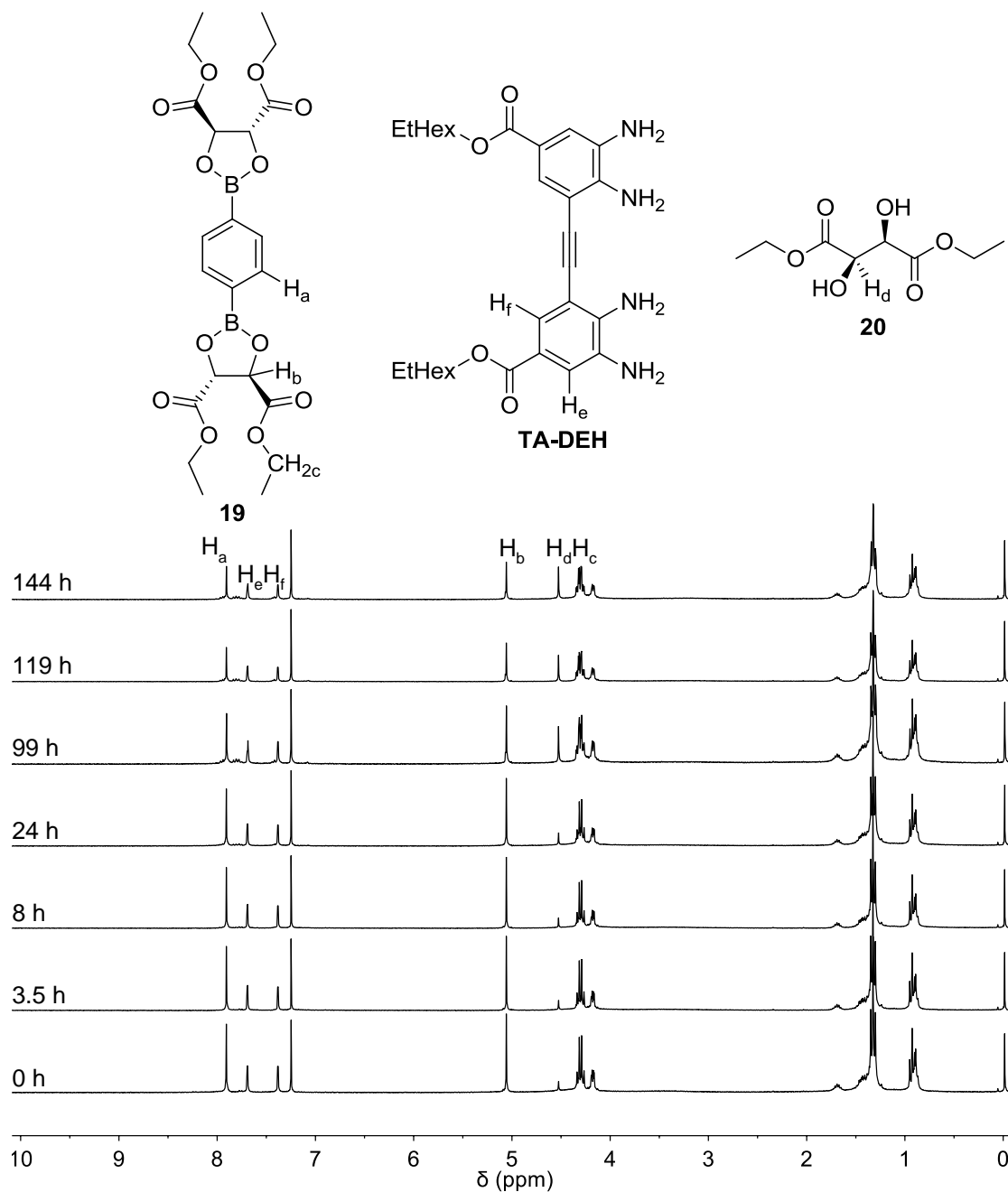


Figure 59.  $^1\text{H}$  NMR spectra of the reaction progress of monomer **TA-DEH** and **BDBA**-based ester **19** with increasing signal of **20** over time.

To investigate this further, bis(dioxaborolane) **19** was reacted with simple **OPD** under the same reaction conditions (Figure 60).

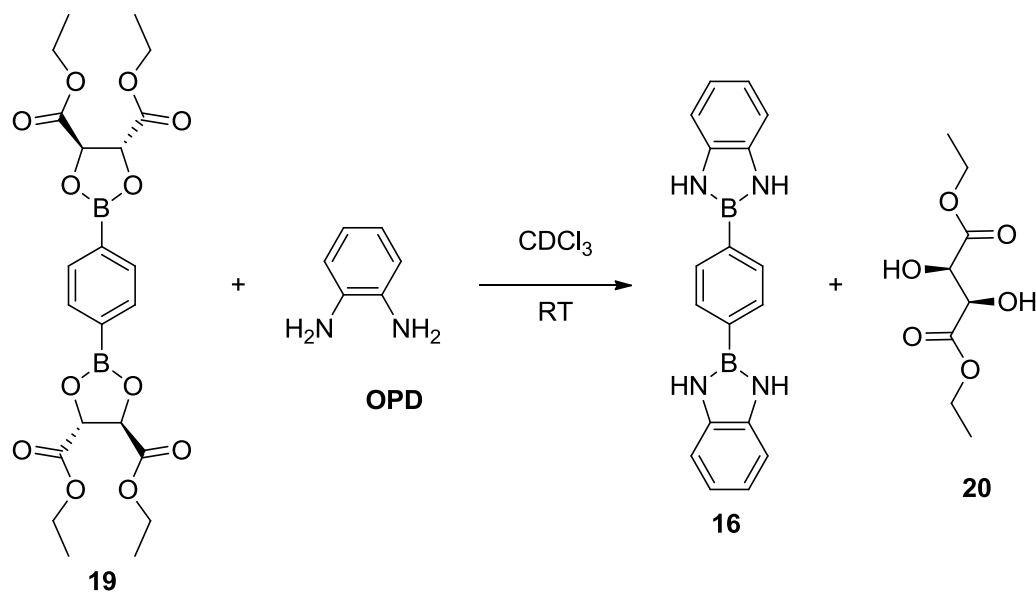


Figure 60. Reaction of **19** and **OPD**.

Analysis using  $^1\text{H}$  NMR spectroscopy revealed a decrease of the aromatic signals of the starting materials ( $\text{H}_a$  and  $\text{H}_{e-f}$ , Figure 61). There was no evidence of the target bis(diazaborole) **16** even after 2 weeks, neither by visible observation of any precipitation nor by examination of the  $^1\text{H}$  NMR spectra. The appearance of the signals at  $\delta = 7.94$  ( $\text{H}_g$ ) and 7.75 ( $\text{H}_h$ ) ppm may result from the potential monosubstituted diazaborole **21** (Figure 62). By integrating these  $^1\text{H}$  NMR signals and those of **17** ( $\text{H}_a$ ), we estimate 28% conversion of **19** to **21** or 14% overall conversion of dioxaborole to diazaborole.

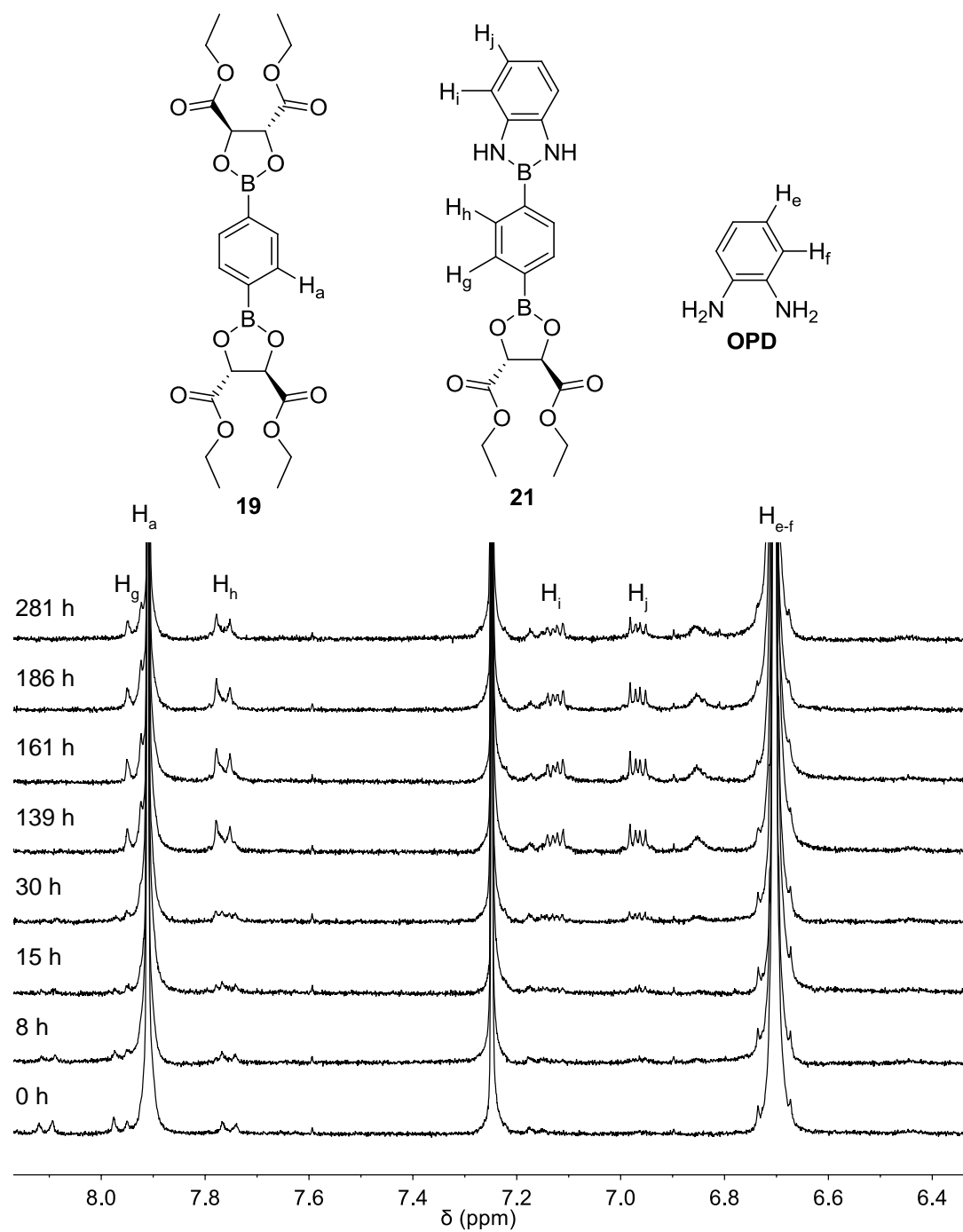


Figure 61.  $^1\text{H}$  NMR spectra of the reaction progress of **BDBA**-based ester **19** and **OPD**.

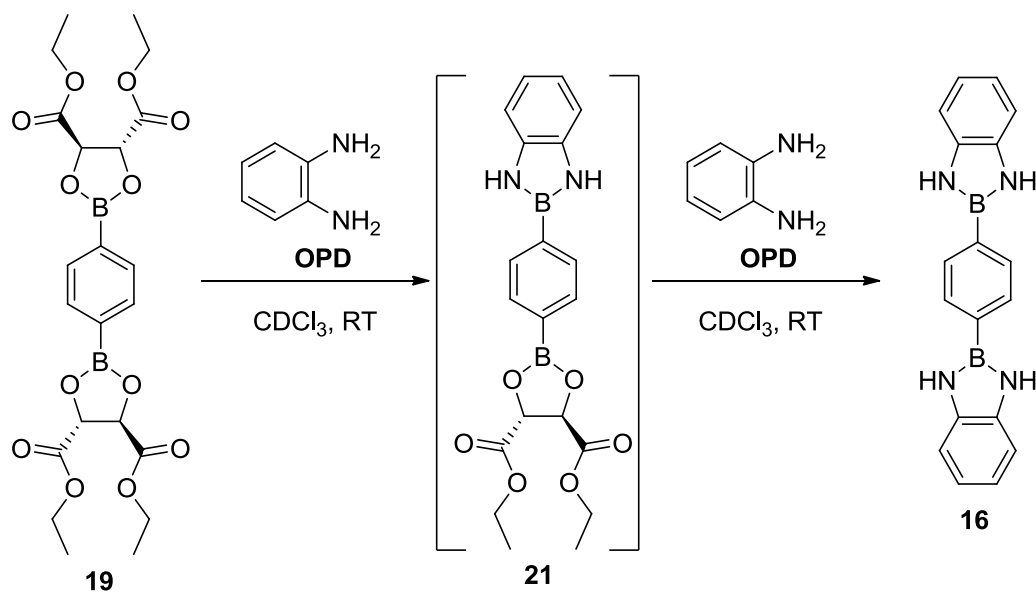


Figure 62. Monosubstituted diazaborole **21**.

The results from these experiments suggest that the **BDBA**-based tartrate esters are more stable than the corresponding diazaborole. To investigate this further, the reaction of ethyl tartrate ester of benzenboronic acid **18** and **OPD** (Figure 56) was reproduced according to Letsinger and Hamilton's reported experimental method.<sup>24</sup> The precursor boronate ester **18** was also prepared based on his reported procedure (Figure 63). Diethyl tartrate **20** and **PBA** were allowed to reflux in toluene for 6 h using a Dean-Stark apparatus. After the removal of solvent, a white solid was obtained. <sup>1</sup>H NMR analysis in CDCl<sub>3</sub> supported the formation of boronate ester **18**.

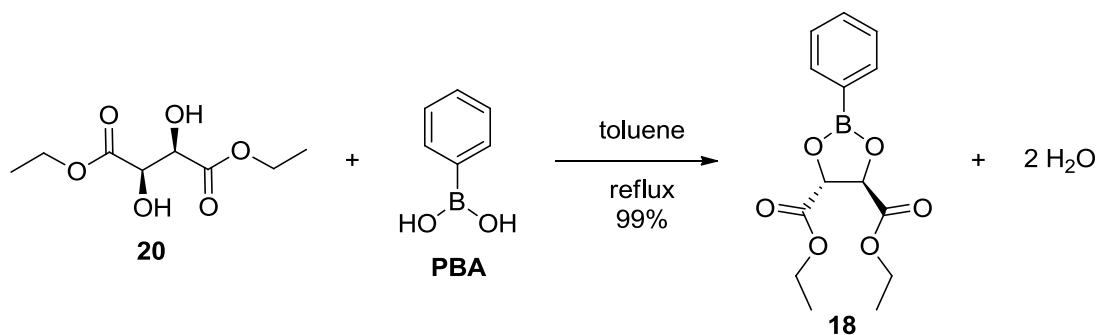


Figure 63. Synthesis of boronate ester **18**.

Next, we attempted to reproduce the synthesis of **DAB** by using the reaction of boronate ester **18** and **OPD**. An equimolar mixture of each of the starting materials in benzene was reacted at room temperature for one hour in a glass vial. The solvent was then removed under reduced pressure at room temperature until the volume was reduced by half. The resulting precipitate was filtered and washed with benzene. The process of concentration, filtration and washing was repeated five times.  $^1\text{H}$  NMR analysis of the resulting product was identified as **DAB**. Under these conditions, **DAB** synthesis was achieved in 60% yield. This may be due to the removal of solvent, which induced precipitation of the **DAB** product, driving the reaction toward the products.

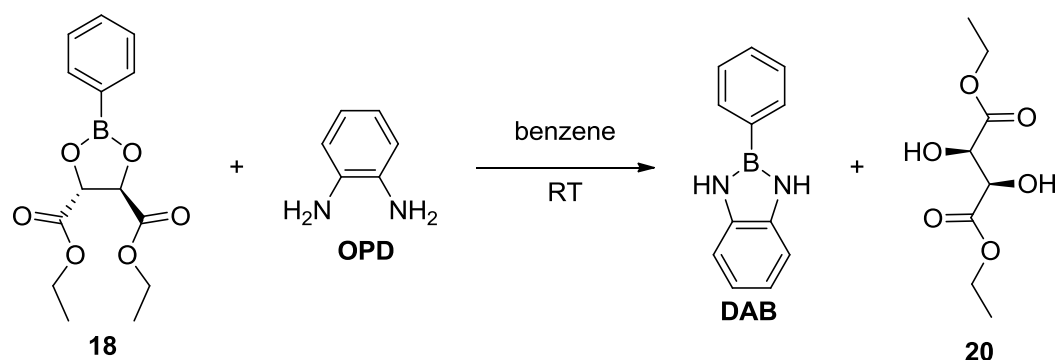


Figure 64. Synthesis of **DAB** from **18** and **OPD**.

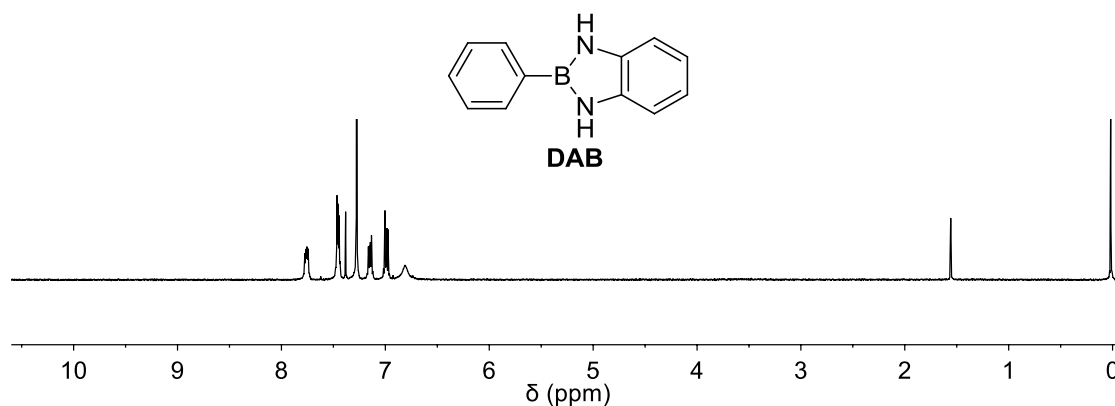


Figure 65.  $^1\text{H}$  NMR spectrum for the product of the reaction in Figure 64.

In order to examine the reaction without any external manipulation, the reaction was studied in benzene- $d_6$  in an NMR tube. The reaction was also repeated in  $\text{CDCl}_3$  in order to understand the impact of solvent on the reaction (Figure 66).

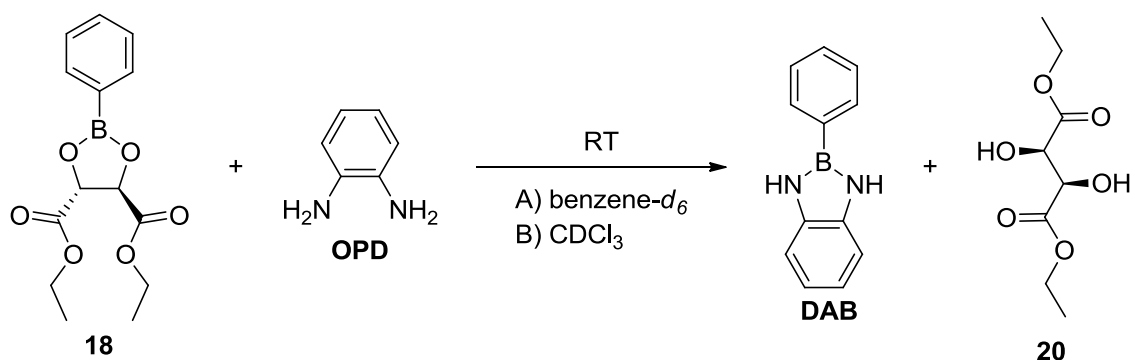


Figure 66. Reaction of **18** and **OPD** in different solvents.

The reaction progress was monitored by integrating the  $^1\text{H}$  NMR signals associated with the protons ortho and meta to nitrogen of **OPD** (benzene- $d_6$ :  $\delta = 6.70$  and  $6.39$  ppm;  $\text{CDCl}_3$ :  $\delta = 6.72$  ppm) and **DAB** (benzene- $d_6$ :  $\delta = 7.02$  and  $6.83$  ppm;  $\text{CDCl}_3$ :  $\delta = 7.12$  and  $6.95$  ppm) (Figure 67). After 10 days, the reaction reached 35% conversion in benzene, which is similar to the same reaction in chloroform, where 31% conversion was observed. These results are different from the former reaction using Letsinger's method where 60% conversion was observed and the equilibration time was significantly shorter. This confirms that the formation of the **DAB** product was promoted by precipitation, which was caused by the removal of solvent under reduced pressure.

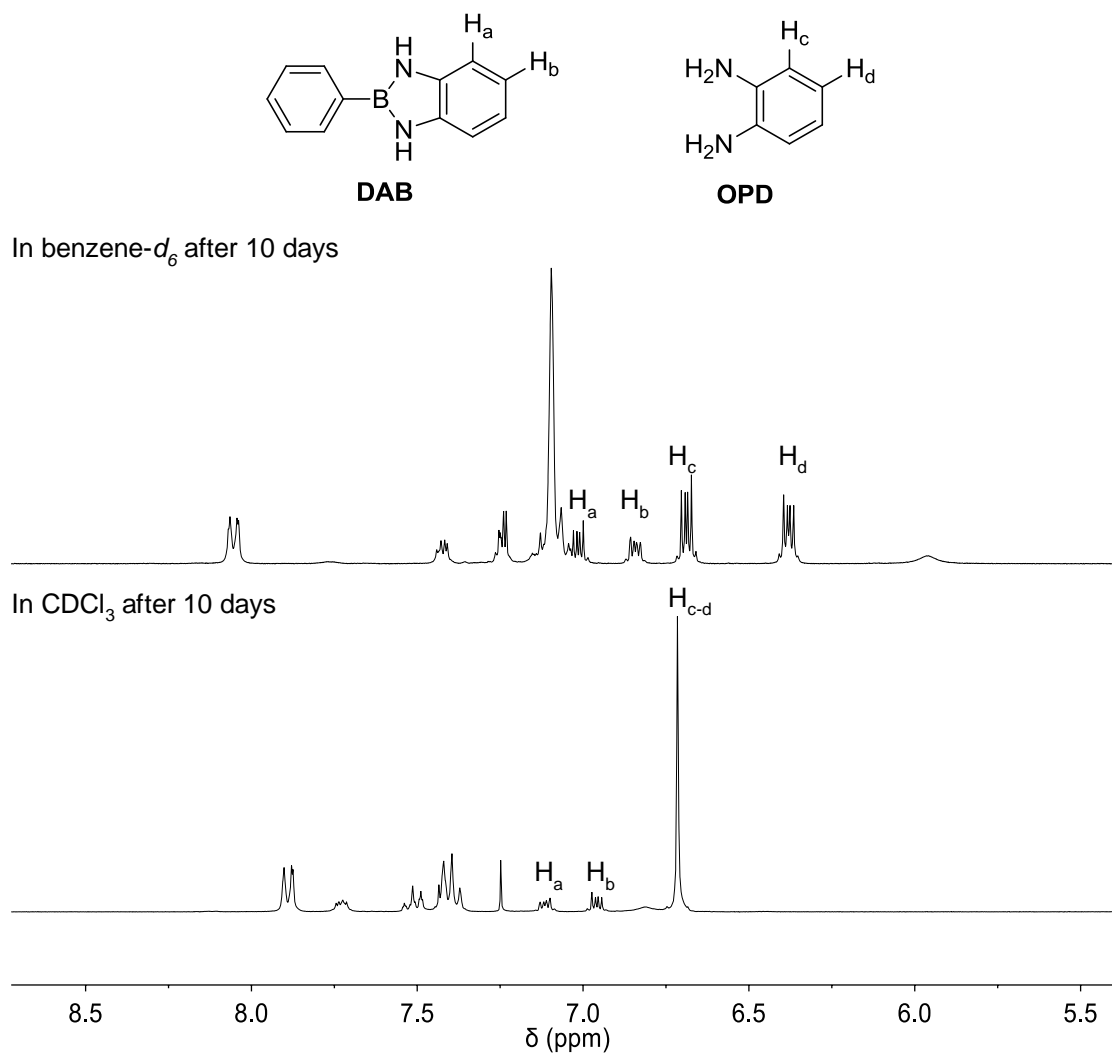


Figure 67. Partial  $^1H$  NMR spectra for the reaction in Figure 66 after 10 days in benzene- $d_6$  and  $CDCl_3$ .

### 3.4 Conclusions

The increased solubility of intermediates **8-10** in common organic solvents revealed that incorporating an ethylhexyl ester into the monomer improves solubility in chloroform. Synthesis of the ethylhexyl ester substituted monomer **TA-DEH** was achieved in multiple steps from benzoic acid **5**. The synthesized monomer **TA-DEH** was more soluble in chloroform than previously studied monomers **TA-DM** and **TA-DTg** by a factor of 10 in

terms of molality. This result confirms the presence of branched 2-ethylhexyl ester in monomer **TA-DEH** has a positive effect on solubility.

The formation of macrocycle **DBM-TEH** from the condensation reaction of monomer **TA-DEH** with **BDBA** was observed in toluene as well as DMSO. Nevertheless, neither the macrocycle nor oligomeric intermediates were soluble in chloroform. Interchain interaction of the branched alkyl is not efficient enough to cause large pi-stacking distance among the aromatic cores of these diazaborole-based macrocycles.

The reactions between **BDBA**-based esters with various di- and tetraamines in chloroform at room temperature was slow. The reaction between simple **OPD** with *t*-butyl **BDBA**-based ester **15** gave the corresponding intermediate in 22% after 9 days, while the tartrate ester moiety **19** gave similar result, reaching 28% conversion after 11 days. The reactions between monomer **TA-DEH** with the same **BDBA**-based esters under similar conditions did not favor the **DBM-TEH** product. No significant progress was observed for up to 2 weeks. On the other hand, **DAB** synthesis between an ethyl tartrate boronate ester **14** and **OPD** was achieved in 60% conversion following Letsinger and Hamilton's method. While the same reaction only reached 35% conversion in benzene and 28% conversion in chloroform for 10 days at room temperature. The results indicate that the simple **DAB** product can be achieved by the removal of solvent to induce precipitation. In the case of diazaborole-linked macrocycles, intramolecular reactions to cyclize could not compete with the stability of the **BDBA**-based esters.

### 3.5 Experimental

All air or moisture sensitive reactions were performed using standard Schlenk techniques under argon atmosphere. Glassware was oven dried before use to achieve the same goal.

Thin layer chromatography (TLC) analyses were performed on silica gel coated with fluorescent indicator F254 aluminum TLC plates. Visualization of TLC plates was performed under a UV light (254 nm) to monitor the consumption of the starting materials and formation of the products. Purification of the synthesized molecules were achieved using silica gel (60 Å) column chromatography.

All starting materials and reagents were purchased from commercial sources (Acros organic, Alfa Aesar, Cambridge Isotope Laboratories, EMD Millipore, Frontier Scientific, J. T. Baker, Oxchem, Sigma Aldrich, T.C.I., V.W.R) and used without further purification, unless otherwise mentioned. The NMR solvents, CDCl<sub>3</sub> and DMSO-d<sub>6</sub>, were stored over activated 3 Å molecular sieves. 3 Å molecular sieves were activated by heating at 130 °C under vacuum for 3 hours. Liquid reagents used for air or moisture sensitive reactions were stored under argon.

<sup>1</sup>H and <sup>13</sup>C NMR spectra were collected using JEOL Eclipse 300+ spectrometer. Chemical shifts are reported in δ (ppm) relative to the <sup>1</sup>H and <sup>13</sup>C {(CDCl<sub>3</sub>: δ 7.26 for <sup>1</sup>H, CDCl<sub>3</sub>: δ 77.23 for <sup>13</sup>C) or (DMSO-d<sub>6</sub>: δ 2.50 for <sup>1</sup>H, DMSO-d<sub>6</sub>: δ 39.52 for <sup>13</sup>C)}. The splitting patterns are designated as s (singlet); d (doublet); t (triplet); q (quartet); dd (doublet of doublets); td (triplet of doublets); m (multiplet); br. s (broaden singlet); ss (slightly broaden singlet).

MALDI-MS analysis was carried out by Michael Raulerson at Texas A&M University using the Macroflex with the following parameters: laser beam attenuation (57.778), laser repetition rate (60 Hz), number of shots (400), positive voltage polarity (POS), ion source voltage 1 (19 kV), ion source voltage 2 (15.65 kV), linear detector voltage (2.799 kV), reflector voltage 1 (20 kV), reflector detector voltage (1.845 kV).

**Synthesis of 2-ethylhexyl 4-amino-3-nitrobenzoate (6).** Commercially available 4-amino-3-nitrobenzoic acid (**5**, 10.6 g, 58.2 mmol, 1 equiv) was dissolved in 2-ethylhexanol (100 mL, 640 mmol, 11 equiv) in a 250 mL round bottom flask. Concentrated H<sub>2</sub>SO<sub>4</sub> (1 mL) was introduced dropwise to the solution with constant mixing. The reaction mixture was refluxed for 4 h using a Vigreux column. The reaction flask was then moved to a distillation apparatus to remove excess 2-ethylhexanol. The resulting dark yellow to brown oil was purified using silica gel column chromatography starting with EtOAc:hexanes (1:9 v/v) and increasing the polarity up to EtOAc:hexanes (1:4 v/v). A yellow solid (14.2 g, 83% yield) was obtained. <sup>1</sup>H NMR (301 MHz, CDCl<sub>3</sub>): δ 8.82 (d, 1H), 7.96 (dd, 1H), 6.84 (d, 1H), 6.44 (br. s, 2H), 4.22 (d, 2H), 1.77-1.70 (m, 1H), 1.48-1.30 (m, 8H), 0.95-0.86 (m, 6H). <sup>13</sup>C NMR (75 MHz, CDCl<sub>3</sub>): δ 165.2, 147.4, 135.9, 131.6, 129.0, 119.5, 118.6, 67.7, 39.0, 30.6, 29.1, 24.0, 23.1, 14.1, 11.1.

**Synthesis of 2-ethylhexyl 4-amino-3-bromo-5-nitrobenzoate (7).** Liquid bromine (2.67 mL, 52.2 mmol, 1.3 equiv) was added dropwise to a methylene chloride solution (200 mL) of 2-ethylhexyl 4-amino-3-nitrobenzoate (**6**, 11.8 g, 40.2 mmol, 1 equiv.). The reaction mixture was stirred for 24 h at room temperature. The product was washed with sodium thiosulfate (54 mL), saturated sodium bicarbonate (35 mL), deionized water (50 mL), and brine (50 mL). The organic layer was dried over anhydrous sodium

sulfate and concentrated to a yellow oil. Diethyl ether (40 mL) was used to dissolve the oil, which was transferred to a separatory funnel (250 mL) and washed with Na<sub>2</sub>CO<sub>3</sub> (saturated 30 mL x1, 25 mL x1), and brine (20 mL). The organic layer was dried over anhydrous sodium sulfate and concentrated to a yellow oil. The product was purified using silica gel column chromatography with EtOAc:hexanes (1:9, v/v) as the eluent. The solvent was removed to give a yellow solid (12.0 g, 80% yield). <sup>1</sup>H NMR (301 MHz, CDCl<sub>3</sub>): δ 8.80 (d, 1H), 8.30 (d, 1H), 6.99 (br. s, 2H), 4.21 (d, 2H), 1.75-1.67 (m, 1H), 1.48-1.30 (m, 8H), 0.95-0.87 (m, 6H). <sup>13</sup>C NMR (75 MHz, CDCl<sub>3</sub>): δ 164.2, 144.8, 138.9, 132.0, 128.1, 119.1, 111.8, 68.1, 38.9, 30.6, 29.1, 24.0, 23.0, 14.1, 11.1.

**Synthesis of 2-ethylhexyl 4-amino-3-((trimethylsilyl)ethynyl)-5-nitrobenzoate (8).**

A) In an Ar atmosphere, 2-ethylhexyl 4-amino-3-bromo-5-nitrobenzoate (**7**, 8.64 g, 23.1 mmol, 1 equiv), Pd(PPh<sub>3</sub>)<sub>2</sub>Cl<sub>2</sub> (0.741 g, 1.06 mmol, 0.05 equiv), and CuI (0.414 g, 2.17 mmol, 0.09 equiv) were added to an oven dried sealed-tube. The materials were dissolved by adding Et<sub>3</sub>N (12 mL) and THF (100 mL). Trimethylsilylacetylene (TMSA, 4.5 mL, 31 mmol, 1.3 equiv) was added slowly for 30 min at room temperature under Ar. Then, the mixture was stirred at 66 °C for 20 h. TLC analysis confirmed the consumption of starting materials. The reaction mixture was then diluted with EtOAc (100 mL) and passed through a silica plug. The EtOAc was removed and the collected organic compound was then purified using silica gel column chromatography with EtOAc:hexanes (1:20, v/v) as the eluent. The product was concentrated into a yellow oil (3.51 g, 37% yield). <sup>1</sup>H NMR (301 MHz, CDCl<sub>3</sub>): δ 8.79 (d, 1H), 8.15 (d, 1H), 7.5 (br. s, 2H), 4.20 (d, 2H), 1.75-1.67 (m, 1H), 1.46-1.24 (m, 8H), 0.96-0.87 (m, 6H), 0.29 (s, 9H). <sup>13</sup>C NMR (75 MHz, CDCl<sub>3</sub>): δ 164.7,

147.8, 138.8, 131.5, 128.9, 118.4, 112.3, 104.4, 98.0, 67.9, 38.9, 30.6, 29.1, 24.0, 23.1, 14.1, 11.1, 0.9.

B) In an Ar atmosphere, 2-ethylhexyl 4-amino-3-bromo-5-nitrobenzoate (**7**, 5.0 g, 13.4 mmol, 1 equiv), PPh<sub>3</sub> (0.353 g, 1.34 mmol, 0.1 equiv), Pd(PPh<sub>3</sub>)<sub>2</sub>Cl<sub>2</sub> (0.471 g, 0.67 mmol, 0.05 equiv), and CuI (0.129 g, 0.67 mmol, 0.05 equiv) were added to an oven-dried sealed tube. The materials were dissolved by adding Et<sub>3</sub>N (20 mL) and THF (50 mL). Trimethylsilylacetylene (TMSA, 3 mL, 21.5 mmol, 1.6 equiv) was added slowly for 30 min at room temperature under Ar. Then, the mixture was stirred at 66 °C for 20 h. TLC confirmed the consumption of starting materials. The reaction mixture was diluted with EtOAc (100 mL) and passed through a silica plug. The collected organic compound was distilled under vacuum, and then purified using silica gel column chromatography with EtOAc:hexanes (1:9 v/v) as the eluent. The product was concentrated into a yellow oil (4.29 g, 82% yield). <sup>1</sup>H NMR (301 MHz, CDCl<sub>3</sub>): δ 8.79 (d, 1H), 8.15 (d, 1H), 7.5 (br. s, 2H), 4.20 (d, 2H), 1.75-1.67 (m, 1H), 1.46-1.24 (m, 8H), 0.96-0.87 (m, 6H), 0.29 (s, 9H). <sup>13</sup>C NMR (75 MHz, CDCl<sub>3</sub>): δ 164.7, 147.8, 138.8, 131.5, 128.9, 118.4, 112.3, 104.4, 98.0, 67.9, 38.9, 30.6, 29.1, 24.0, 23.1, 14.1, 11.1, 0.9.

**Synthesis of 2-ethylhexyl 4-amino-3-ethynyl-5-nitrobenzoate (9).** Tetrabutylammonium fluoride (TBAF, 8.25 mL, 1.0 M, 48.25 mmol, 1.3 equiv) was added to a solution of **8** (2.37 g, 6.35 mmol, 1 equiv) in wet THF (50 mL). After 30 s of stirring, the reaction mixture was filtered through a silica plug using EtOAc:hexanes (1:9 v/v) as the diluent. The collected eluate was concentrated and purified by silica gel column chromatography using EtOAc:hexanes (1:20 v/v) as the eluent to give a yellow solid (1.37 g, 68% yield). <sup>1</sup>H NMR (301 MHz, CDCl<sub>3</sub>): δ 8.82 (s, 1H), 8.19 (s, 1H), 4.20 (d, 2H), 3.59

(s, 1H), 1.75-1.65 (m, 1H), 1.48-1.29 (m, 8H), 0.95-0.87 (m, 6H).  $^{13}\text{C}$  NMR (75 MHz,  $\text{CDCl}_3$ ):  $\delta$  164.5, 148.0, 139.3, 131.6, 129.4, 118.5, 111.0, 86.0, 67.9, 38.9, 30.6, 29.1, 24.0, 23.1, 14.1, 11.1.

**Synthesis of 3,3'-(ethyne-1,2-diyl)bis((2-ethylhexyl 5-nitro-4-aminobenzoate)**

**(10)**. In an Ar atmosphere, 2-ethylhexyl 4-amino-3-bromo-5-nitrobenzoate (**7**, 0.560 g, 1.76 mmol, 1 equiv), the deprotected alkyne (**9**, 0.694 g, 1.86 mmol, 1 equiv),  $\text{Pd}(\text{PPh}_3)_4$  (0.106 g, 0.09 mmol, 0.05 equiv), and  $\text{CuI}$  (0.0168 g, 0.09 mmol, 0.05 equiv) were added to a oven dried sealed-tube (50 mL).  $\text{Et}_3\text{N}$  (9.0 mL, 64.6 mmol, 37 equiv) was added to dissolve all of the reagents. The reaction mixture was stirred at 70 °C for 18 h. TLC analysis confirmed the consumption of starting materials **7** and **9**. The reaction mixture was then cooled, diluted with  $\text{EtOAc}$  (50 mL), and passed through a silica plug. The solvent was removed to reveal the crude product.  $^1\text{H}$  NMR showed the presence of impurities. The orange product was again suspended in  $\text{EtOAc}$ :hexanes (1:5 v/v), vacuum filtered and washed with diethyl ether. After solvent was removed, the product obtained was a bright yellow solid (0.756 g, 67% yield).  $^1\text{H}$  NMR (301 MHz,  $\text{CDCl}_3$ ):  $\delta$  8.86(s, 2H), 8.26 (s, 2H), 7.08 (br, 4H), 4.23 (d, 4H), 1.77-1.69 (m, 2H), 1.56-1.34 (m, 16H), 0.96-0.88 (m, 12H).  $^{13}\text{C}$  NMR (75 MHz,  $\text{CDCl}_3$ ):  $\delta$  164.4, 147.5, 139.2, 131.9, 129.7, 118.9, 110.8, 90.6, 68.1, 38.9, 30.6, 29.1, 24.0, 23.1, 14.1, 11.1.

**Synthesis of 3,3'-(ethyne-1,2-diyl)bis(2-ethylhexyl 4,5-diaminobenzoate) (TA-**

**DEH)**. In a 100 mL round bottom flask, compound **10** (0.50 g, 0.82 mmol, 1 equiv) was combined with  $\text{SnCl}_2 \cdot 2\text{H}_2\text{O}$  (3.69 g, 16 mmol, 20 equiv) and  $\text{EtOAc}$  (50 mL). The solution was stirred at 80 °C for 24 h. The reaction mixture was washed with a mixture of  $\text{NaOH}$  (2 M, 30 mL) and water (15 mL). It was then passed through a vacuum filter to remove

the white precipitate. EtOAc (10 mL x2) was used to wash the precipitate cake. The washings were combined with the organic and aqueous filtrates into a separatory funnel. After draining the aqueous layer, the organic layer was washed with water (30 mL x2), brine (30 mL x2) and dried over anhydrous Na<sub>2</sub>SO<sub>4</sub>. The solvent was removed to reveal a dark brown solid. The collected organic compound was purified by silica gel column chromatography using EtOAc:hexanes (2:1 v/v) as the eluent. Solvent was then removed to give a yellow solid (0.32 g, 71% yield). <sup>1</sup>H NMR (301 MHz, CDCl<sub>3</sub>) δ 7.68 (s, 2H), 7.38 (s, 2H), 4.48 (br, 2H), 4.20-4.16 (m, 2H), 3.43 (br, 2H), 1.73-1.65 (m, 2H), 1.48-1.24 (m, 16H), 0.95-0.86 (m, 12H). <sup>13</sup>C NMR (75 MHz, CDCl<sub>3</sub>): δ 166.6, 142.0, 132.7, 126.2, 120.7, 118.4, 107.8, 90.5, 67.2, 39.0, 30.6, 29.1, 24.0, 23.1, 14.2, 11.2.

**Solubility comparison of monomers TA-DEH, TA-DM, and TA-DTg.** Into each small test tube, **TA-DEH** (2.3 mg, 0.0042 mmol, 1 equiv), **TA-DM** (1.1 mg, 0.0041 mmol, 1 equiv), and **TA-DTg** (2.6 mg, 0.0042 mmol, 1 equiv) were added. Chloroform was introduced dropwise. The weight of CHCl<sub>3</sub> drops it took to completely dissolve each material was recorded.

Monomer	Amount of CHCl <sub>3</sub> used (mg)
<b>TA-DEH</b>	48.5
<b>TA-DM</b>	504.7
<b>TA-DTg</b>	1289.5

**Synthesis of macrocycle (DBM-DEH) in toluene.** In a 65 mL round bottom flask, monomer **TA-DEH** (83.0 mg, 0.15 mmol, 1 equiv) and **BDBA** (24.5 mg, 0.15 mmol, 1 equiv) were dissolved in ethanol (5 mL) for 5 minutes. After toluene (25 mL) was added, the reaction was allowed to reflux for 5 days. The reaction mixture was then concentrated and cooled to room temperature. A light-coral precipitate was filtered and washed with

cold toluene (2 mL) and cold hexane (2 mL). The product was vacuum dried to obtain a light-coral solid (84.0 mg). The following peaks correspond to the macrocycle product;  $^1\text{H}$  NMR (301 MHz,  $\text{DMSO-}d_6$ )  $\delta$  10.26 (s, 8H), 9.80 (s, 8H), 8.35 (s, 8H), 7.80 (s, 4H), 7.72 (s, 4H), 4.21 (d, 8H), 1.73-1.67 (m, 4H), 1.45-1.34 (m, 32H), 0.95-0.88 (m, 24H).  $^{13}\text{C}$  NMR (75 MHz,  $\text{DMSO-}d_6$ )  $\delta$  166.5, 142.1, 138.2, 134.3, 125.4, 121.3, 112.1, 104.5, 90.2, 66.9, 38.3, 30.7, 29.0, 24.1, 23.0, 14.5, 11.5.

**Reaction of monomer TA-DEH and BDBA in  $\text{DMSO-}d_6$ .** In an NMR tube, monomer **TA-DEH** (6.8 mg, 0.01 mmol, 1 equiv) and **BDBA** (1.9 mg, 0.01 mmol, 1 equiv) were dissolved in  $\text{DMSO-}d_6$ . The reaction progress was monitored over time using  $^1\text{H}$  NMR at 100 °C. The following peaks correspond to the macrocycle product;  $^1\text{H}$  NMR (301 MHz,  $\text{DMSO-}d_6$ )  $\delta$  10.26 (s, 8H), 9.80 (s, 8H), 8.35 (s, 8H), 7.80 (s, 4H), 7.72 (s, 4H), 4.21 (d, 8H), 1.73-1.67 (m, 4H), 1.45-1.34 (m, 32H), 0.95-0.88 (m, 24H).

**Synthesis of 2,2'-(1,4-phenylene)bis(1,3,2-benzodioxaborole) (13).** **BDBA** (101.2 mg, 0.611 mmol, 1 equiv) was combined with catechol (**12**, 134.6 mg, 1.222 mmol, 2 equiv) and methanol (5 mL) in a 100 mL round bottom flask. After the starting materials were mixed well to dissolve, toluene (50 mL) and 3 Å molecular sieves were added. The reaction mixture was allowed to reflux for 90 min with a Dean-Stark trap. Then, the solution was concentrated and cooled to room temperature to induce precipitation. Vacuum filtration was performed to obtain a white solid (181.0 mg, 94% yield).  $^1\text{H}$  NMR (301 MHz,  $\text{CDCl}_3$ )  $\delta$  8.20 (s, 4H), 7.33, (dd, 4H), 7.14 (dd, 4H).  $^1\text{H}$  NMR (301 MHz,  $\text{DMSO-}d_6$ )  $\delta$  7.36 (s, 4H), 6.70, (dd, 4H), 6.57 (dd, 4H).  $^{13}\text{C}$  NMR analysis could not be obtained in  $\text{CDCl}_3$  due to the low solubility of the product.  $^{13}\text{C}$  NMR (75 MHz,  $\text{DMSO-}d_6$ )  $\delta$  152.0, 131.1, 119.2, 109.7.

**Synthesis of a *t*-butyl ester of BDBA 15.** BDBA (95 mg, 0.57 mmol, 1 equiv) was combined with tert-butyl catechol (**14**, 190.6 mg, 1.147 mmol, 2 equiv) and methanol (5 mL) in a 100 mL round bottom flask. After the starting materials were mixed well to dissolve, toluene (50 mL) and 3 Å molecular sieves (about 10) were added. The reaction mixture was allowed to reflux for 90 min with a Dean-Stark trap. Then, the solution was concentrated and cooled to room temperature to induce precipitation. Vacuum filtration was performed to obtain a white solid (219.8 mg, 94% yield). <sup>1</sup>H NMR (301 MHz, CDCl<sub>3</sub>) δ 8.17 (s, 4H), 7.38 (d, 2H), 7.22-7.15 (m, 4H), 1.36 (s, 18H). <sup>13</sup>C NMR (75 MHz, CDCl<sub>3</sub>) δ 148.4, 146.8, 146.2, 134.5, 119.7, 111.7, 110.1, 35.0, 31.8.

**Reaction of BDBA-based ester 15 and OPD.** In an NMR tube, compound **15** (6.1 mg, 0.014 mmol, 1 equiv) and **OPD** (3.1 mg, 0.029 mmol, 2 equiv) were dissolved in CDCl<sub>3</sub>. The reaction progress was monitored using <sup>1</sup>H NMR at room temperature.

**Reaction of BDBA-based ester 15 and monomer TA-DEH.** In an NMR tube, compound **15** (4.0 mg, 0.0094 mmol, 1 equiv) and monomer **TA-DEH** (5.2 mg, 0.0094 mmol, 1 equiv) were dissolved in CDCl<sub>3</sub>. The reaction progress was monitored using <sup>1</sup>H NMR at room temperature.

**Synthesis of an ethyl tartrate ester of BDBA (19).** BDBA (321.7 mg, 1.941 mmol, 1 equiv) was combined with (2*R*,3*R*)-diethyl tartrate (**20**, 800.4 mg, 3.882 mmol, 2 equiv) and ethanol (5 mL) in a 100 mL round bottom flask. After the starting materials were mixed well to dissolve, toluene (50 mL) was added. The reaction mixture was allowed to reflux for 90 min with a Dean-Stark trap. Then, the solution was concentrated and cooled to room temperature before leaving in a freezer (-20 °C) for 6 h. The crystals formed were isolated by vacuum filtration and washed with cold toluene and cold hexane

to give a white solid (973.8 mg, 99% yield).  $^1\text{H}$  NMR (301 MHz,  $\text{CDCl}_3$ )  $\delta$  7.91 (s, 4H), 5.06 (s, 4H), 4.29 (q, 8H), 1.53 (t, 12H).  $^{13}\text{C}$  NMR (301 MHz,  $\text{CDCl}_3$ )  $\delta$  169.4, 134.6, 78.1, 62.4, 14.2.

**Reaction of BDBA-based ester 19 and monomer TA-DEH.** In an NMR tube, compound **19** (2.4 mg, 0.0058 mmol, 1 equiv) and monomer **TA-DEH** (3.2 mg, 0.0058 mmol, 1 equiv) were dissolved in  $\text{CDCl}_3$ . The reaction progress was monitored over time using  $^1\text{H}$  NMR at room temperature.

**Reaction of BDBA-based ester 19 and OPD.** In an NMR tube, compound **16** (4.7 mg, 0.0093 mmol, 1 equiv) and **OPD** (2.0 mg, 0.018 mmol, 2 equiv) were dissolved in  $\text{CDCl}_3$ . The reaction progress was monitored over time using  $^1\text{H}$  NMR at room temperature.

**Synthesis of diethyl 2-phenyl-1,3,2-dioxaborolane-4,5-dicarboxylate (18).** In a 100 mL round bottom flask, a mixture of **PBA** (460.1 mg, 3.773 mmol, 1 equiv) and (2*R*,3*R*)-diethyl tartrate (**15**, 778.0 mg, 3.773 mmol, 1 equiv) in toluene (50 mL) was heated under reflux for 6 h using a Dean Stark apparatus. Then, the reaction flask was cooled to room temperature and the solvent was removed to reveal a white solid (1.089 g, 99% yield).  $^1\text{H}$  NMR (301 MHz,  $\text{CDCl}_3$ )  $\delta$  7.90 (d, 2H), 7.50 (m, 1H), 7.42 (m, 2H), 5.05 (s, 2H), 4.31 (q, 4H), 1.32 (t, 6H).  $^{13}\text{C}$  NMR (75 MHz,  $\text{CDCl}_3$ )  $\delta$  169.6, 135.4, 132.3, 128.0, 78.1, 62.3, 14.2.

**Synthesis of DAB from boronate ester 18 and OPD.** In a 20 mL glass vial, **OPD** (111.4 mg, 1.030 mmol, 1 equiv) in benzene (4 mL) was mixed with a solution of boronate ester **18** (300.9 mg, 1.030 mmol, 1 equiv) in benzene (4 mL). After 1 h of mixing at room temperature, benzene was removed under vacuum without raising the temperature until the

volume was reduced by half. The resulting crystals were filtered and washed with benzene. The process of concentration, filtration and washing was repeated five times. The obtained product was a white solid. The total product formed was 120.4 mg (60% yield). It was identified as **DAB** using  $^1\text{H}$  NMR.  $^1\text{H}$  NMR (301 MHz,  $\text{CDCl}_3$ )  $\delta$  7.77-7.69 (m, 2H), 7.52-7.43 (m, 3H), 7.22-7.11 (m, 2H), 7.03-6.90 (m, 2H), 6.79 (br. s, 2H).  $^{13}\text{C}$  NMR (75 MHz,  $\text{CDCl}_3$ )  $\delta$  136.4, 133.1, 129.9, 128.3, 119.5, 111.3. All washings and filtrates were combined and the solvent was removed.  $^1\text{H}$  NMR analysis of the filtrate revealed a mixture of the diethyl tartrate **15** byproduct and the leftover **DAB** product.

**Reaction of boronate ester **18** and OPD in benzene- $d_6$  and  $\text{CDCl}_3$ .**

- A) In an NMR tube, compound **18** (10.9 mg, 0.0037 mmol, 1 equiv) and **OPD** (4.0 mg, 0.037 mmol, 1 equiv) were dissolved in benzene- $d_6$ . The reaction progress was monitored over time using  $^1\text{H}$  NMR.
- B) In an NMR tube, compound **18** (10.9 mg, 0.0037 mmol, 1 equiv) and **OPD** (4.0 mg, 0.037 mmol, 1 equiv) were dissolved in  $\text{CDCl}_3$ . The reaction progress was monitored over time using  $^1\text{H}$  NMR.

## REFERENCES

- (1) Zhang, W.; Moore, J. S. Shape-Persistent Macrocycles: Structures and Synthetic Approaches from Arylene and Ethynylene Building Blocks. *Angew. Chem. Int. Ed.* **2006**, *45*, 4416–4439.
- (2) Iritani, K.; Ikeda, M.; Yang, A.; Tahara, K.; Hirose, K.; Moore, J.; Tobe, Y. Hexagonal Molecular Tiling by Hexagonal Macrocycles at the Liquid/Solid Interface: Structural Effects on Packing Geometry. *Langmuir* **2017**, *33*, 12453–12462.
- (3) Gong, B.; Shao, Z. Self-Assembling Organic Nanotubes with Precisely Defined, Sub-nanometer Pores: Formation and Mass Transport Characteristics. *Acc. Chem. Res.* **2013**, *46*, 2856–2866.
- (4) Zhong, Y.; Yang, Y.; Shen, Y.; Xu, W.; Wang, Q.; Connor, A.; Zhou, X.; He, L.; Zeng, X.; Shao, Z.; Lu, Z.; Gong, B. Enforced Tubular Assembly of Electronically Different Hexakis(m-Phenylene Ethynylene) Macrocycles: Persistent Columnar Stacking Driven by Multiple Hydrogen Bonding Interactions. *J. Am. Chem. Soc.* **2017**, *139*, 15950–15957.
- (5) Staab, H. A.; Neunhoeffer, K. [2.2.2.2.2.2] Metacyclophane-1,9,17,25,33,41-hexayne from m-Iodophenylacetylene by Sixfold Stephens-Castro Coupling. *Synth.* **1974**, 424.
- (6) Zhao, D.; Moore, J. S. Shape-Persistent Arylene Ethynylene Macrocycles: Syntheses and Supramolecular Chemistry. *Chem. Commun.* **2003**, 807–818.
- (7) Goldberg, A. R.; Northrop, B. H. Spectroscopic and Computational Investigations of the Thermodynamics of Boronate Ester and Diazaborole Self-Assembly. *J. Org.*

*Chem.* **2016**, *81*, 969–980.

- (8) Rowan, S. J.; Cantrill, S. J.; Cousins, G. R. L.; Sanders, J. K. M.; Stoddart, J. F. Dynamic Covalent Chemistry. *Angew. Chem. Int. Ed. Engl.* **2002**, *41*, 898–952.
- (9) Jin, Y.; Yu, C.; Denman, R. J.; Zhang, W. Recent Advances in Dynamic Covalent Chemistry. *Chem. Soc. Rev.* **2013**, *42*, 6634–6654.
- (10) Zhang, W.; Moore, J. S. Arylene Ethynylene Macrocycles Prepared by Precipitation-Driven Alkyne Metathesis. *J. Am. Chem. Soc.* **2004**, *126*, 12796.
- (11) Chavez, A. D.; Evans, A. M.; Flanders, N. C.; Bisbey, R. P.; Vitaku, E.; Chen, L. X.; Dichtel, W. R. Equilibration of Imine-Linked Polymers to Hexagonal Macrocycles Driven by Self-Assembly. *Chem. Eur. J.* **2018**, *24*, 3989–3993.
- (12) Brooks, W. L. A.; Sumerlin, B. S. Synthesis and Applications of Boronic Acid-Containing Polymers: From Materials to Medicine. *Chem. Rev.* **2016**, *116*, 1375–1397.
- (13) El-Kaderi, H. M.; Hunt, J. R.; Mendoza-Cortés, J. L.; Côté, A. P.; Taylor, R. E.; O’Keeffe, M.; Yaghi, O. M. Designed Synthesis of 3D Covalent Organic Frameworks. *Science* **2007**, *316*, 268–272.
- (14) Kaur, P.; Hupp, J. T.; Nguyen, S. T. Porous Organic Polymers in Catalysis: Opportunities and Challenges. *ACS Catal.* **2011**, *1*, 819–835.
- (15) Nishiyabu, R.; Kubo, Y.; James, T. D.; Fossey, J. S. Boronic Acid Building Blocks: Tools for Sensing and Separation. *Chem. Commun.* **2011**, *47*, 1106–1123.
- (16) Côté, A. P.; Benin, A. I.; Ockwig, N. W.; O’Keeffe, M.; Matzger, A. J.; Yaghi, O. M. Porous, Crystalline, Covalent Organic Frameworks. *Science* **2005**, *310*, 1166–1170.

- (17) Smith, M. K.; Powers-Riggs, N. E.; Northrop, B. H. Discrete, soluble covalent organic boronate ester rectangles. *Chem. Commun.*, **2013**, *49*, 6167–6169.
- (18) Klotzbach, S.; Scherpf, T.; Beuerle, F. Dynamic covalent assembly of tribenzotriquinacenes into molecular cubes. *Chem. Commun.* **2014**, *50*, 12454–12457.
- (19) Entwistle, C. D.; Marder, T. B. Applications of Three-Coordinate Organoboron Compounds and Polymers in Optoelectronics. *Chem. Mater.* **2004**, *16*, 4574–4585.
- (20) Liu, Z.; Shi, M.; Li, F.; Fang, Q.; Chen, Z.; Yi, T.; Huang, C. Highly Selective Two-Photon Chemosensors for Fluoride Derived from Organic Boranes. *Org. Lett.* **2005**, *7*, 5481–5484.
- (21) Ulrich, G.; Ziessel, R.; Harriman, A. The Chemistry of Fluorescent Bodipy Dyes: Versatility Unsurpassed. *Angew. Chem. Int. Ed.* **2008**, *47*, 1184–1201.
- (22) Kahveci, Z.; Sekizkardes, A. K.; Arvapally, R. K.; Wilder, L.; El-Kaderi, H. M. Highly Porous Photoluminescent Diazaborole-Linked Polymers: Synthesis, Characterization, and Application to Selective Gas Adsorption. *Polym. Chem.* **2017**, *8*, 2509–2515.
- (23) Weber, L.; Stammler, H. G.; Neumann, B. Synthetic, Structural, and Electrochemical Studies of 2-ferrocenyl- and 2-cymantrenyl-functionalized 2,3-dihydro-1H-1,3,2-diazaboroles and 1,3,2-diazaborolidenes. *Eur. J. Inorg. Chem.* **2005**, 4715–4722.
- (24) Letsinger, R. L.; Hamilton, S. B. Organoboron Compounds. VIII. Dihydrobenzoboradiazoles. *J. Am. Chem. Soc.* **1958**, *80*, 5411–5413.
- (25) Mulvaney, J. E.; Bloomfield, J. J.; Marvel, C. S. Polybenzborimidazolines. *J.*

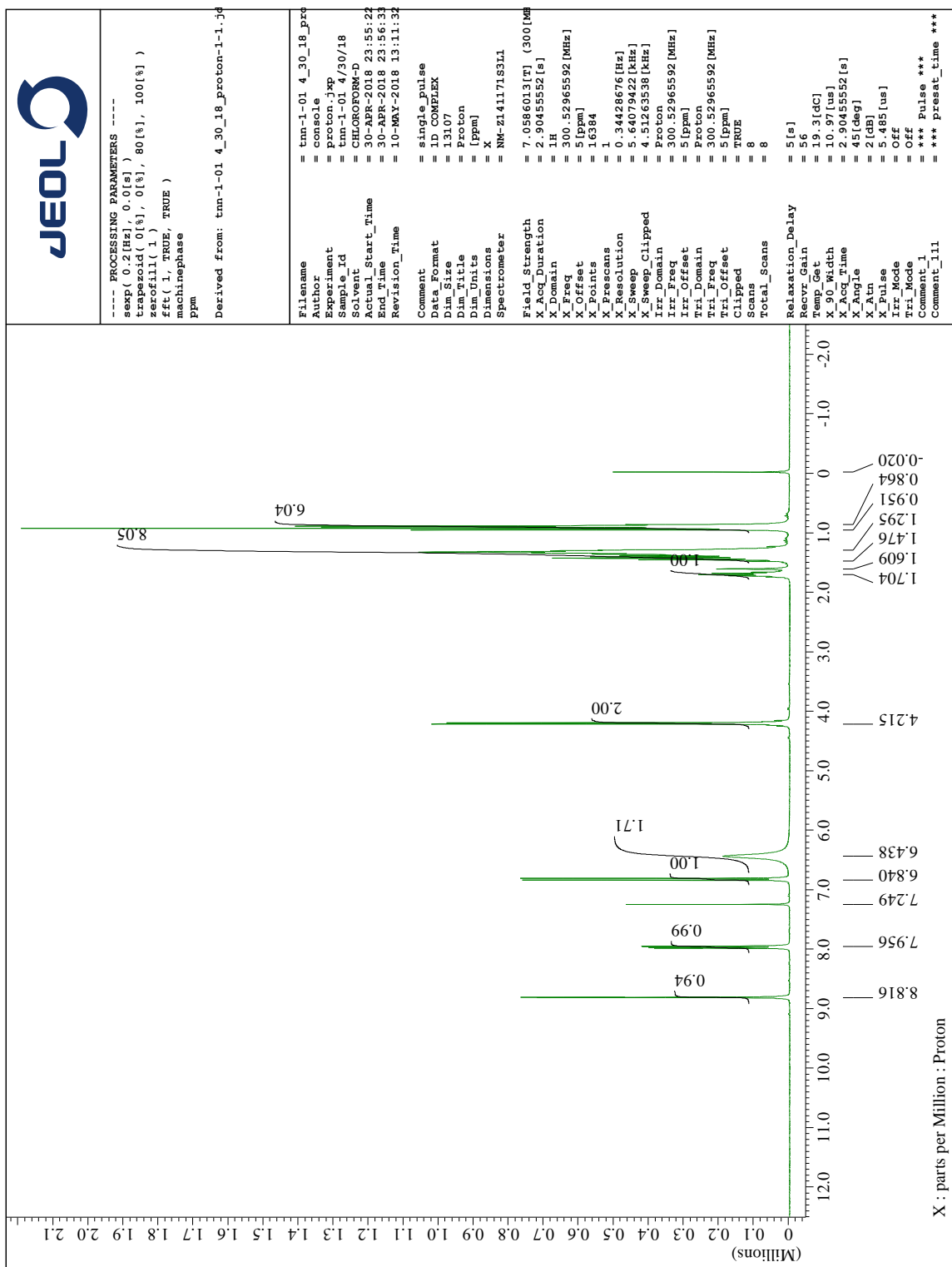
*Polym. Sci.* **1962**, *62*, 59–72.

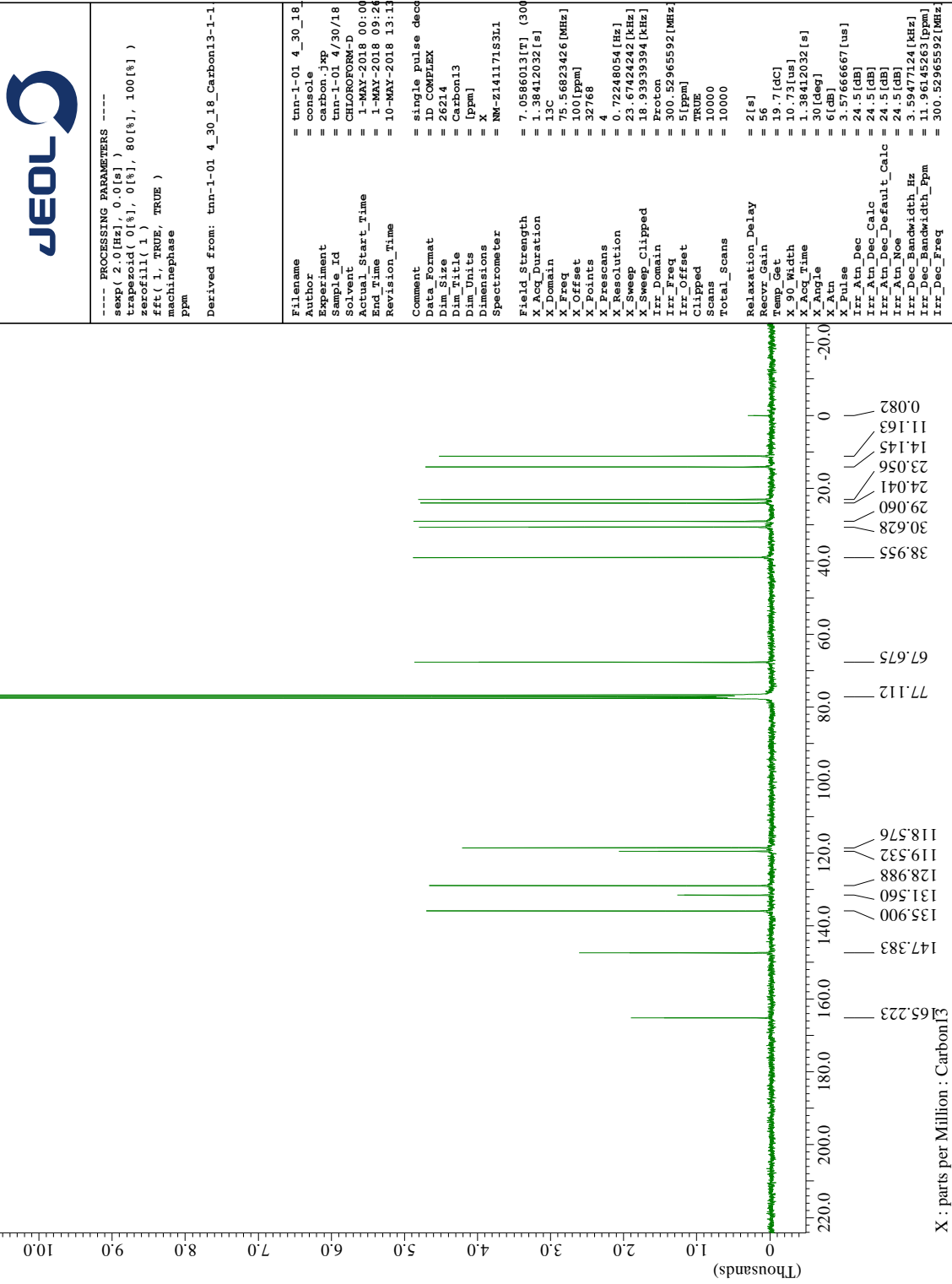
- (26) Kojima, T.; Kumaki, D.; Nishida, J.; Tokito, S.; Yamashita, Y. Organic field-effect transistors based on novel organic semiconductors containing diazaboroles. *J. Mater. Chem.* **2011**, *21*, 6607–6613.
- (27) Lokugama, S. Synthesis of Diazaborole Linked Oligomers using Aryl Boronic Acid Derivatives. M.S. Thesis, Sam Houston State University, 2015.
- (28) Manankandayalage, C. Synthesis of Diazaborole Based Macrocycles with Pendent Triethylene Glycol (Tg) Groups. M.S. Thesis, Sam Houston State University, 2016.
- (29) Maruyama, S.; Kawanishi, Y. Syntheses and Emission Properties of Novel Violet-Blue Emissive Aromatic bis(diazaborole)s. *J. Mater. Chem.* **2002**, *12*, 2245–2249.
- (30) Yamaguchi, I.; Choi, B.; Koizumi, T.; Kubota, K.; Yamamoto, T.  $\pi$ -Conjugated Polyphenylenes with Diazaborole Side Chains Synthesized via 1,2-Phenylenediamine Polymer. *Macromolecules* **2007**, *40*, 438–443.
- (31) Hawkins, R. T.; Lennarz, W. J.; Snyder, H. R. Arylboronic acids. V. Methyl-substituted boronic acids, borinic acids, and triarylborons. *J. Am. Chem. Soc.* **1960**, *82*, 3053–3059.
- (32) Slabber, C. A.; Grimmer, C. D.; Robinson, R. S. Solution-state  $^{15}\text{N}$  NMR and solid-state single-crystal XRD study of heterosubstituted diazaboroles and borinines prepared via an effective and simple microwave-assisted solvent-free synthesis. *J. Organomet. Chem.* **2013**, *723*, 122–128.
- (33) Son, J. H.; Jang, G.; Lee, T. S. Synthesis of water-soluble, fluorescent, conjugated polybenzodiazaborole for detection of cyanide anion in water. *Polym.* **2013**, *54*,

3542–3547.

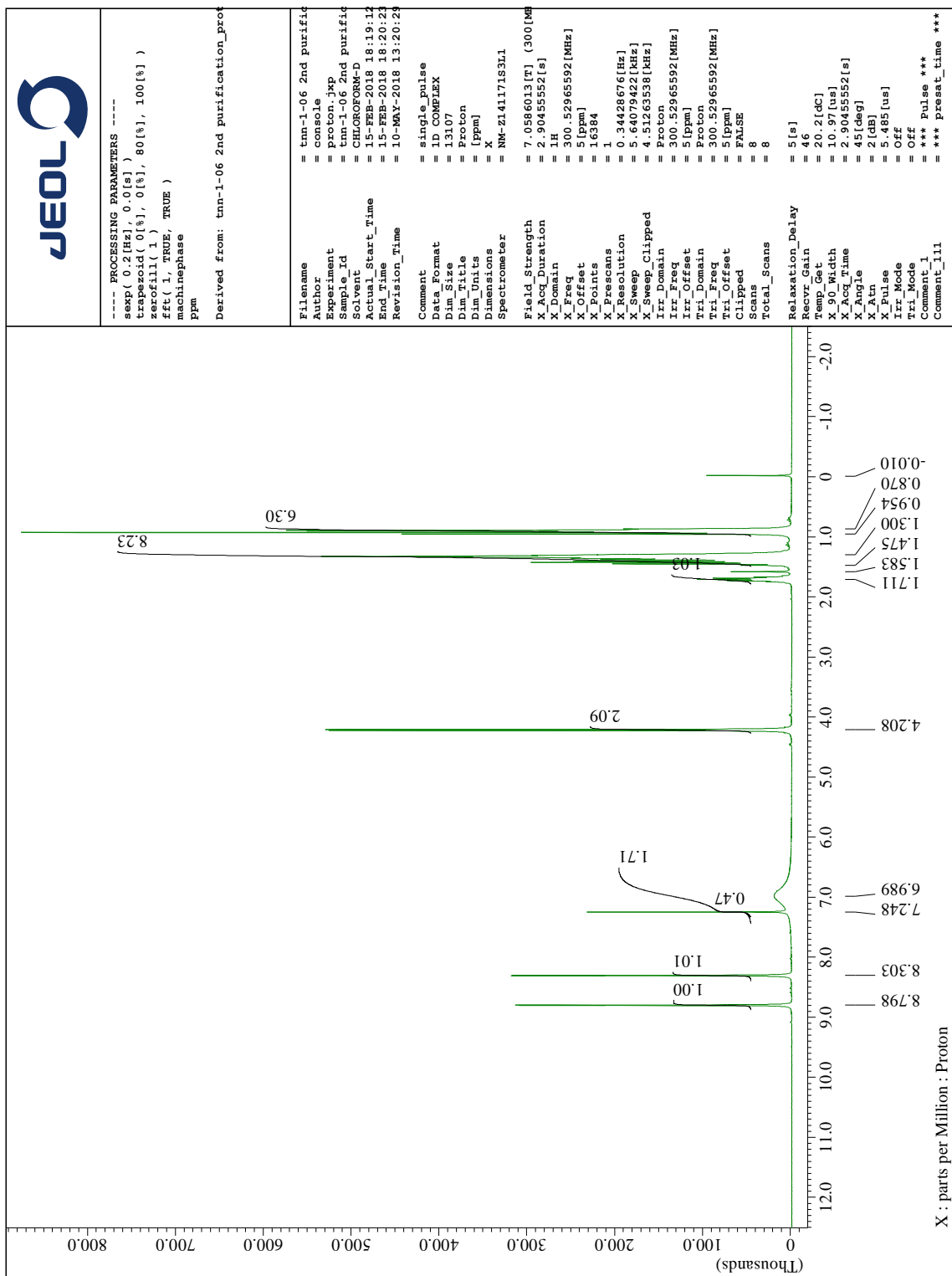
- (34) Abeysinghe, J. Diazaboroles: Experimental Investigations of their Dynamic Covalent Nature and Computational Chemistry. M.S. Thesis, Sam Houston State University, 2017.
- (35) Goldberg, A. R.; Northrop, B. H. Spectroscopic and Computational Investigations of The Thermodynamics of Boronate Ester and Diazaborole Self-Assembly. *J. Org. Chem.* **2016**, *81*, 969–980.
- (36) Pelletier, M. J. Quantitative Analysis Using Raman Spectrometry. *Appl. Spectrosc.* **2003**, *57*, 20A–42A.
- (37) Rambo, B. M.; Lavigne, J. J. Defining Self-Assembling Linear Oligo(dioxaborole)s. *Chem. Mater.* **2007**, *19*, 3732–3739.
- (38) *Unpublished data obtained by Angela Caffey.*
- (39) Roy, C.; Brown, H. A Comparative Study of the Relative Stability of Representative Chiral and Achiral Boronic Esters Employing Transesterification. *Monatsh. Chem.* **2007**, *138*, 879–887.

## APPENDIX – NMR spectra for the synthesized compounds

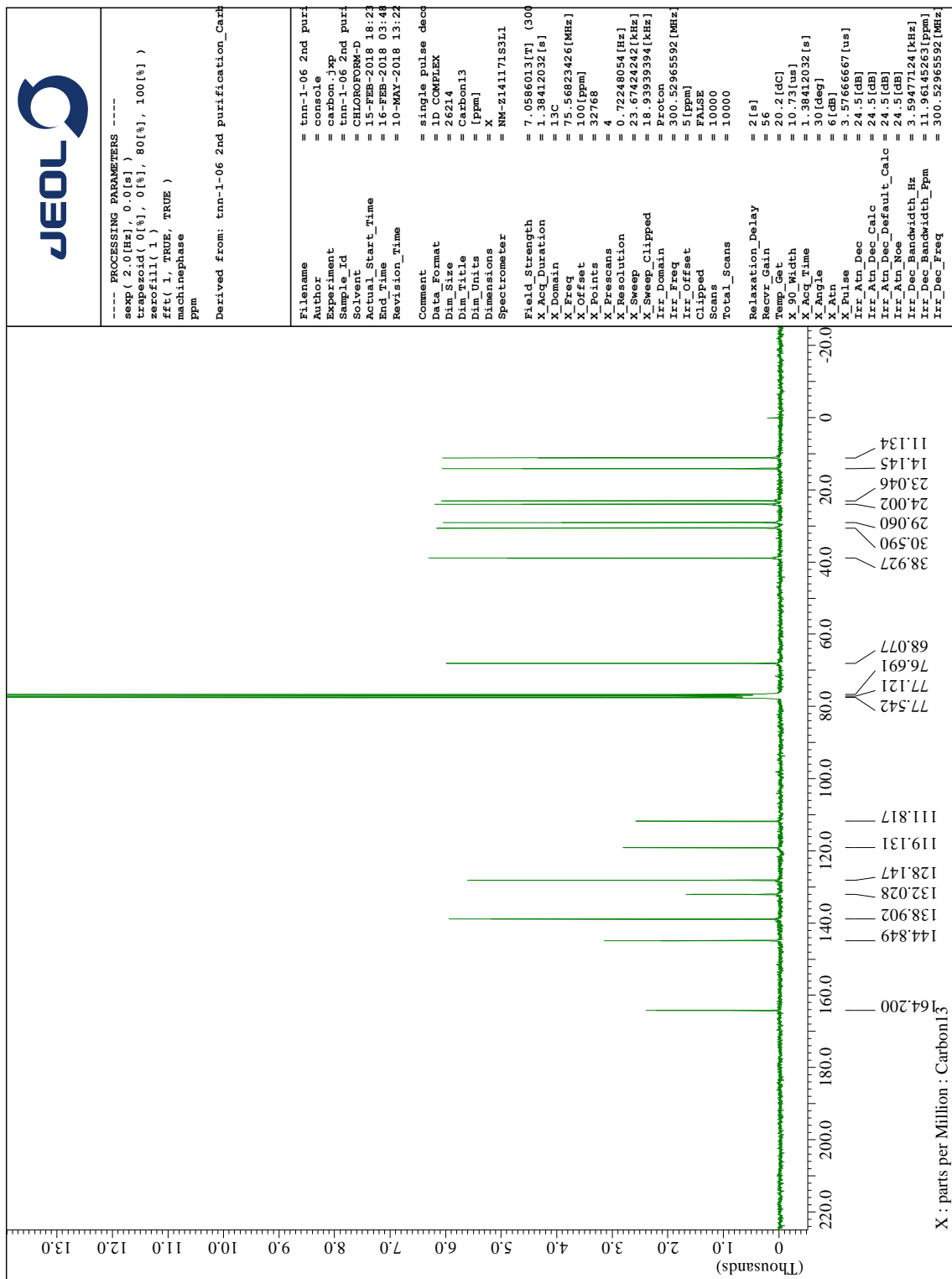
<sup>1</sup>H NMR spectrum of 2-ethylhexyl 4-amino-3-nitrobenzoate (**6**) in CDCl<sub>3</sub>



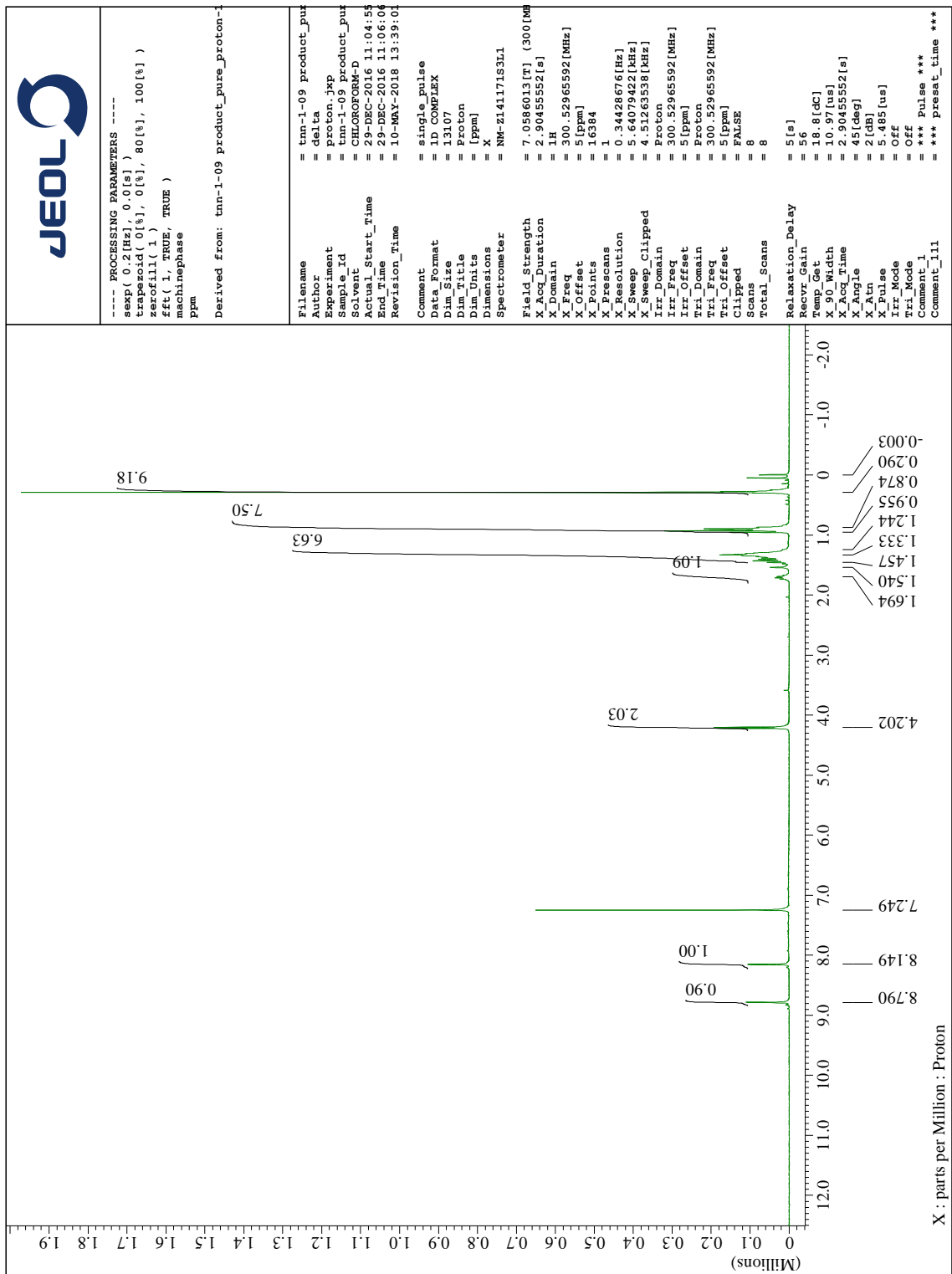
$^{13}\text{C}$  NMR spectrum of 2-ethylhexyl 4-amino-3-nitrobenzoate (**6**) in  $\text{CDCl}_3$



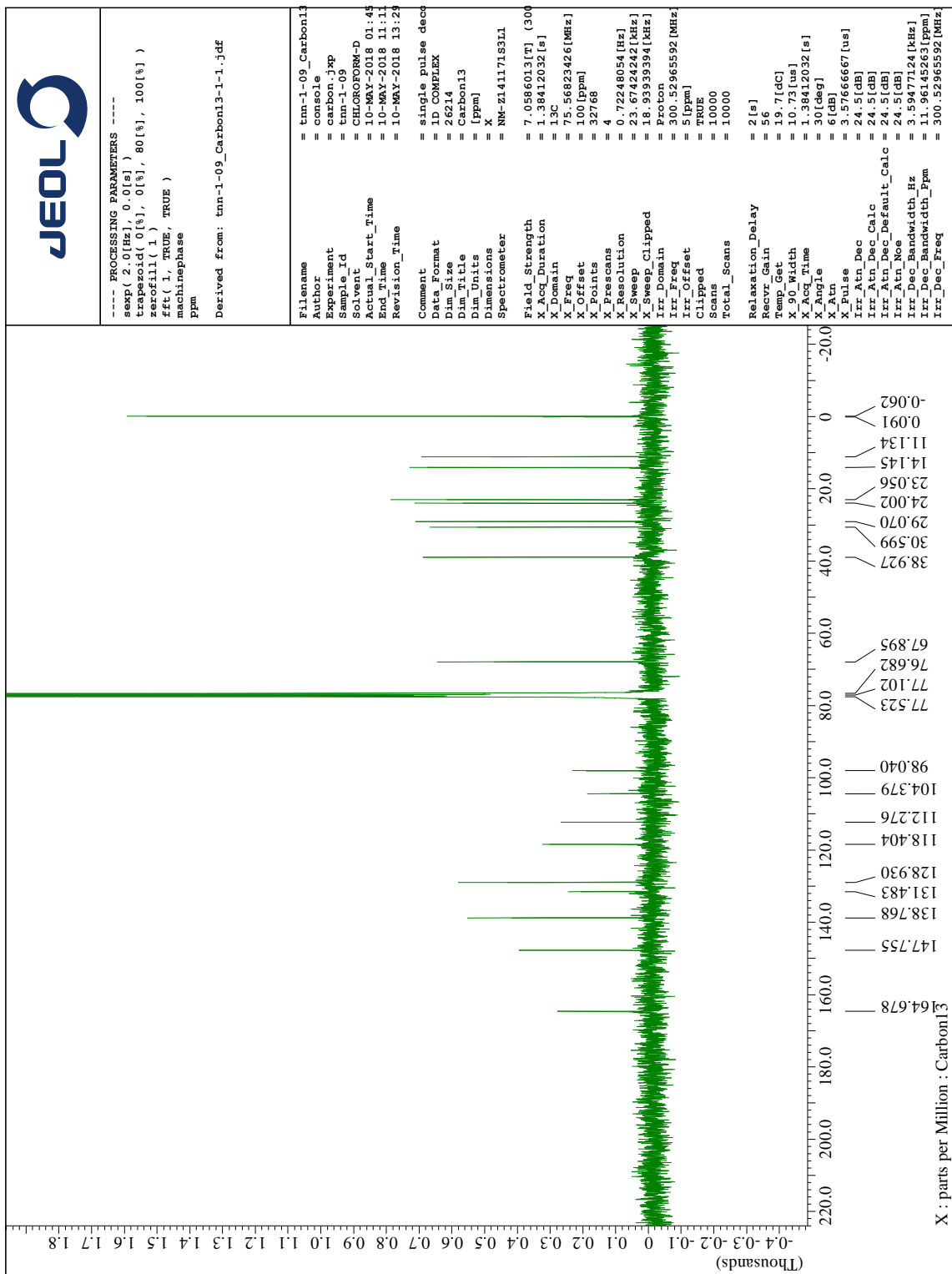
$^1\text{H}$  NMR spectrum of 2-ethylhexyl 4-amino-3-bromo-5-nitrobenzoate (**7**) in  $\text{CDCl}_3$



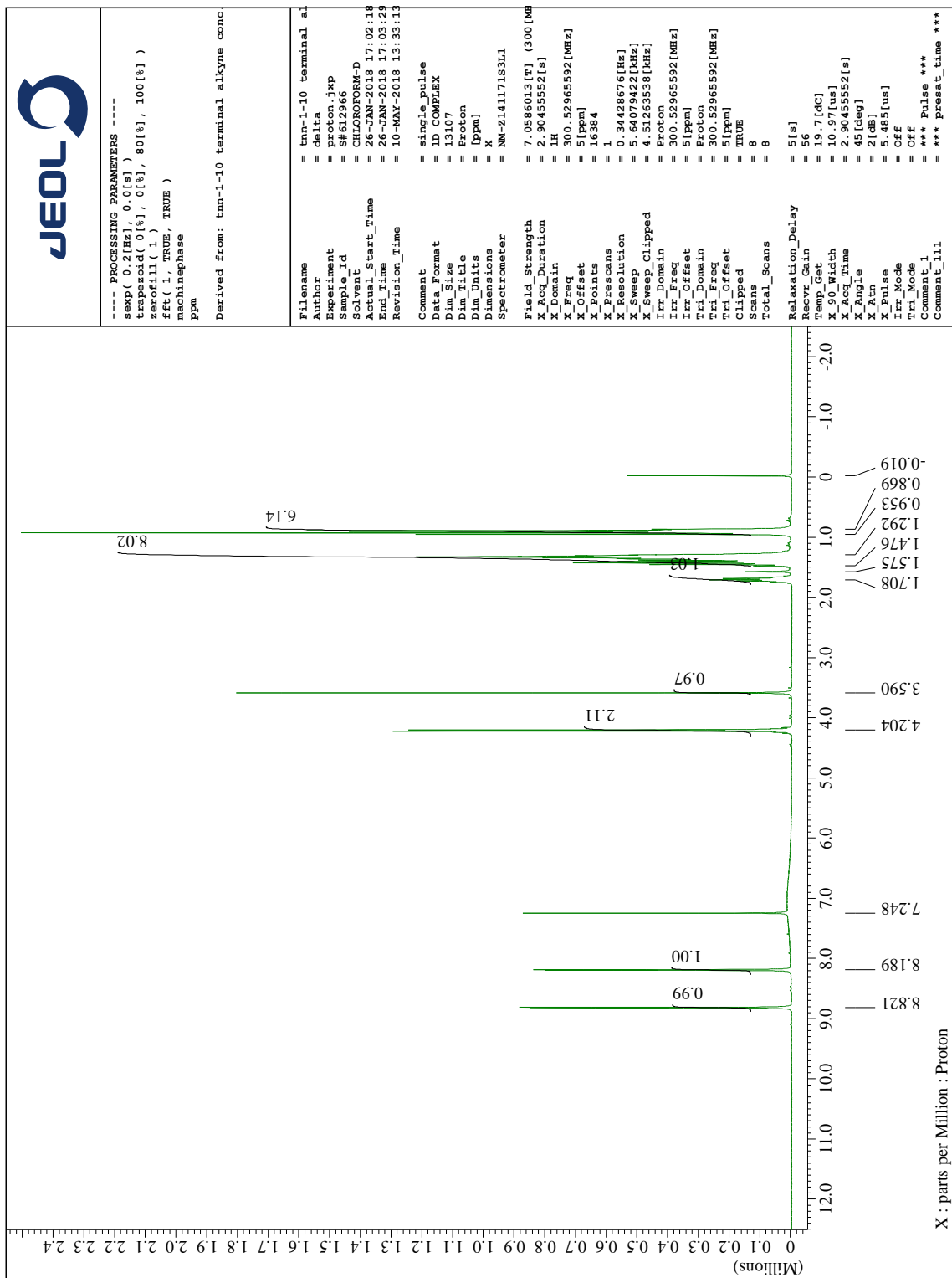
$^{13}\text{C}$  NMR spectrum of 2-ethylhexyl 4-amino-3-bromo-5-nitrobenzoate (**7**) in  $\text{CDCl}_3$



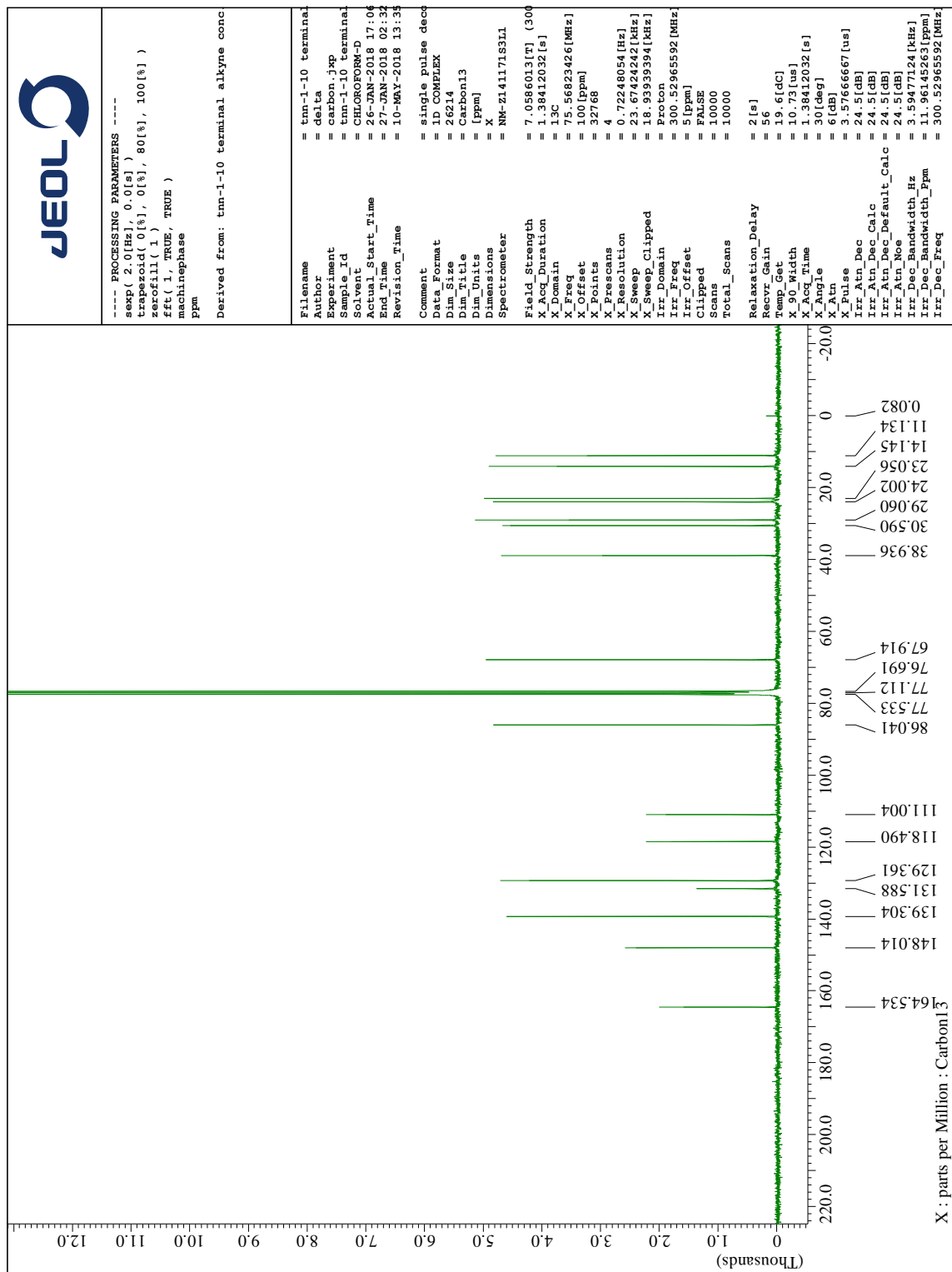
$^1\text{H}$  NMR spectrum of 2-ethylhexyl 4-amino-3-((trimethylsilyl)ethynyl)-5-nitrobenzoate (**8**) in  $\text{CDCl}_3$



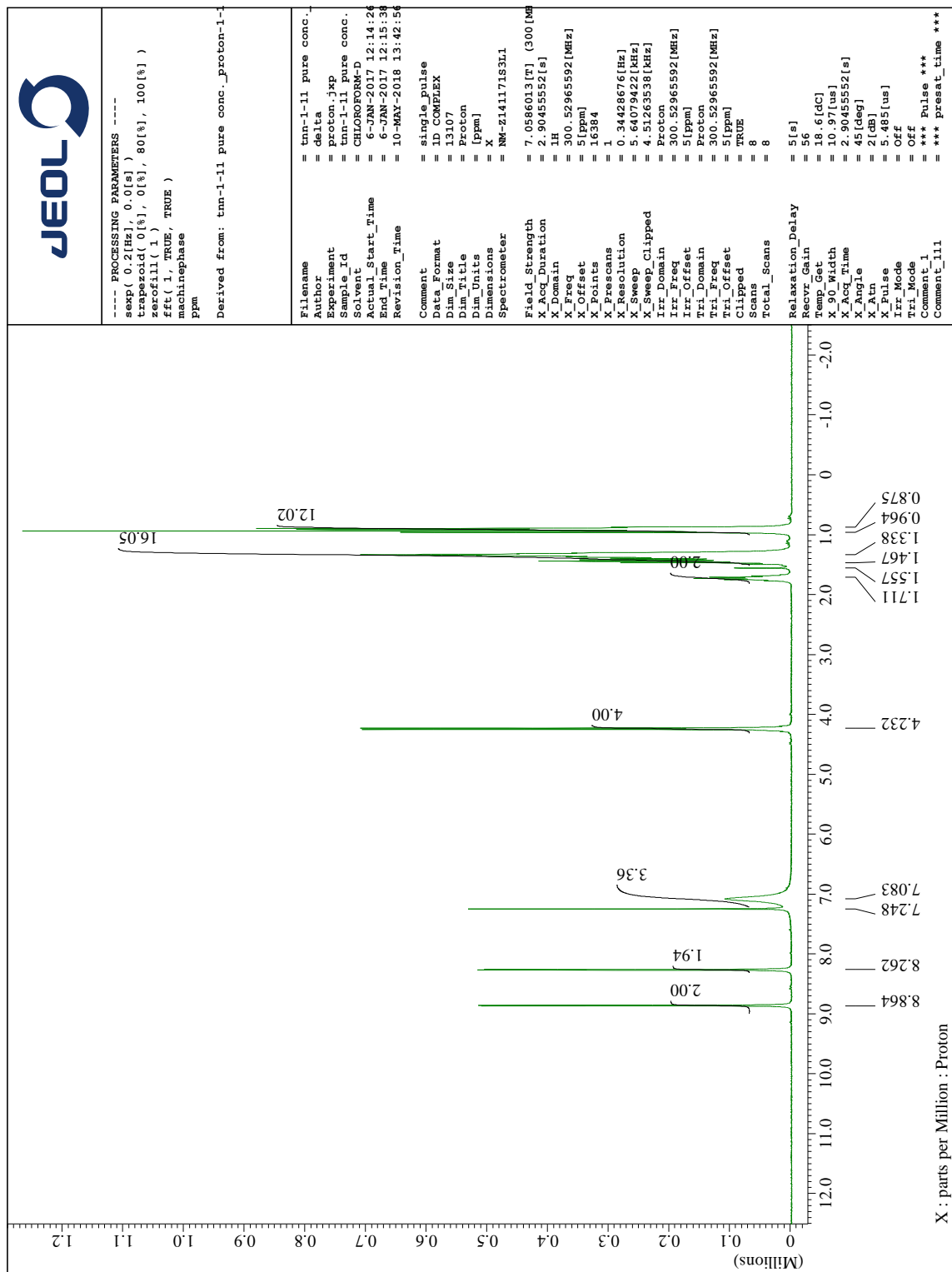
$^{13}\text{C}$  NMR spectrum of 2-ethylhexyl 4-amino-3-((trimethylsilyl)ethynyl)-5-nitrobenzoate (**8**) in  $\text{CDCl}_3$



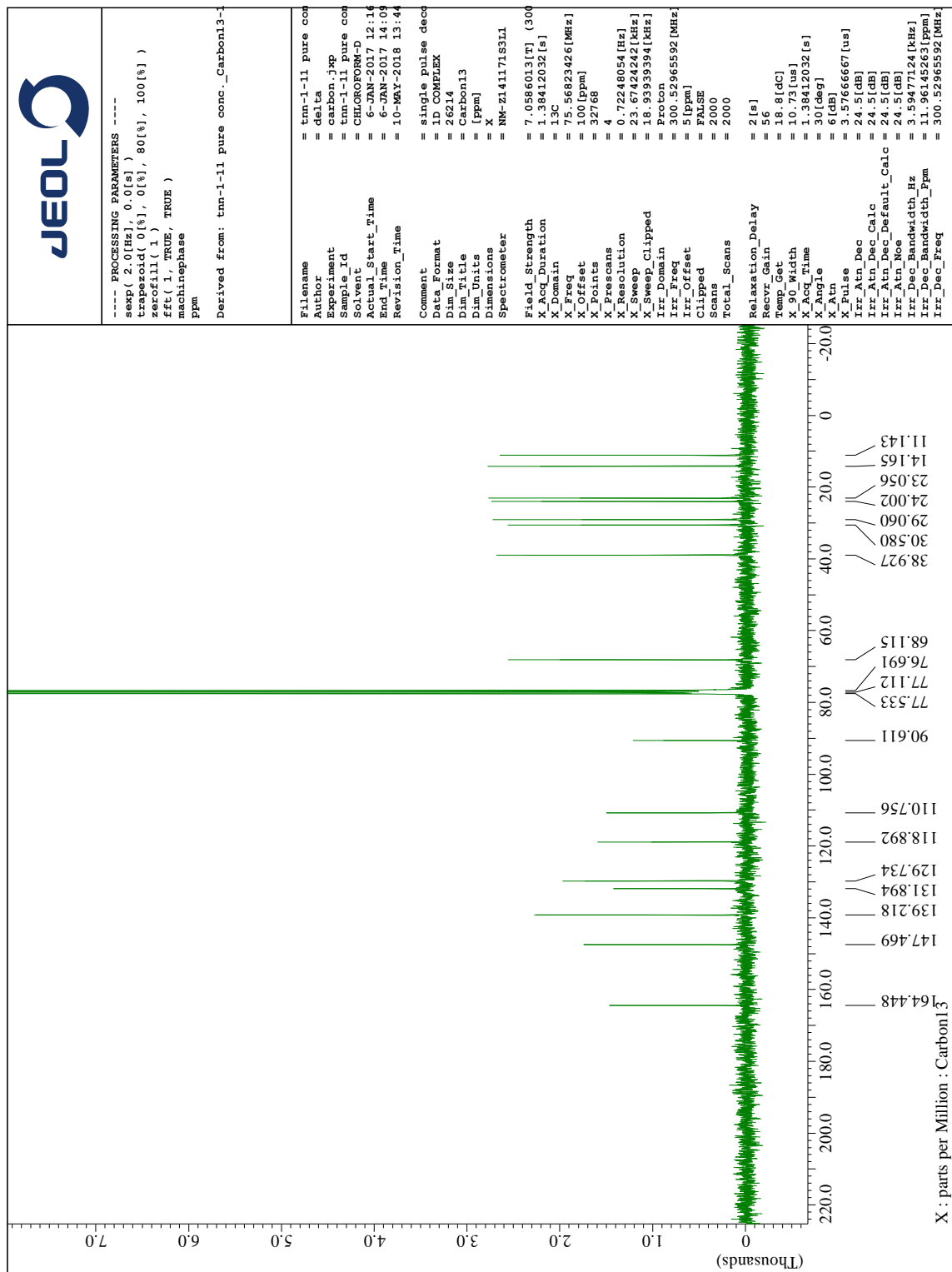
<sup>1</sup>H NMR spectrum of 2-ethylhexyl 4-amino-3-ethynyl-5-nitrobenzoate (**9**) in CDCl<sub>3</sub>



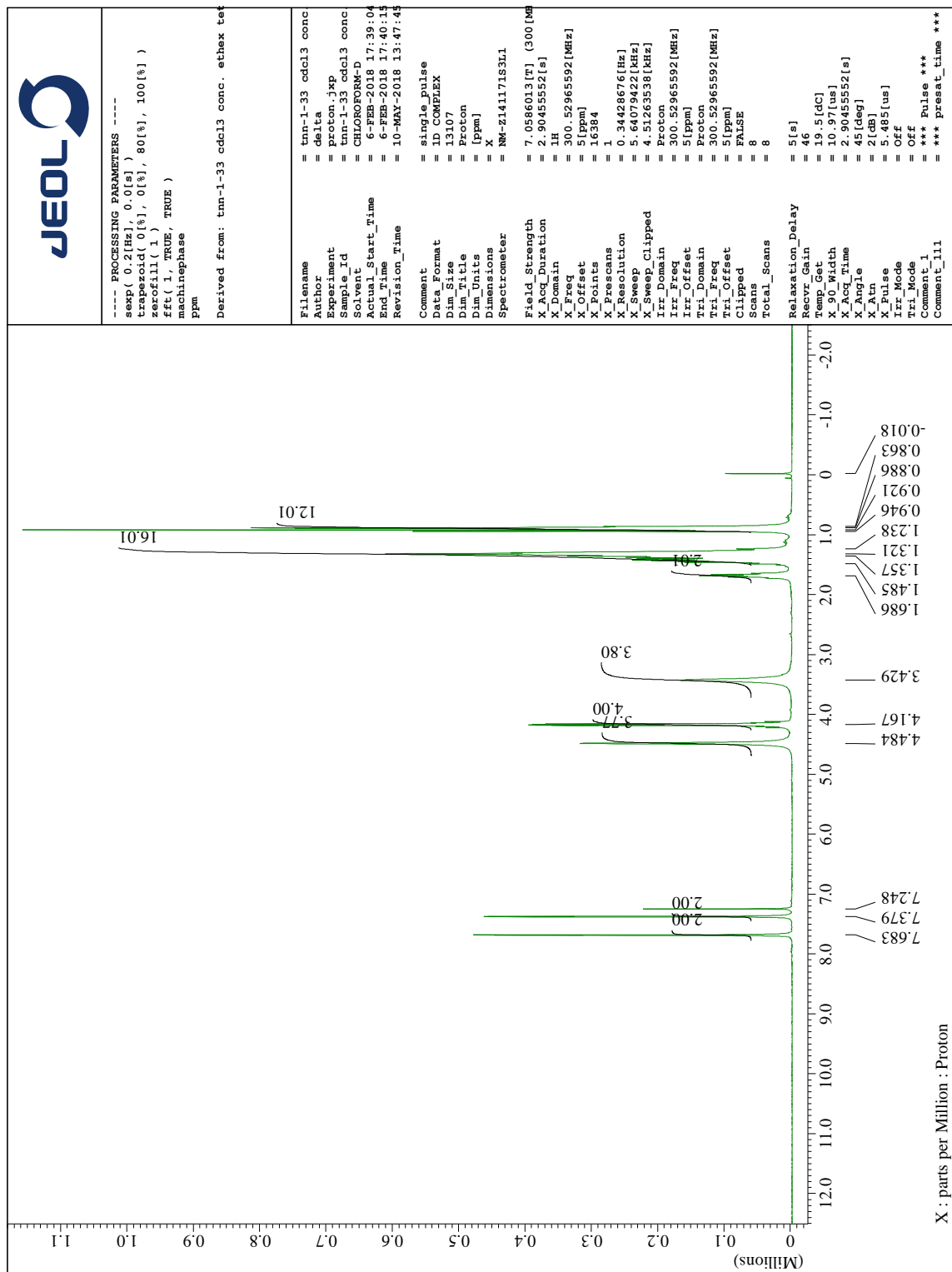
$^{13}\text{C}$  NMR spectrum of 2-ethylhexyl 4-amino-3-ethynyl-5-nitrobenzoate (**9**) in  $\text{CDCl}_3$



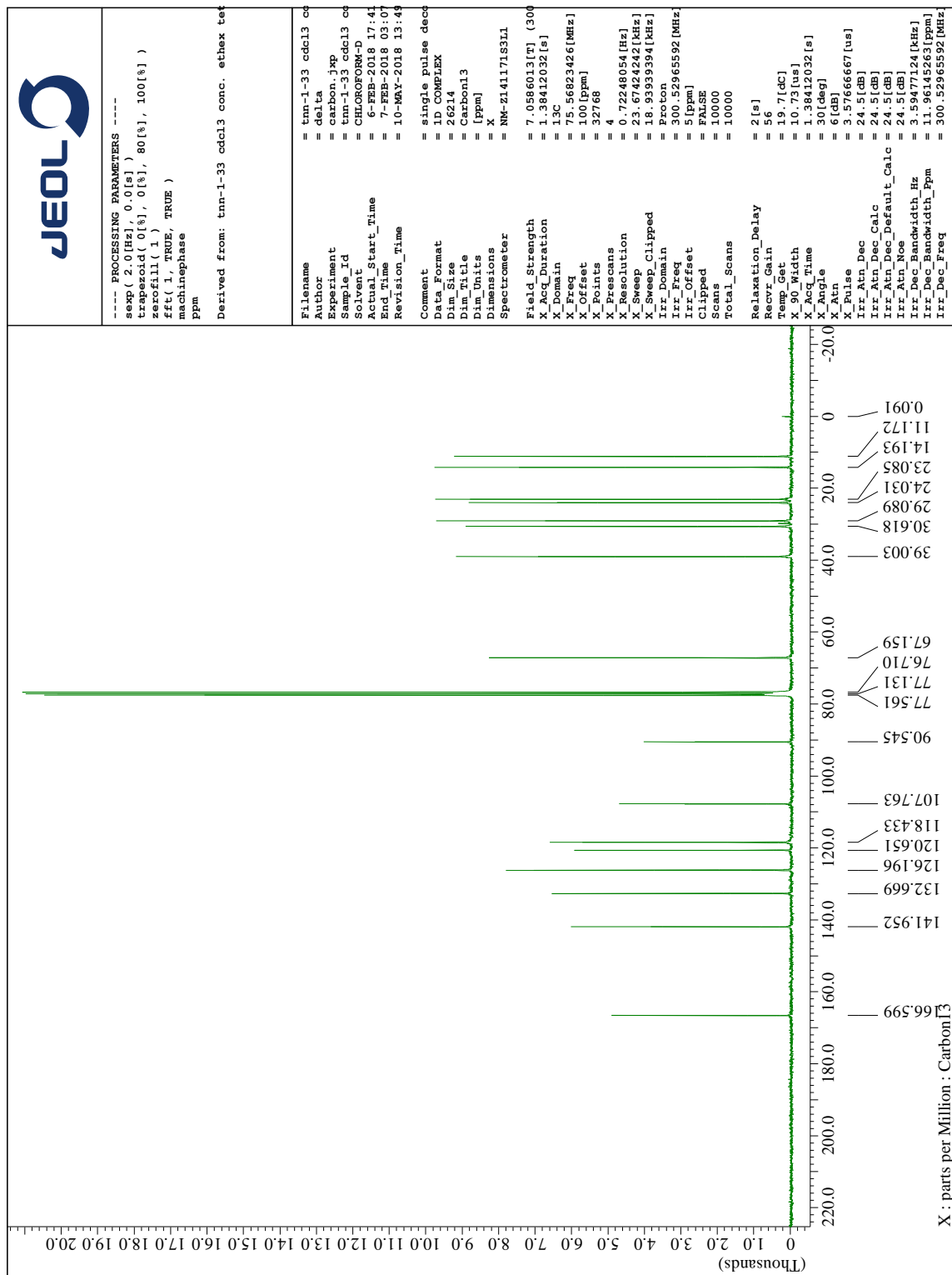
$^1\text{H}$  NMR spectrum of 3,3'-(ethyne-1,2-diyl)bis(2-ethylhexyl 5-nitro-4-aminobenzoate) (**10**) in  $\text{CDCl}_3$



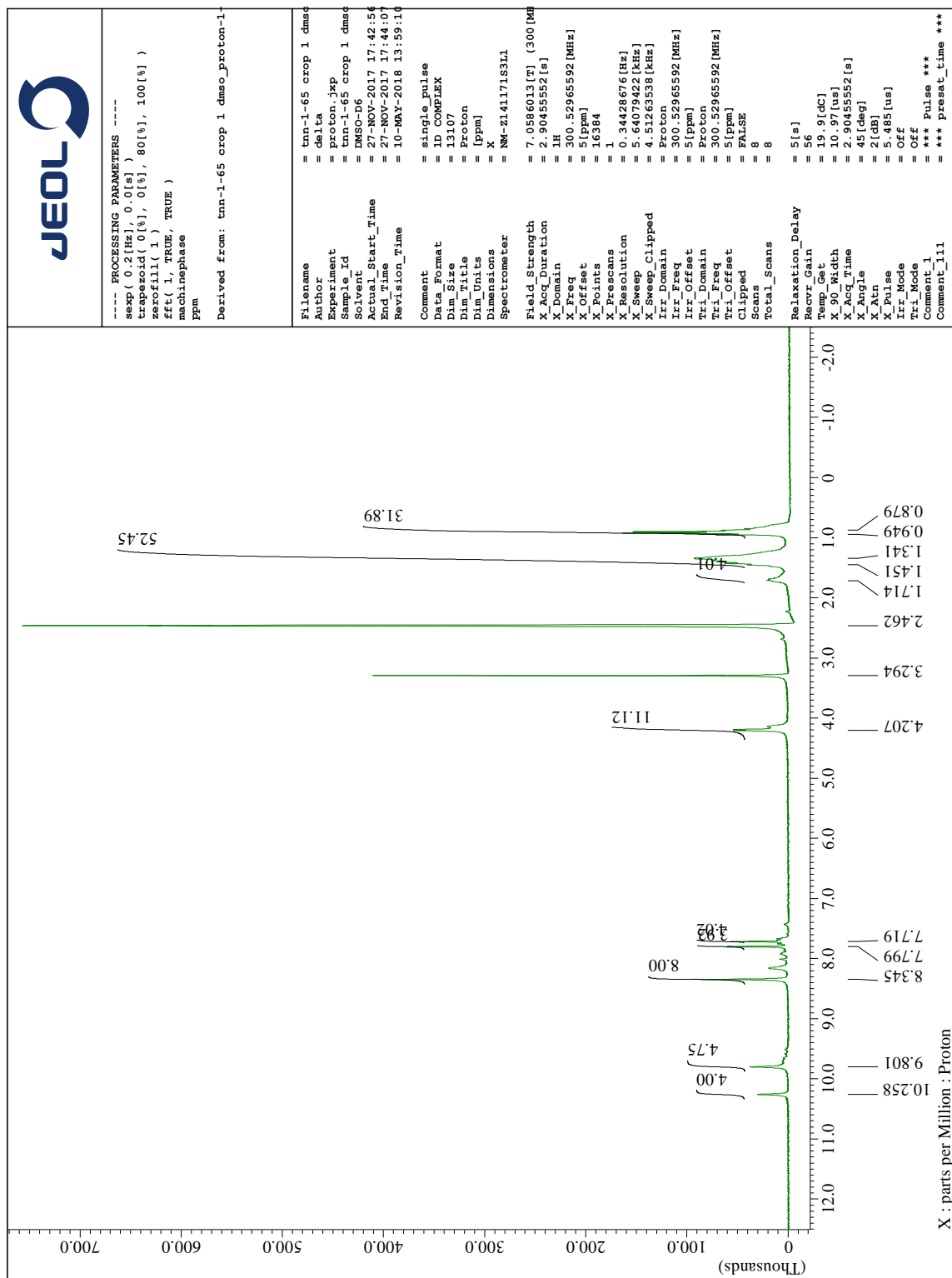
$^{13}\text{C}$  NMR spectrum of 3,3'-(ethyne-1,2-diyl)bis(2-ethylhexyl 5-nitro-4-aminobenzoate) (10) in  $\text{CDCl}_3$



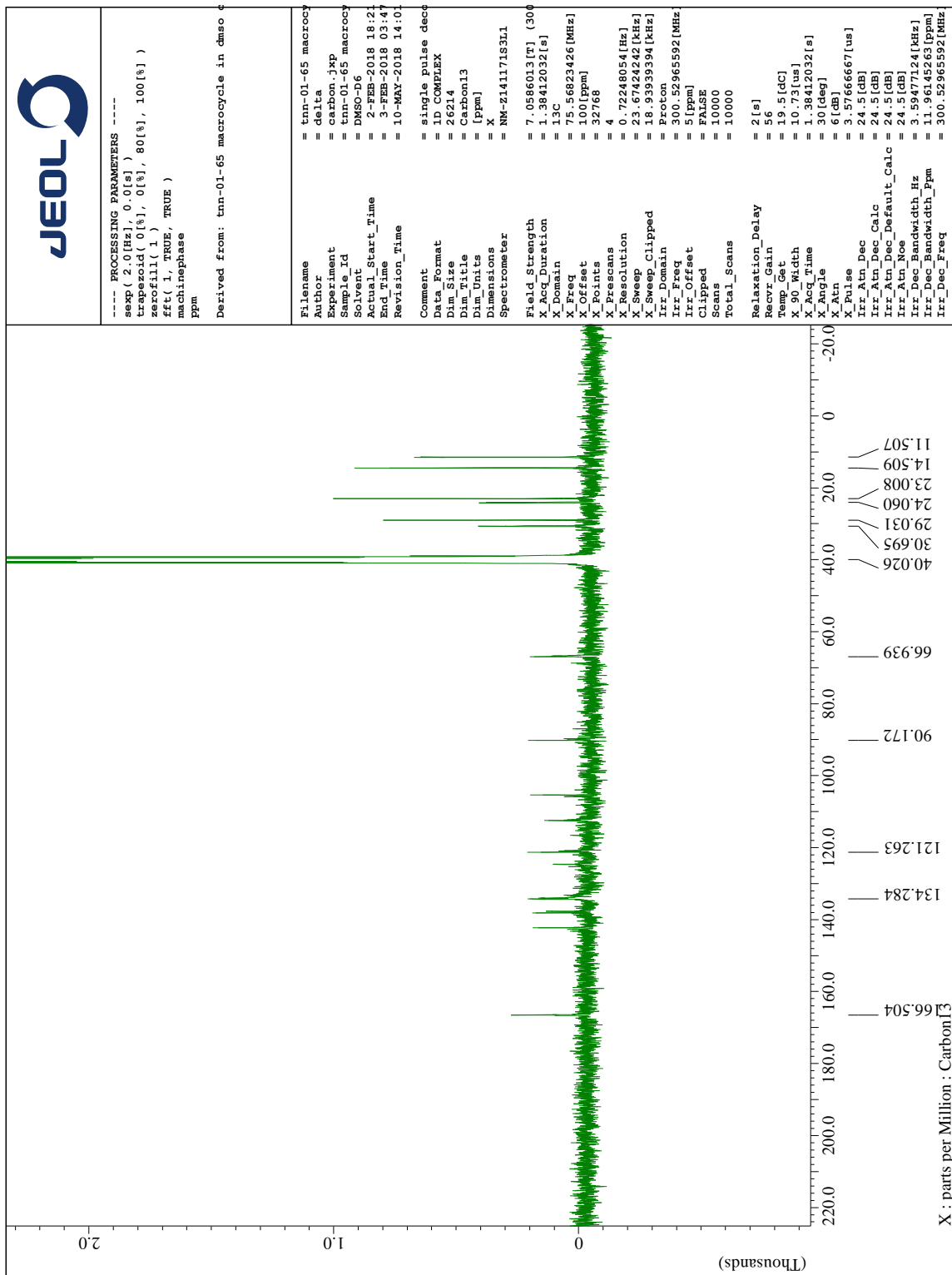
$^1\text{H}$  NMR spectrum of 3,3'-(ethyne-1,2-diyl)bis(2-ethylhexyl 4,5-diaminobenzoate) (TA-DEH) in  $\text{CDCl}_3$



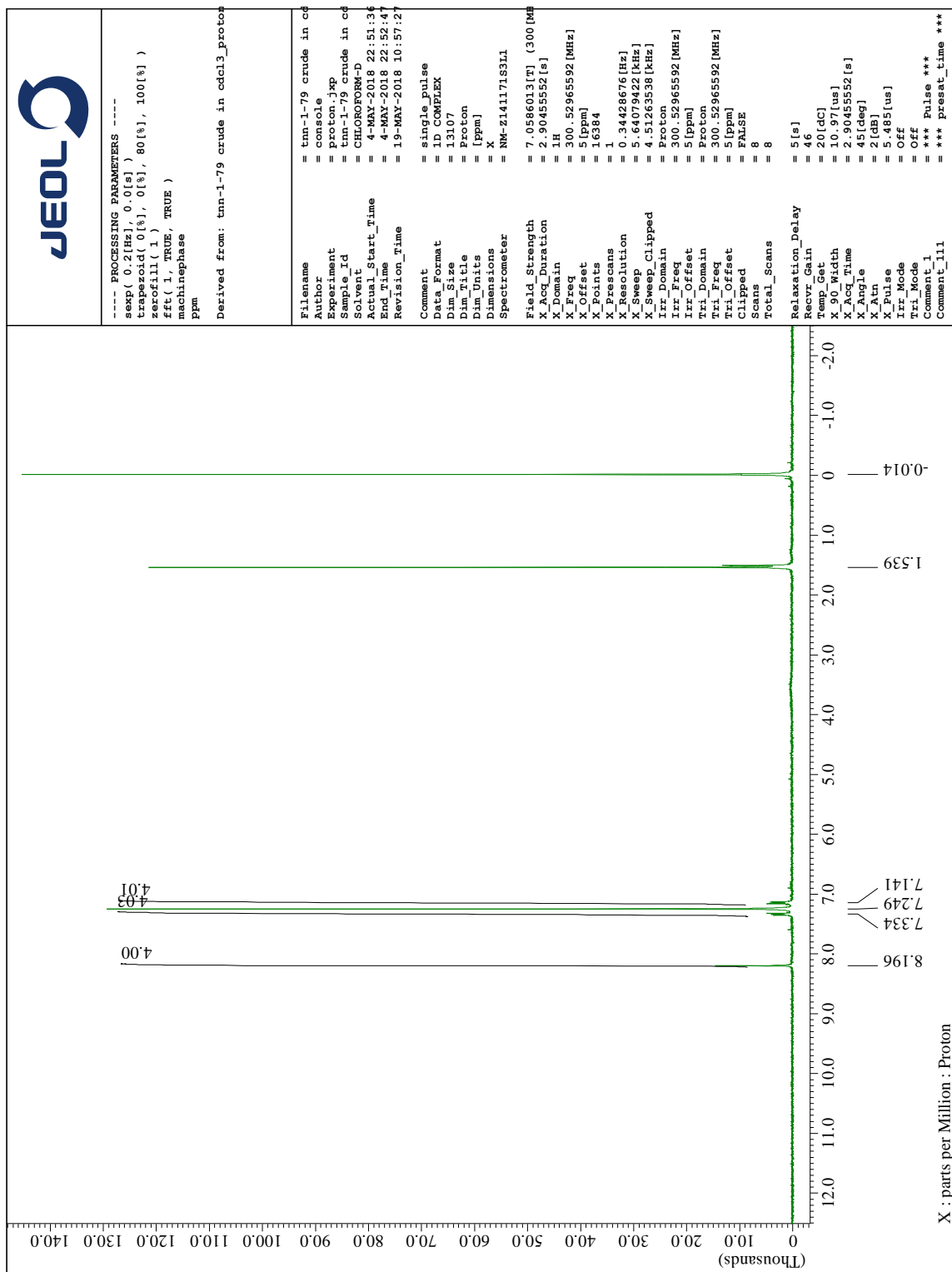
<sup>13</sup>C NMR spectrum of 3,3'-(ethyne-1,2-diyl)bis(2-ethylhexyl 4,5-diaminobenzoate) (TA-DEH) in CDCl<sub>3</sub>

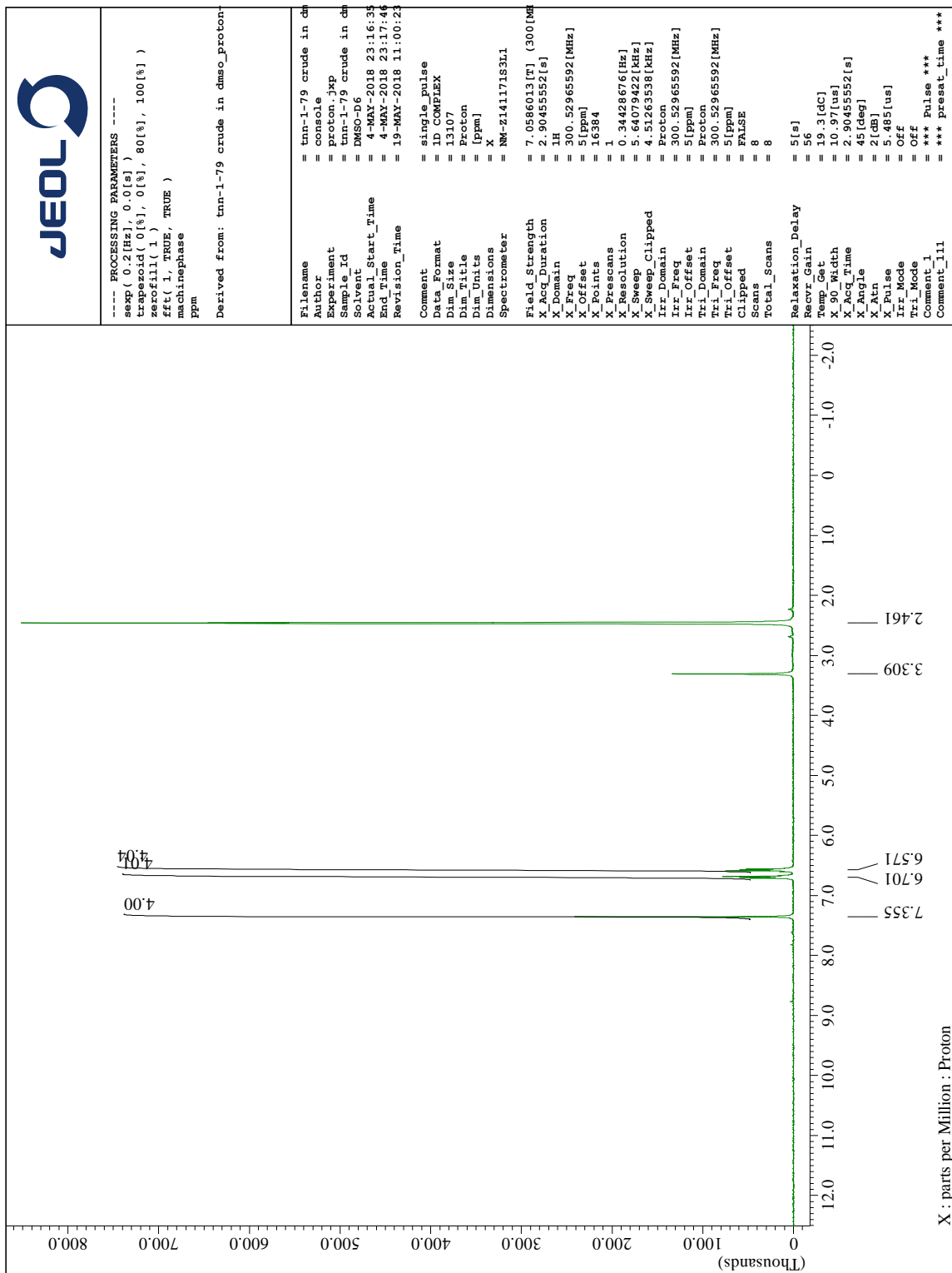


$^1\text{H}$  NMR spectrum of the product mixture from Figure 42 in  $\text{DMSO-}d_6$

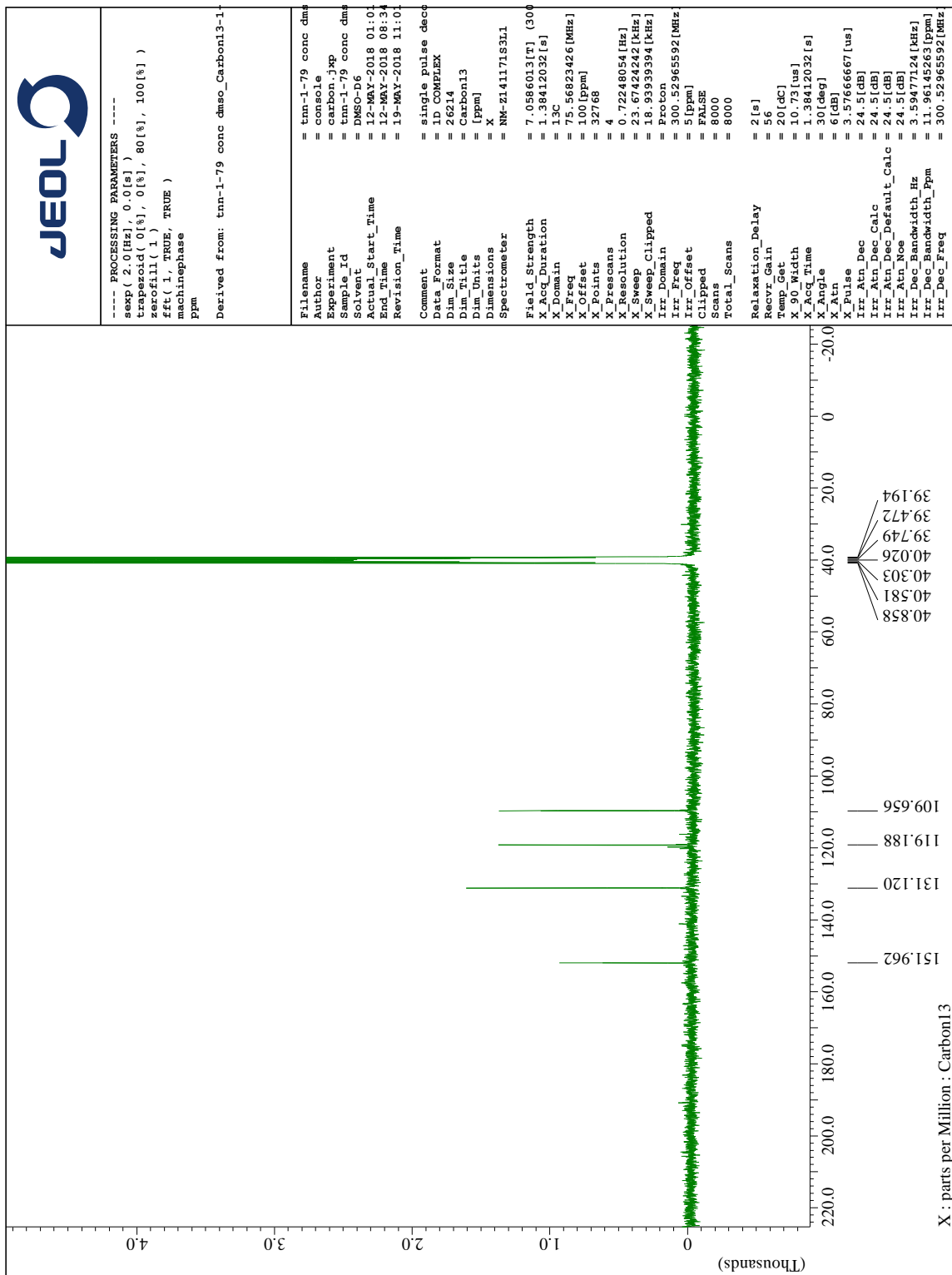


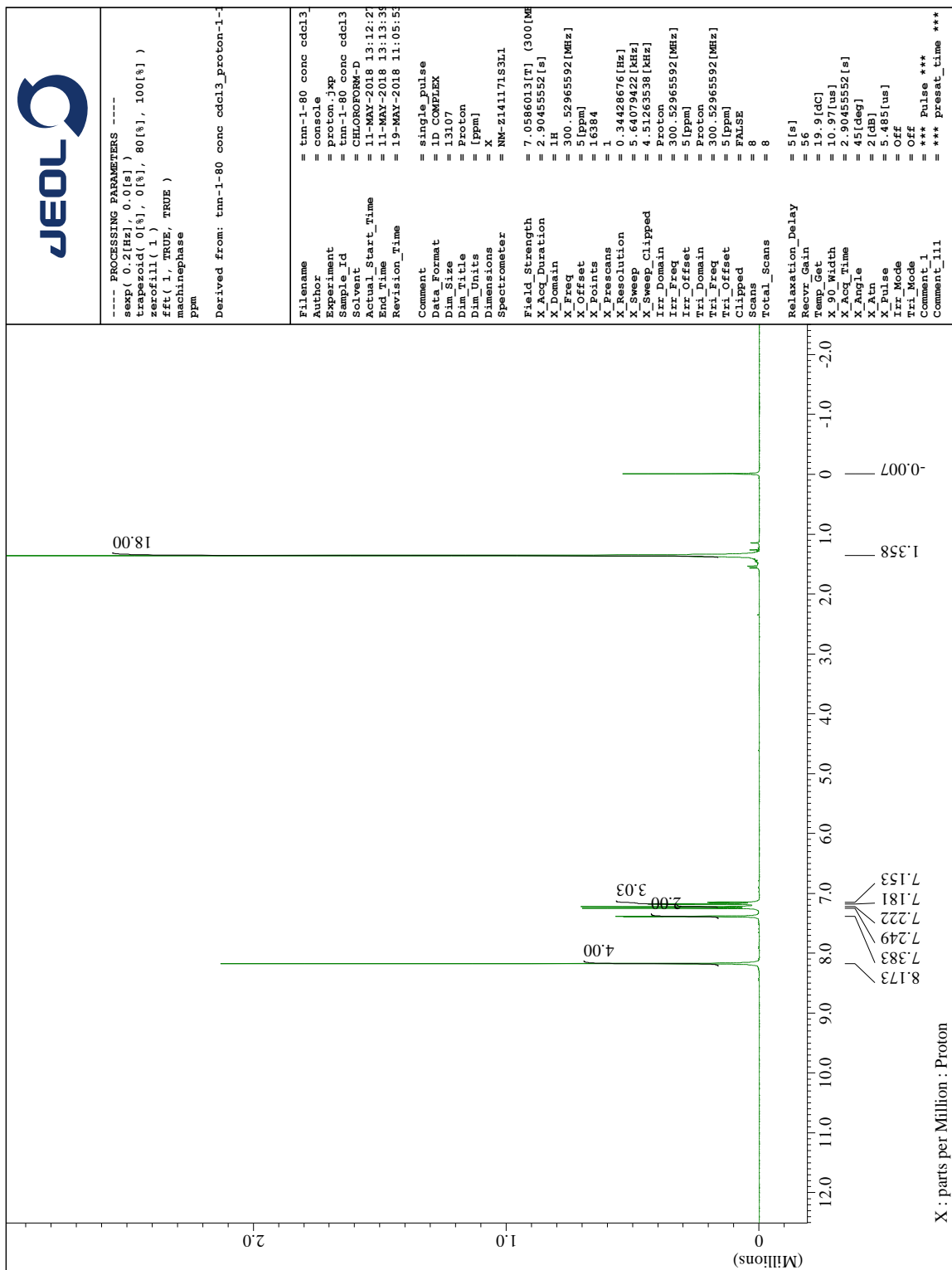
<sup>13</sup>C NMR spectrum of the product mixture from Figure 42 in DMSO-*d*<sub>6</sub>

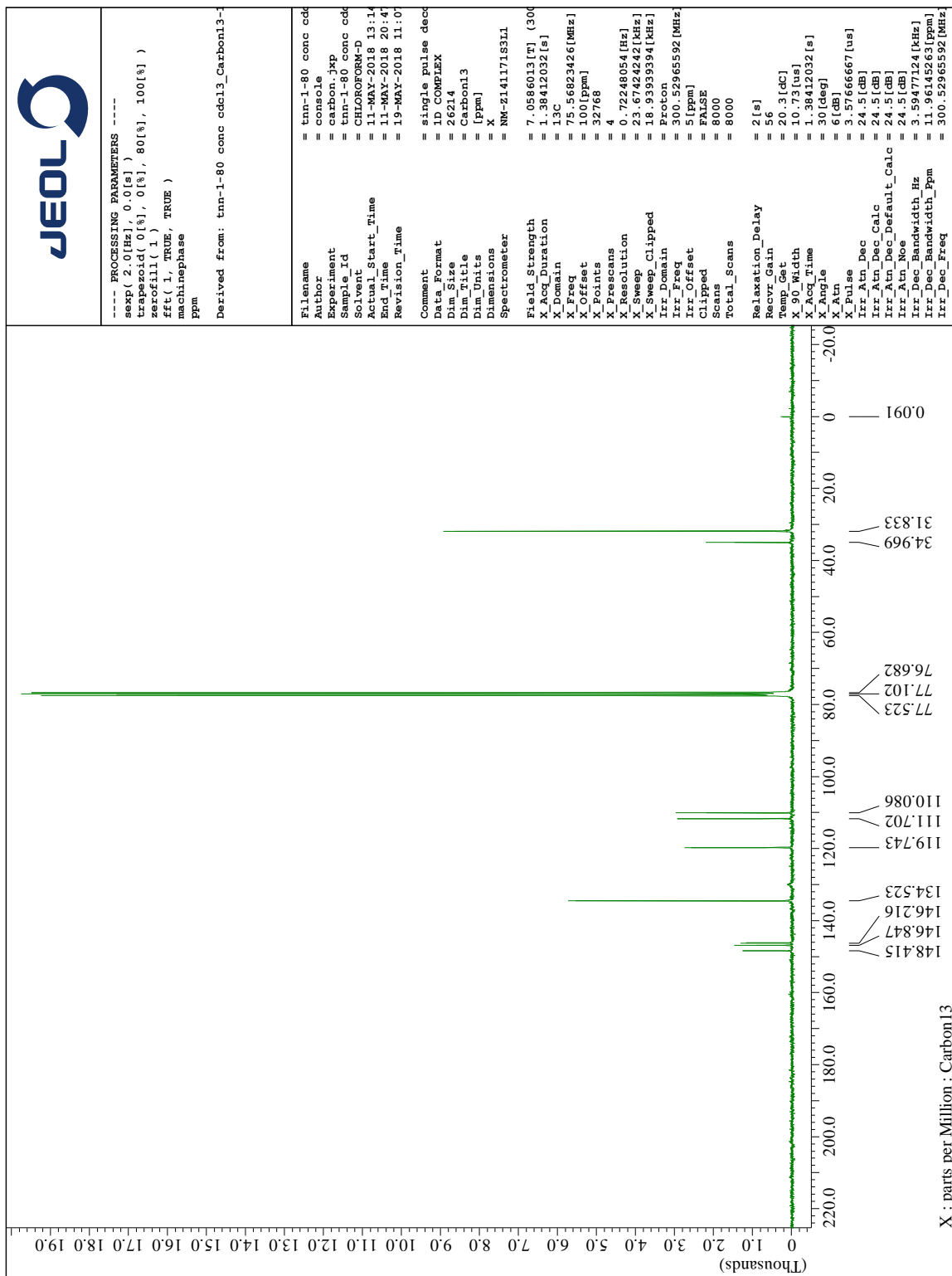

 $^1\text{H}$  NMR of 2,2'-(1,4-phenylene)bis(1,3,2-benzodioxaborole) (**13**) in  $\text{CDCl}_3$



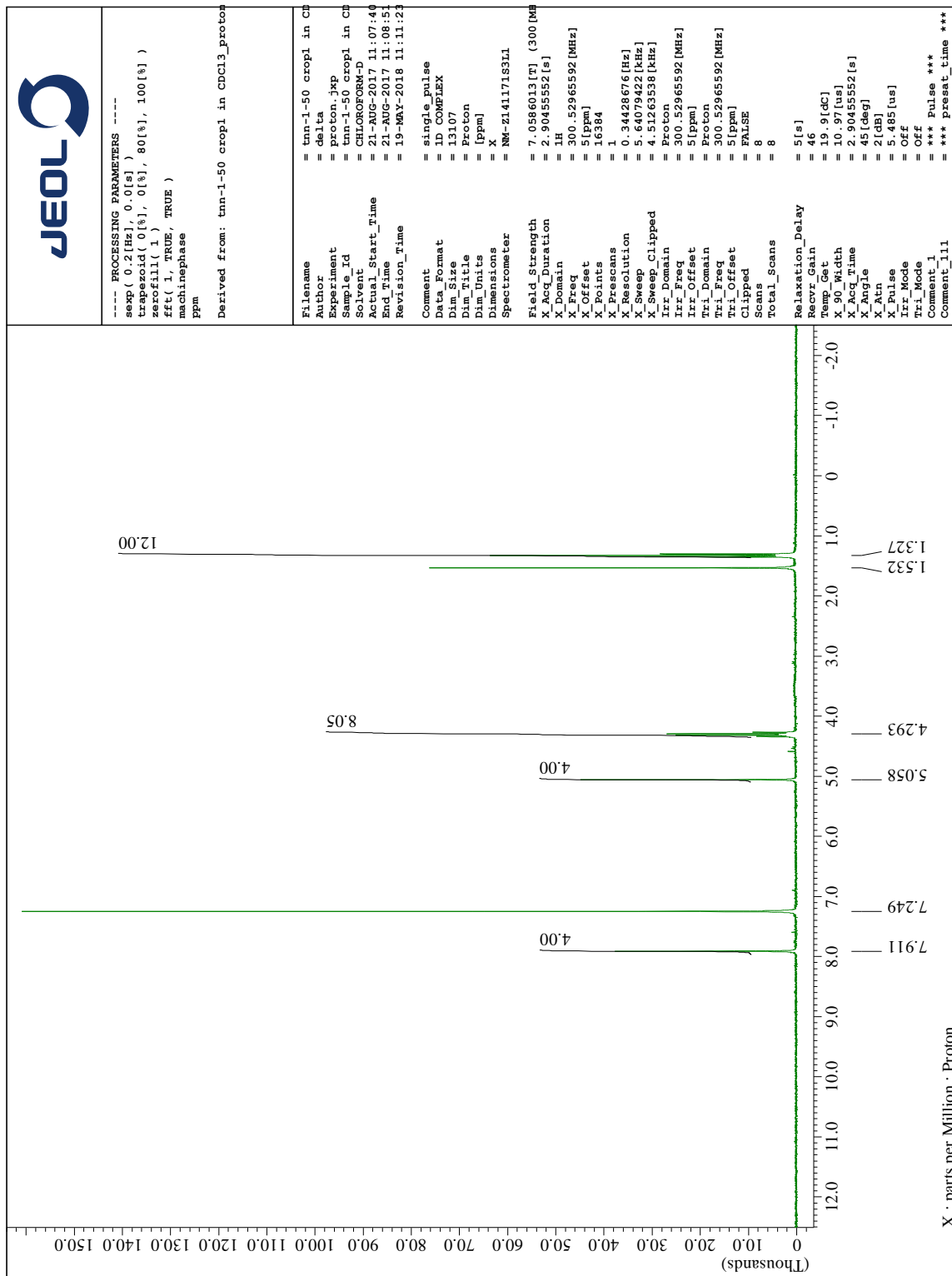
$^1\text{H}$  NMR of 2,2'-(1,4-phenylene)bis(1,3,2-benzodioxaborole) (**13**) in DMSO- $d_6$

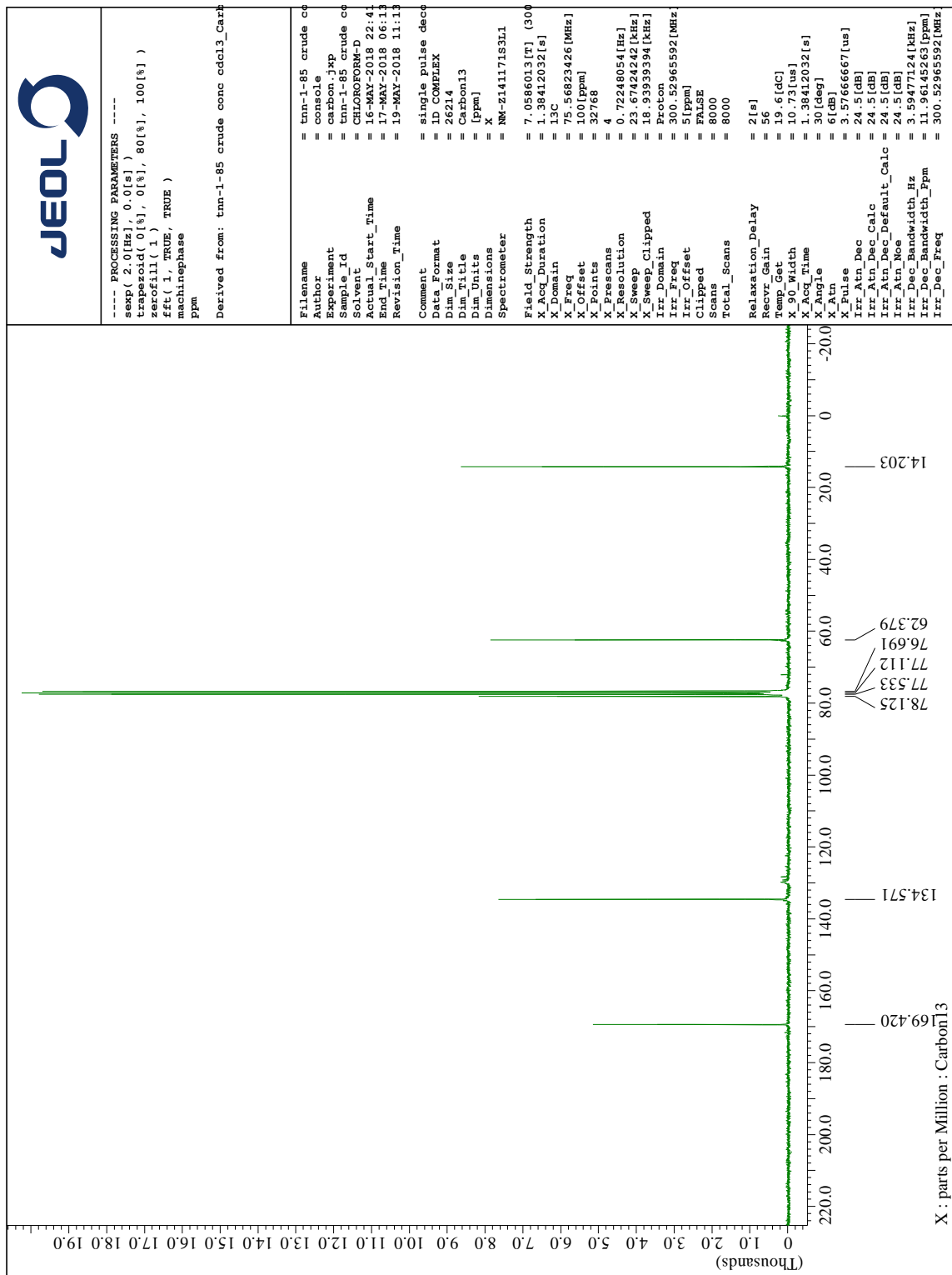

 $^{13}\text{C}$  NMR of 2,2'-(1,4-phenylene)bis(1,3,2-benzodioxaborole) (**13**) in DMSO- $d_6$

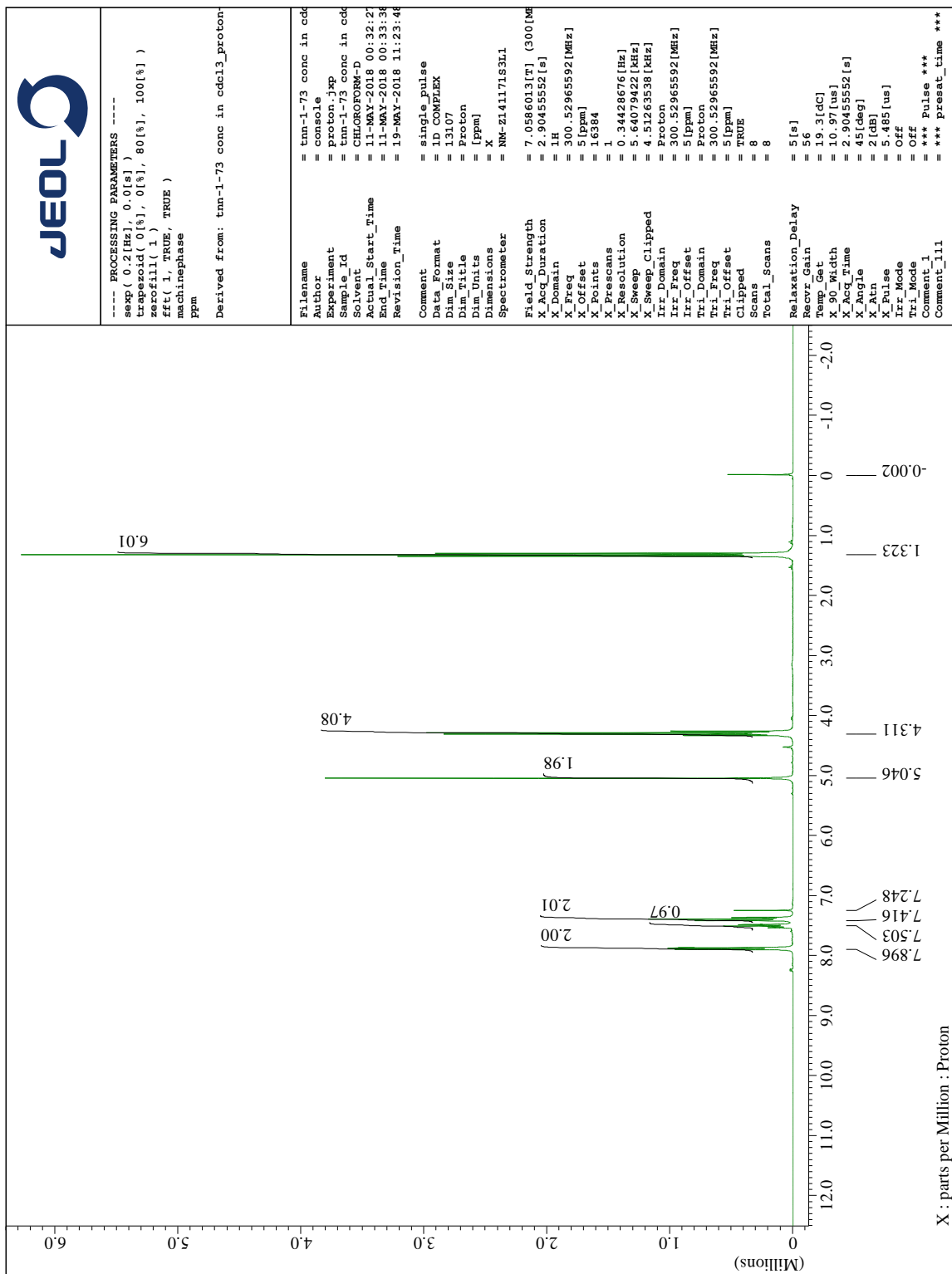

 $^1\text{H}$  NMR of the *t*-butyl BDBA-based ester **15** in  $\text{CDCl}_3$



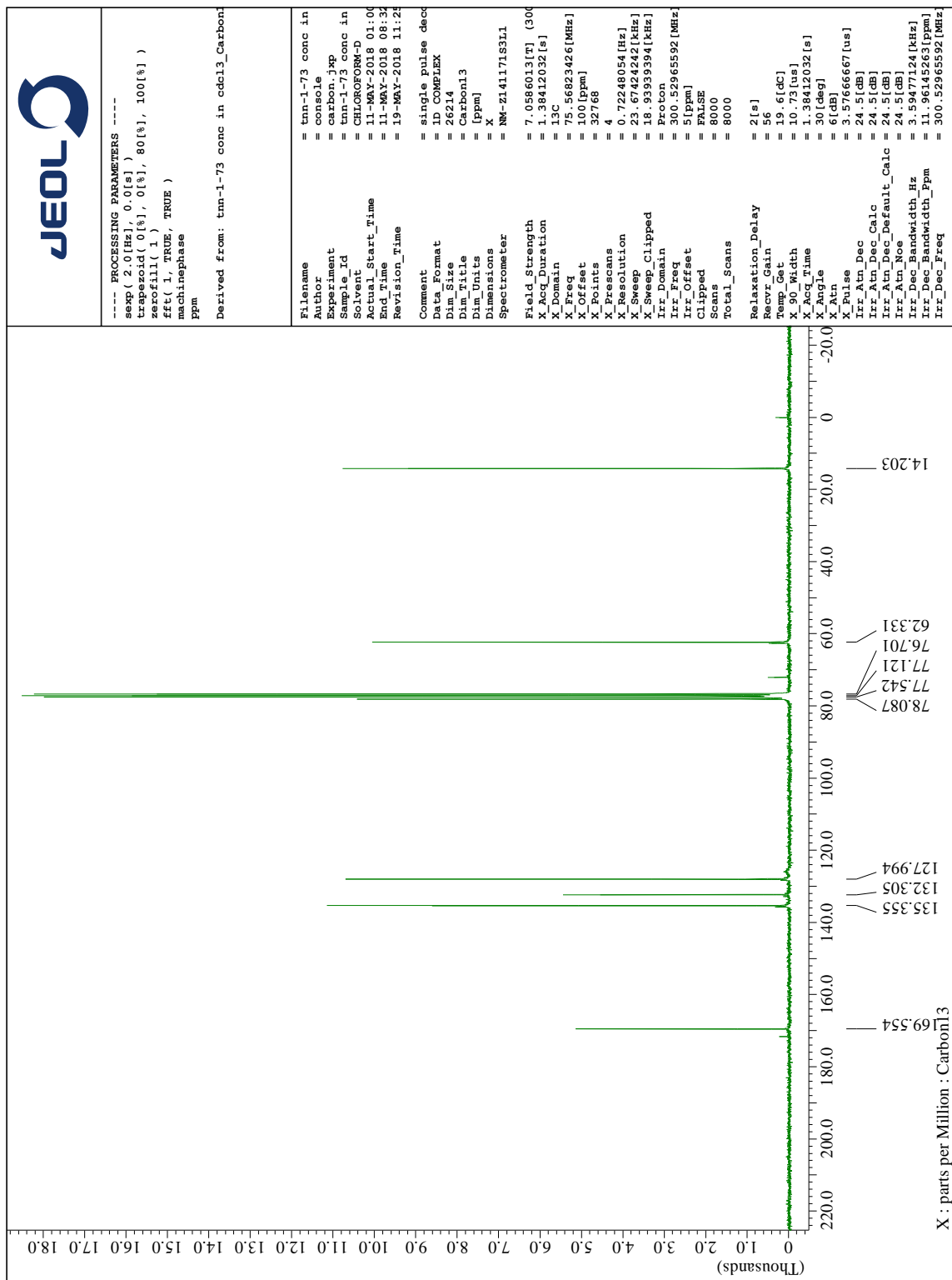
$^{13}\text{C}$  NMR of the *t*-butyl BDBA-based ester **15** in  $\text{CDCl}_3$

 $^1\text{H}$  NMR of the ethyl tartrate ester of **BDBA 19** in  $\text{CDCl}_3$


 $^{13}\text{C}$  NMR of the ethyl tartrate ester of **BDBA 19** in  $\text{CDCl}_3$



$^1\text{H}$  NMR of the ethyl tartrate ester of phenylboronic acid (**18**) in  $\text{CDCl}_3$

 $^{13}\text{C}$  NMR of the tartrate ester of phenyl boronic acid **18** in  $\text{CDCl}_3$

## VITA

**Thao Nguyen**

### EDUCATION

**Sam Houston State University, College of Science and Engineering Technology** –  
Huntsville, TX

**Master of Science in Chemistry**

August 2016 – Present (GPA 3.7, expected to graduate in August 2018)

**Houston Baptist University, College of Science and Mathematics** – Houston, TX

**Bachelor of Science in Chemistry**

September 2008 – December 2013

### SPECIAL SKILLS

Knowledgeable in wet chemistry,  $^1\text{H}$  and  $^{13}\text{C}$  NMR, liquid chromatography (LC), gas chromatography (GC), GC-MS, TLC, AA, FT-IR, fluorescence, UV-Visible spectrophotometers, polarimeter, direct and potentiometric titration, Karl Fischer titration; familiar with pH meters, electrochemical cells, rotary evaporators, viscometers; proficient with stoichiometry, statistics and other mathematical conversions on numbers; fluent in English and Vietnamese.

### EXPERIENCE

**Sam Houston State University** in Huntsville, TX

Graduate Teaching Assistant August 2016 – May 2018

- Instructed and supervised lab courses; graded exams, quizzes, homework problem sets, and lab reports; kept course records; held regular tutoring hours for both lab and lecture courses.

2016 (fall)	Organic Chemistry I, laboratory	Lecturer: Dustin Gross
	Instrumental Analysis, laboratory	Lecturer: David Thompson
2017 (spring)	Organic Chemistry I, laboratory	Lecturer: Dustin Gross
2017 (fall)	Instrumental Analysis, laboratory	Lecturer: David Thompson
2018 (spring)	Structural Spectroscopic Method, laboratory	Lecturer: Benny Arney
	Advanced Integrated, laboratory	Lecturer: Benny Arney

Graduate Research Assistant August 2016 – Present

- Planned, coordinated and performed laboratory experiments to improve molecular designs for organic materials using dynamic covalent reactions.
- Experienced in organic synthesis, temperature and air sensitive synthesis, column chromatography, NMR instrument and MNOVA software.
- Presented research at regional and national conferences.
- Supported other research group members on the usage of various equipment and apparatus.

Woodfield Pharmaceutical – Houston, TX

Analytical Chemist July 2014 – July 2016

- Planned, coordinated and conducted laboratory tests to assess physical/chemical properties and performance of raw materials in pharmaceutical chemistry on various instruments such as HPLC, GC, FTIR, Karl Fischer Titrator, polarimeter, and etc.
- Evaluated the physical properties of flavors as well as packaging components to meet defined quality standards.
- Resolved nonconforming test data.
- Compiled expired reagents, both solid and liquid, as well as laboratory wastes, which had been collected for more than 10 years for proper disposal.
- Updated and performed qualification processes for the in-house Standards.
- Operated, repaired, and performed the maintenance and annual calibration for analytical instruments.
- Reviewed annual batch records.
- Supported the R&D and Stability/Finished Product groups on the usage of the GC unit.
- Thoroughly familiar with current Good Manufacturing Practice (cGMP) and Good Laboratory Practice (GLP), maintained a safe work environment as per OSHA regulations.
- Regularly communicated with manufacturing to ensure materials being tested on time when needed.

Welch Scholar – Houston Baptist University (Grant #BF0016)

Research Assistant September 2013 – June 2014

- Provided analytical support for the synthesis and purification studies of diruthenium complexes following procedures described in the literature.
- Investigated the UV-visible spectroscopic and electrochemical properties of newly synthesized diruthenium complexes.